NASA
Technical
Paper
2589

September 1986

Impact Data From a Transport Aircraft During a Controlled Impact Demonstration

Edwin L. Fasanella,
Emilio Alfaro-Bou,
and Robert J. Hayduk

NASA

NASA Technical Paper 2589

1986

Impact Data From a Transport Aircraft During a Controlled Impact Demonstration

Edwin L. Fasanella
PRC Kentron, Inc.
Hampton, Virginia

Emilio Alfaro-Bou
and Robert J. Hayduk
Langley Research Center
Hampton, Virginia

NASA
National Aeronautics
and Space Administration

Scientific and Technical Information Branch

Contents

Summary

On December 1, 1984, the Federal Aviation Administration (FAA) and the National Aeronautics and Space Administration (NASA) conducted the first remotely piloted air-to-ground crash test of a transport aircraft. NASA and the FAA had many objectives during the joint planning and conducting of the controlled impact demonstration (CID). NASA's interest was primarily the structural behavior associated with impact. The FAA's primary objective was the demonstration of an antimisting kerosene (AMK). Improved design for damage minimization and improved seats were secondary test considerations for the FAA.

This paper reports the structural crash impact data collected by NASA Langley Research Center during the CID for the 1-sec period after initial impact, and contains appendixes with over 330 time histories of accelerations and loads. Acceleration and load levels measured in the CID were substantially lower overall than anticipated because the left-wing impact reduced the center-of-gravity sink rate from approximately 17 ft/sec to 12 ft/sec. A pitch rate was induced by the wing impact, causing the aircraft to impact 2.5° nose-down. Consequently, the peak normal (i.e, approximately vertical) accelerations along the floor were highest in the cockpit and the forward cabin near the nose wheel well and were approximately $14G$. The remaining cabin floor received peak normal accelerations typically about $7G$ or less. The peak longitudinal accelerations showed a similar distribution, with the highest acceleration being $7G$ in the cockpit and the forward cabin. The accelerations were generally less than $4G$ over the rest of the floor. The peak transverse accelerations on the floor ranged from about $5G$ in the cockpit to $1G$ in the aft fuselage.

This paper does not address loads experienced when the aircraft impacted wing-opening obstacles, effectiveness of AMK, or analysis of the post-crash fire.

Introduction

On December 1, 1984, the Federal Aviation Administration (FAA) and the National Aeronautics and Space Administration (NASA) conducted the first remotely piloted air-to-ground crash test of a transport aircraft. The Full-Scale Transport Controlled Impact Demonstration (CID) was the culmination of 4 years of effort by the two agencies.

The FAA initiated the program, provided the Boeing 720 airplane, and directed the project for the primary purpose of testing an antimisting fuel additive, a product of extensive research. NASA accepted the invitation to conduct experiments on structural behavior because of the NASA Langley Research Center's extensive experience in general aviation full-scale crash testing, crash data acquisition and analysis, crash photography, energy-absorbing-seat development, and finite-element structural analysis (refs. 1 to 3). In addition, NASA Ames Research Center Dryden Flight Research Facility, at Edwards Air Force Base, California, assumed the responsibility for the developmental flight program and remote piloting of the unmanned vehicle to the impact site.

NASA's interest was primarily to make airframe structural loads measurements and to acquire and assess baseline structural crash dynamics data. The FAA's primary interest was to demonstrate that antimisting kerosene (AMK) could be used to fly the airplane and to prevent the characteristic fireball when spilled at impact. Demonstration of improved design features, such as fire-blocking materials and seats improved for crash conditions, was a secondary objective for the FAA.

Langley was responsible for the selection, testing, and installation of instrumentation for measuring impact loads throughout the aircraft structure and for measuring transmission of loads into the anthropomorphic dummies (i.e., seat performance), a galley, and the overhead bins. Langley developed, tested, and qualified 2 independent 176-channel data acquisition systems (DAS's), including hardware and software, for recording and transmitting aircraft impact loads. In addition, Langley developed a 10-camera photographic system to provide onboard high-speed film coverage during the controlled impact. Langley was also responsible for acquisition of the airframe structural response data, subsequent analysis of the airframe data, and development and validation of an aircraft structural mathematical model using the finite-element code DYCAST (DYnamic Crash Analysis of STructures, ref. 4).

Dryden developed the remotely piloted vehicle (RPV) control system and supporting simulator for unmanned remote piloting of the Boeing 720 aircraft to the impact site. Dryden also developed a telemetry system for ground-based control of the aircraft and for activation of the DAS recorders, lights, and cameras. Dryden was also systems integrator for the FAA's AMK, fireworthiness, and crashworthiness design features experiments, as well as Langley's structural measurements experiment, associated electronics, onboard photographic system, and experimental seats.

A preliminary report on the structural loads data (for selected channels) plus detailed information about the design of the DAS, data reduction, fireproofing of cameras and equipment, and background

information leading up to the CID was released to the public at a government-industry CID workshop held April 10, 1985, at NASA Langley Research Center, Hampton, Virginia (ref. 5). Other information describing results from the CID is contained in references 6 and 7.

This paper presents the rationale behind the selection of the planned CID crash scenario, a description of the test article, the data gathering system used, the test, the results from the NASA seat experiments, a survey of the fuselage accelerations for locations from nose to tail, and the data from 331 of the 350 data channels for the 1-sec time interval after the initial left-wing (outboard engine) impact with the ground. In the appendixes, the data are divided into fuselage (appendix A), wing (appendix B), and seat and dummy (appendix C) accelerations and loads. Accelerations from the impact with the wing-opening obstacles, which occurred approximately 1.8 sec after initial wing contact with the ground, are not addressed in this report.

Symbols and Abbreviations

Accelerations are expressed in dimensionless form as a multiple of the acceleration of gravity g. In this paper G (or G units) is used to denote that only magnitudes are being compared; that is, the direction of acceleration being measured is generally not in the direction of gravity.

L	longitudinal (X) direction with respect to floor, positive forward
N	normal (Z) direction with respect to floor (approximately vertical), positive downward
T	transverse (Y) direction with respect to floor, positive out right wing; time, sec
V	velocity, ft/sec
X, Y, Z	longitudinal, transverse, and normal axis of aircraft
x_d, y_d, z_d	longitudinal, transverse, and normal axis of dummies
x, y, z	coordinate along X-, Y-, and Z-axis

Abbreviations:

AMK	antimisting kerosene
BS	body station
c.g.	center of gravity
CID	controlled impact demonstration
CPR	cardiopulmonary resuscitation
PCM	pulse code modulation
XMTR	transmitter

CID Crash Scenario

In 1980, in preparation for the CID, NASA and FAA initiated study contracts with the three major U.S. transport airframe manufacturers: The Boeing Co., Lockheed-California Co., and McDonnell Douglas Corp. The objectives of these study contracts were to review and evaluate all company and government transport accident data, to define a range of survivable crash scenarios that could form the basis for improving design technology, and to identify test techniques and analytical methods needed to evaluate impact dynamic response of transport aircraft.

Between the years 1958 and 1979, 993 jet transport accidents occurred worldwide. From this total, 176 well-documented survivable accidents were selected for detailed evaluation. Generally, the three manufacturers examined accidents associated with their own aircraft, with the diagram of figure 1 illustrating the degree of multiple review. This study effort provided definition of accident scenarios throughout the transport aircraft operational regime. The actual CID air-to-ground crash scenario evolved from these data (ref. 8). The data show that approximately 28 percent of the transport accidents occur during take-off and climb and 54.5 percent during approach and landing. Consequently, the most frequent air-to-ground crash scenario was selected for CID.

The planned CID crash scenario resulting from these detailed studies is depicted in figure 2. This scenario is representative of an "impact-survivable" accident, that is, an accident in which the livable volume is maintained (i.e., the airframe does not break up) and in which crash impact forces are survivable for many of the passengers. The transport aircraft in the planned scenario had the landing gears stowed to prevent fuselage fracture aft of the main landing gear and followed a 3.3° to 4.0° glide slope in a 1.0° nose-up attitude. The aircraft had a nominal 17 ft/sec sink rate, with no roll or yaw attitude or velocity and a longitudinal velocity of approximately 150 knots.

Planned impact conditions called for symmetric impact prior to encountering obstructions. It was planned for the fuselage to slide through a corridor between two rows of heavy steel wing-opening structures. These wing openers were designed to guarantee fuel spillage of 20 to 100 gallons per second. Powered frangible landing lights and a packed stone bed

beyond the wing openers provided additional ignition sources for the fuel. Two jet-fueled flame generators were mounted in the tail cone to provide an onboard positive ignition source. The planned take-off gross weight of the aircraft was 175 000 to 195 000 lb.

CID Test Aircraft

The aircraft used in this demonstration was a four-engine, intermediate range Boeing 720 jet transport that had entered FAA service in the mid-1960's and was ready for retirement. Even though the Boeing 720 is now considered obsolete, its structural design and construction are still representative of narrow-body transport aircraft used by domestic and foreign airlines.

Because this paper deals with NASA's structural and seat experiments, the modifications to the aircraft for the AMK experiment are not described in detail. The fuel delivery system was extensively modified and each engine carried a turbine-driven AMK fuel degrader. This device mechanically "degraded" the properties of the AMK so that the fuel characteristics were nearly those of Jet A fuel prior to entering each engine. Further information on this fuel delivery system is in reference 9.

The floor plan of the CID aircraft is presented in figure 3. Two sets of coordinates are used in the figure, both running fore to aft. The usual body station (BS) system is supplemented by an x-coordinate, which is the distance in inches measured from the nose of the aircraft. (The origin of the coordinate system used as reference for all accelerations was located at the nose, with positive X-axis forward, positive Y-axis to the right, and positive Z-axis downward. For convenience, the x-coordinate distances shown in the various figures are all positive.) Instrumentation hardware consisted of 2 DAS pallets (1 in the forward cabin and 1 aft), 4 power pallets (cameras and lights), 11 cameras (10 NASA plus 1 FAA), and associated lights. Experiments onboard included seats, galley, overhead bins, simulated hazardous cargo, and flight recorders.

There were 27 seats aboard, with a capacity of 75 occupants. (See table 1.) A variety of typical transport seats from various manufacturers was used as well as modified seats incorporating desirable features for impact. The seats were arranged in widely spaced rows so that one seat experiment would not interfere with any other seat in case a failure occurred. NASA had one row of experimental seats aboard at BS 1220. The other seats were all FAA seats, with the exception of one triple seat that belonged to France. Of the 73 dummies placed onboard, only 17 were of anthropomorphic research quality (with 13 instrumented). The remaining dummies were noninstrumented cardiopulmonary resuscitation (CPR) type. The 13 instrumented anthropomorphic dummies were located strategically to maximize coverage of the experimental seats. Instrumentation of the dummies consisted of accelerometers, located in the pelvis, chest, and head cavities, and of restraint load cells. The minimum dummy instrumentation was three accelerometers located in the pelvis and two lap-belt load cells. All dummies were in a seated, upright position except for the dummies in the NASA triple seats, which were bent over and tied in a crash position.

A total of 350 instruments were distributed throughout the fuselage structure, wings, storage bins, seats, and dummies, as shown in table 2. The distribution was 45 percent on the seats and dummies and 55 percent on the structures. Most transducers (305) were accelerometers; the remaining 45 channels were strain-gage-type transducers. The instrumentation layout of the aircraft is shown in figure 4. Seven major frames spaced along the length of the fuselage were instrumented from belly to crown to measure load transmission during impact (fig. 4(a)). The cross-sectional views show the distribution at a particular frame. Eight bending bridges along the fuselage near six of these major frames were installed to obtain the vertical bending moments during impact.

The wing instrumentation (fig. 4(b)) was limited in number and was primarily intended for measurement of vertical loads transmitted along the spars. Both inboard pylons had two accelerometers at the engine connections (fig. 4(c)). These accelerometers measured the load transmission from the engines to the wings. Each wing also had two strain-gage bending bridges for measuring vertical bending moments.

The NASA row of seats was located in the aft end of the aircraft in anticipation of an aft-end primary impact. On the right-hand side of the aircraft at BS 1220 (see fig. 3), a standard Airest 2000 triple passenger seat manufactured by Jebson-Burns Co. carried three dummies. A modified Airest 2000 seat was situated on the left-hand side, opposite the aisle. Langley researchers modified the Airest seat into a collapsible, energy-absorbing configuration (ref. 10). As shown in figure 5, several innovative design changes converted the standard triple passenger seat frame into a forward and downward collapsing four-bar linkage. Split sleeves and nylon bearings were installed at the connections between the legs and the seat pan tubes. Conventional aircraft bolts were used as hingepins at the leg–floor-rail attachment points. The four-bar linkage system provided proper kinematics for seat stroking. Two

graphite-epoxy energy-absorbing tubes, installed diagonally between the forward and rear seat legs, provided stability during normal flight and energy-absorption capability under crash conditions. The graphite-epoxy tubes progressively crushed under axial load during aircraft impact if the loads exceeded design levels.

The schematic drawing in figure 6 illustrates the crash position of the center-seated anthropomorphic dummy and the seat–dummy–restraint-system instrumentation. Both the standard and energy-absorbing NASA seats had similar center-seated instrumented dummies.

CID Instrumentation and Data Acquisition System

Langley developed the complete instrumentation and data acquisition system (DAS) (fig. 7) for the CID. All accelerometers were piezoresistive and capable of measuring acceleration from 0 Hz to greater than 1000 Hz. The accelerometer maximum levels were set to approximately $\pm 150G$ for the normal (i.e, vertical) direction, $\pm 100G$ for the longitudinal direction, and $\pm 50G$ for the transverse direction.

Each channel was filtered with the appropriate low-pass four-pole Butterworth filter before sampling to prevent aliasing errors. There were 101 channels filtered at 180 Hz, 243 at 100 Hz, and 6 at 60 Hz. All anthropomorphic-dummy acceleration channels were 180-Hz data channels. The structure acceleration channels were primarily 100-Hz channels, although some 180-Hz channels also were used. The strain-gage-type instruments, load cells and bending bridges, were connected to 100- or 60-Hz data channels.

The DAS, as designed, included two independent systems each capable of collecting and processing data from 180 sensors. The signal conditioning units (used in the DAS) had 30 channels per unit. There were six of these systems in each DAS for a total of 180 channels, of which 176 were used for data and the balance for system monitoring. The gain in the units ranged from 1 to 1000, with a full-scale output of 5 V into the pulse code modulation (PCM) system.

The PCM format for the data was set up in a frame format with 129 8-bit words per frame at a bit rate of 1 megabit per second. Within this format, 60 words were assigned to the 180-Hz channels and 58 words were assigned to the 100- and 60-Hz channels. The sampling rates for these data channels were as follows: (1) 180-Hz data at 5.38 samples per cycle (approximately 969 samples per second); (2) 100-Hz data at 4.85 samples per cycle (approximately 485 samples per second); and (3) 60-Hz data at 8.08 samples per cycle (approximately 485 samples per second). Since the 100- and 60-Hz channels were sampled at half the rate of the 180-Hz (mainframe) channels, a particular 100- or 60-Hz (subframe) channel was sampled each alternate PCM frame. With the resources available (i.e., a rate of 1 megabit per second), the word size was limited to 8 bits to allow for the relatively high sample rates and the large number of channels.

The conversion of the sensor data in the PCM system was accomplished with a master converter which processed all data sequentially from the analog multiplexing input cards in the PCM system. The PCM data from each DAS were recorded redundantly on two onboard 14-track airborne tape recorders. The PCM data on four tracks per recorder were digitally delayed 256 msec to ensure data acquisition in the event of a momentary tape speed perturbation during the impact. The PCM data, although recorded redundantly onboard, were also being transmitted redundantly from air to ground via four telemetry transmitting systems to the ground receiver control station and mobile recording vans.

Data Reduction and Filtering

The data shown in this report were taken from the onboard data tapes. Processing was for four groups: DAS 1 and DAS 2 mainframe data, sampled at 969 Hz; and DAS 1 and DAS 2 subframe data, sampled for each alternating PCM frame at 485 Hz. The "prefires," or zero initial conditions, were taken just prior to aircraft take-off. Accelerations were zero and anthropomorphic-dummy restraint (belt) forces were near zero before CID take-off. However, static wing and fuselage bending moments were nonzero at this time. Thus, data presented in the appendixes for bending moments represent the incremental moments above or below the moments that existed just before CID take-off. Some acceleration traces were further adjusted in plotting when the zero was obviously shifted.

Posttest low-pass digital filtering with a computer algorithm was performed on the data. In the frequency domain, a cosine function was arbitrarily used to represent the roll-off region (ref. 11). The digital filter was used to "smooth" the digital nature of the data and to remove unwanted high-frequency variations that were associated with the sample rate (fig. 8). All structural accelerations were digitally filtered with a low-pass 100-Hz digital filter, and the strain-gage instruments (restraint forces, bending bridges, and load links) were filtered with a low-pass 50-Hz digital filter.

The acceleration traces were all integrated to obtain velocity time histories. When acceleration

offsets are not present, the integrated acceleration can be used to determine the velocity change of the structure. If a very large velocity change is noted, the acceleration data are suspect and may have been degraded by electrical anomalies (voltage shifts or voltage surges), or the accelerometer may have been struck (overloaded), loosened, or separated from its mounting.

CID Flight and Crash Impact Parameters

With ideal weather conditions on the morning of December 1, 1984, the CID aircraft took off from Edwards AFB under the ground-based remote control of Fitzhugh Fulton, an experienced NASA test pilot. The gross take-off weight was 200 455 lb, with 76 058 lb of AMK fuel onboard. During descent to the impact site, a modified instrument landing system and a video camera mounted in the aircraft nose aided the pilot in guiding the aircraft to an extremely small impact footprint 30 ft wide and 200 ft long.

At an altitude of 200 ft the aircraft was off to the right of the target centerline, but not far enough for the pilot to abort the approach and go around for another attempt. The 150-ft altitude was the decision altitude below which the test could not be aborted because of activation of time-critical, limited-duration onboard photographic and data recording systems. At the 150-ft altitude the pilot made a fairly sharp left-aileron control input to bring the aircraft back to the target centerline. This control input initiated a lateral (rolling) oscillation after commitment but prior to impact. The pilot concentrated his efforts on damping the oscillations, achieving the best possible alignment with the target centerline and meeting a critical project requirement of impacting the ground in front of the wing openers. The structural and seat experiments were planned for an impact and slide prior to contacting the artificial obstructions (wing openers) intended for the FAA AMK experiment. Impact beyond the wing openers would have jeopardized the AMK experiment if fuel spillage had not occurred.

Approximately 8000 lb of fuel were consumed in the flight, leaving about 68 000 lb in the tanks. The gross aircraft weight at impact was approximately 192 000 lb. Figure 9 is a sequence of photographs illustrating the CID impact. The left outboard engine (No. 1) impacted the ground first with 13° roll, 13° yaw, and approximately 0° pitch (fig. 9(a)). The aircraft forward speed was approximately 150 knots and the sink rate was about 17 ft/sec. Impact occurred 285 ft short of the planned impact area. The fuselage, pitching nose down after left-wing impact, struck the ground 0.46 sec later at the forward cabin (fig. 9(b)), with a pitch of $-2.5°$ and a center-of-gravity (c.g.) sink rate of 12 ft/sec. The wing absorbed some of the vertical kinetic energy and significantly reduced the severity of the fuselage impact except for the forward cabin area near the pilot. The pitch rate that developed after wing impact increased the sink rate of the forward cabin to 18 ft/sec (about 6 ft/sec above the c.g. sink rate) and decreased the aft sink rate proportionally below the c.g. sink rate. Acceleration traces were integrated for locations fore and aft of the c.g. to determine the variation of vertical velocity change at impact.

The aircraft continued to yaw during the slide following impact and contacted the first wing opener at approximately 38° left yaw (fig. 9(c)). This wing opener (the third one on right-hand side of centerline) cut through the right inboard engine (No. 3) and diagonally opened the leading edge and lower wing. The right wing failed, lifted upward as the aircraft continued to slide, and separated, dumping fuel during the process (fig. 9(d)). All four wing openers on the right-hand side opened the fuselage, permitting fuel to enter the fuselage from the bottom. Since the right inboard engine was sliced in half, large quantities of degraded AMK fuel were exposed to an extremely high-temperature ignition source. These conditions were beyond the design envelope for AMK and a huge "fireball" erupted.

The sequence of events during the first few seconds after impact is shown in figure 10 by a select set of vertical acceleration time histories. The time origin was chosen as 09:22:11 Pacific standard time (PST). The time from initial left-wing impact to the impact of the right-wing inboard engine with the wing opener was almost 2 sec. Since the fuselage impact was nose down, the nose-to-tail progression of structural response can be seen from the pilot-floor and BS 960 curves in figure 10.

The wing-opener impact, an unpredictable air-to-ground flight into an obstruction type of accident, is not discussed in detail and loads data from that impact are not presented in this report. Major structural damage to the right wing and to the fuselage occurred at contact with the three right-wing openers. The major fuselage damage occurred when the inboard right wing opener cut through the wing and entered the fuselage center wing box near BS 720. The wing box was cut diagonally and the massive center section keel beam was cut through and separated from the airplane. The wing-opener damage, along with the fire damage (fig. 11), made it difficult to correlate the initial fuselage impact data with corresponding final structural damage. Fortunately, the aircraft forward of the wings was not as severely weakened by fire or impacted by the wing openers.

Results From CID Initial Impact

Results presented here and in the appendixes are from the impact and subsequent slide prior to contacting the wing openers. This initial impact of the aircraft fuselage is the event of interest for the structural impact experiments. This event occurred in the 1-sec period from 09:22:11 to 09:22:12 PST, which is the period that is being simulated with crash impact computer models.

The overall performance of the NASA DAS and the onboard photographic system was excellent. Ninety-seven percent of the transducers were active at impact and all 11 onboard cameras functioned properly. The DAS and the photographic system were enclosed in thermal insulation to assure data survival in case of fire. The insulation prevented fire damage to all information recorded onboard, even though the fire lasted for hours and was hot enough to melt large holes in the fuselage and to consume the floor beams, floor, and seats in the aft section. The onboard film survived the fire and provided unique insight into the propagation of fire and smoke in the aircraft interior. The aircraft slid for approximately 11 sec after initial impact. By this time the smoke was so dense in the cockpit that the visibility was very poor. After another 5 to 10 sec, visibility was near zero throughout the aircraft.

The distribution of impact-induced accelerations along the floor of the aircraft is presented in figure 12. The abscissa is the distance (in inches) measured from the nose. (See fig. 3 for body station–x-coordinate equivalence.) Acceleration levels are plotted along the ordinate in G units. The square symbol represents an acceleration peak read from the individual filtered time history. The plus symbol represents a further refinement, or "peak averaging," of the data which is believed to be more significant for structural or human response.

The peak averaged acceleration data point corresponding to a particular time history is determined in this manner: The pulse duration corresponding to the primary impact is determined. Integration over this interval yields the change in velocity which, when divided by the duration, yields the average acceleration. Doubling the average acceleration to obtain the data points represented by pluses is effectively a triangularization of the actual acceleration pulse. (See fig. 13.)

Overall, the fuselage impact loads, as measured along the floor, were survivable as defined by accepted criteria for human tolerance (ref. 12). The loads were substantially lower than anticipated because the left-wing impact reduced the c.g. sink velocity. Loads in the aft section were further reduced due to the wing-induced pitching moment which caused the nose to hit first instead of the aft end as planned. Consequently, the peak normal (i.e., approximately vertical) accelerations along the floor were highest in the cockpit and the forward cabin near the nose wheel well and were approximately $14G$ (fig. 12(a)). The remaining cabin floor received peak normal accelerations typically about $7G$ or less. The aft fuselage experienced accelerations below $4G$. These accelerations were disappointingly low for the seat experiments since the NASA energy-absorbing seat in the aft end of the aircraft was designed to initiate stroking at approximately $10G$.

Peak longitudinal accelerations showed a similar distribution, with the highest acceleration being $7G$ in the cockpit and the forward cabin (fig. 12(b)). The accelerations were generally less than $4G$ over the rest of the floor. Peak transverse accelerations on the floor also were generally low. They ranged from about $5G$ in the cockpit to $1G$ in the aft fuselage (fig. 12(c)).

Generally, the peak averaging technique (triangularization) produced good correlation with the peak data except at a few locations. Sharp spikes, producing high peak points, do not correlate with the triangularization peaks. The triangularized peaks are believed to be more significant than values taken from unrefined sharp peaks for indicating structural and human response (ref. 2).

Histograms in figure 14 illustrate the structural response interaction and the load path definition at various locations along the fuselage at primary impact. As discussed earlier, the loads were generally higher in the forward fuselage than in the aft section because of the nose-down impact of the fuselage, with increased sink velocity at the nose caused by the wing-induced pitch rate. Values at locations B and C demonstrate that the load transmission through the fuselage section to the subfloor and dummies was significantly reduced by the crushing and energy absorption of the fuselage structure. At fuselage location B (BS 540), for example, the fuselage bottom experienced a sharp peak normal acceleration of $32G$ and 0.04 sec duration (fig. 15(a)). At the subfloor, the transmitted load was reduced by structural deformation to about $7G$, with duration increased to 0.15 sec (fig. 15(b)). The loads at floor level were nearly the same as at the subfloor at this location (fig. 15(c)). The acceleration time histories (fig. 15(d)) from the seat and the dummy's pelvis at this location show that the higher frequencies have been filtered out by the seat cushion, pan, and soft dummy material, but that the

acceleration and duration were essentially unchanged. No seat dynamic load amplification occurred during load transmission to the dummy's pelvis at this location.

The large peak accelerations at the fuselage bottom at BS 960 (the rear main landing gear bulkhead) occurred later than the peak accelerations at BS 400 and 540. The fuselage bottom at BS 960 contacted the ground at 0.86 sec after initial impact with low impact velocity. The floor and subfloor accelerations peaked at approximately 3G at BS 960 over the entire primary impact sequence. The accelerometers on the rigid bulkhead at the fuselage bottom at BS 960 were overloaded and show very high peaks (see figs. 14(a) and 14(b)). Consequently, the peak values from accelerometers at the fuselage bottom may not be accurate. (See appendix A.)

The overall fuselage crush, as shown in figure 16, was determined after the test by measuring the distance from floor to ground on both sides of the fuselage. The left and right fuselage measurements were averaged and this value was subtracted from the pretest floor-to-underbelly height to obtain overall crush data. Since the aircraft was rolled and impacted the left side first, the left side showed more deformation than the right.

These data indicate 6 to 7 in. of average vertical crush in the forward cabin area at the point of contact near the nose wheel well, 9 in. of crush forward of the wing, and 6 in. of crush aft of the wing. The fact that the forward cabin did not contact the wing openers gives some credence to those crush measurements, even though intense heat may have contributed to the deformation. However, the crush data aft of the wing is suspect because of the loss of structural integrity after impact with the wing openers and because of the intense heat.

The NASA energy-absorbing seat in the aft fuselage experienced loads well below the 10G required to initiate stroking, and consequently it did not stroke. Figure 17(a) contains the normal acceleration time histories of the energy-absorbing seat and the dummy's pelvis superimposed to illustrate these low accelerations and the similarity of response, with the pelvis response (without amplification) lagging the seat response, as expected.

The corresponding normal acceleration time histories for the standard triple seat across the aisle from the NASA energy-absorbing seat are presented in figure 17(b). The performance results are comparable to the NASA energy-absorbing seat within the accuracy of the measuring equipment at this low load level.

Concluding Remarks

NASA and the FAA have conducted the first remotely piloted transport crash test of a Boeing 720 aircraft. The primary interest of NASA in the Full-Scale Transport Controlled Impact Demonstration (CID) was the structural behavior of the aircraft associated with impact. The FAA was interested in the fire-retardant behavior of antimisting kerosene. Acceleration and load levels measured in the CID were substantially lower overall than anticipated because the left-wing impact reduced the center-of-gravity sink velocity from approximately 17 ft/sec to 12 ft/sec. A pitch rate was induced by the wing impact, causing the aircraft to impact with the nose down 2.5°. Consequently, peak normal (i.e., approximately vertical) accelerations along the floor were highest in the cockpit and the forward cabin near the nose wheel well and were approximately 14G. (All accelerometer data were passed through a 100-Hz low-pass digital filter.) The remaining cabin floor received peak vertical accelerations typically about 7G or less. The aft fuselage experienced acceleration magnitudes below 4G. The peak longitudinal accelerations showed a similar distribution, with the highest accelerations being 7G in the cockpit and the forward cabin. The accelerations were generally less than 4G over the rest of the floor. Peak transverse accelerations on the floor were also low. They ranged from about 5G in the cockpit to 1G in the aft fuselage.

The appendixes contain over 330 data traces of accelerations and loads for the first second after wing impact. These data offer insight into the transmission of loads through the structure and into the seats and the dummies. These data are also being used to corroborate nonlinear dynamic finite-element structural analysis computer programs developed to simulate transport crashes. Since all 11 interior cameras functioned properly, the crash behavior of the interior of the aircraft was graphically captured. The films are unique and contain significant information on fire propagation and smoke obscuration.

From an occupant human tolerance standpoint, the CID primary impact loads were survivable. The pilot and crew area received the greatest impact forces. The NASA energy-absorbing seat in the aft fuselage experienced low load levels, well below the 10G required to initiate stroking, and consequently it did not stroke. Data from the impact with the wing openers and the effectiveness of the antimisting kerosene were not assessed in this paper.

NASA Langley Research Center
Hampton, VA 23665-5225
June 5, 1986

TABLE 1. CID AIRCRAFT SEAT AND DUMMY SUMMARY

(a) Dummies

Type	Total number	Number instrumented
Anthropomorphic (NASA)	6	2
Anthropomorphic (FAA)	11	11
CPR	55	
Baby	1	
Total	73	13

(b) Seats

Type	Number of seats	Occupant places
Pilot seat (single)	1	1
Flight attendant (double)	2	4
Aft facing	2	4
Triple seats	22	66
Total	27	75

TABLE 2. CID AIRCRAFT INSTRUMENTATION SUMMARY

Accelerometers:	
Dummies	52
Seats	75
Structures:	
Overhead bins	3
Wing pylons	4
Wing (other)	14
Floor near seats	43
Frames	109
Center of gravity	3
Tail	2
Total	305
Bending bridges:	
Wing	4
Fuselage	8
Total	12
Load cells:	
Overhead storage bins	3
Lap belt	26
Shoulder harness	4
Total	33
Total channels	350

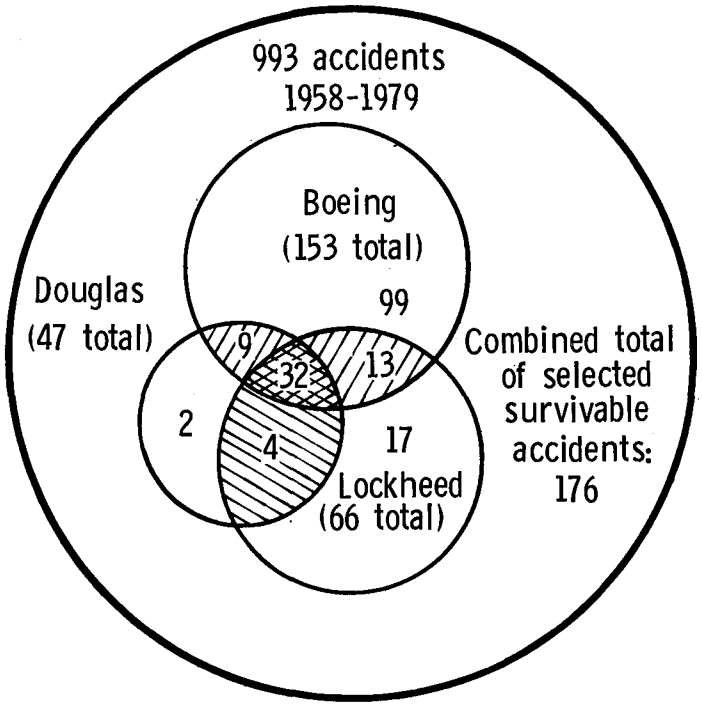

Figure 1. The transport accident data base and study selection.

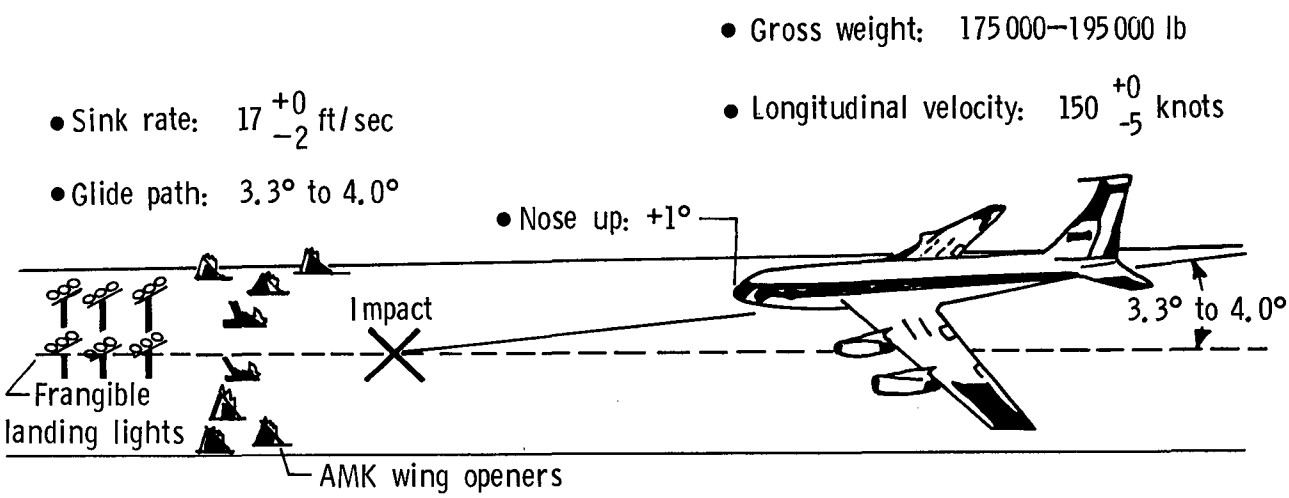

Figure 2. Planned CID crash scenario.

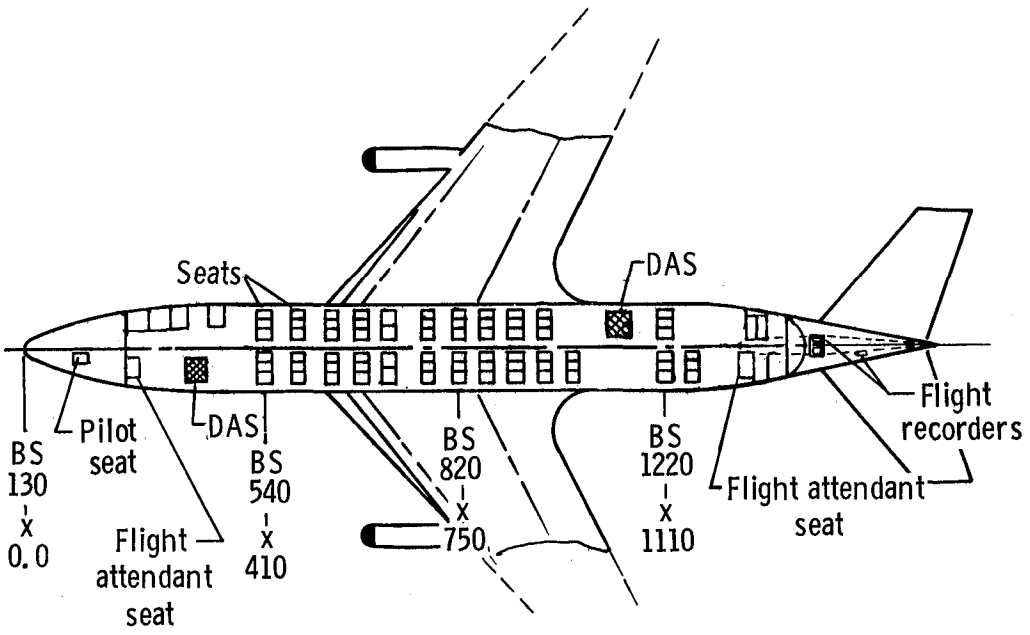

Figure 3. Floor plan of hardware and experiments aboard CID aircraft.

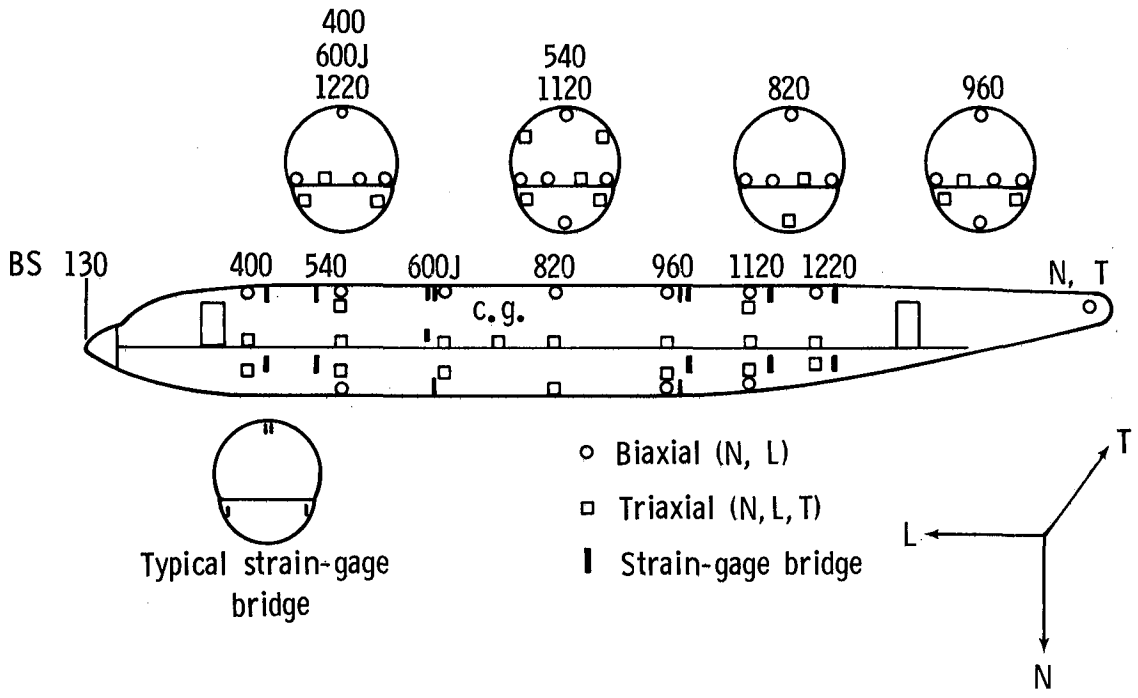

(a) Fuselage.

Figure 4. Accelerometer and strain-gage locations.

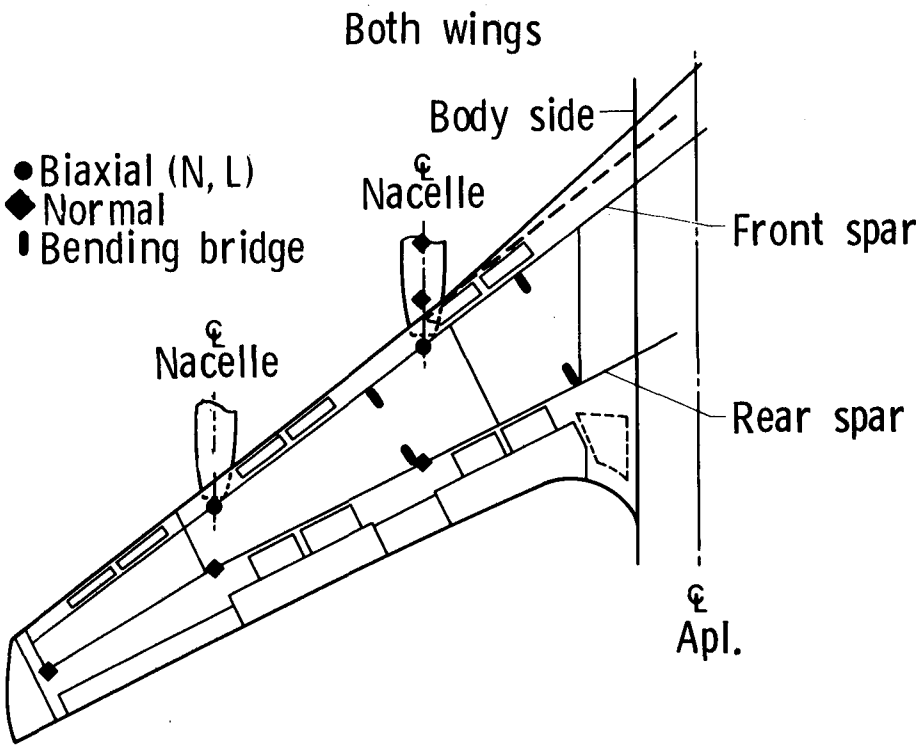

(b) Wing.

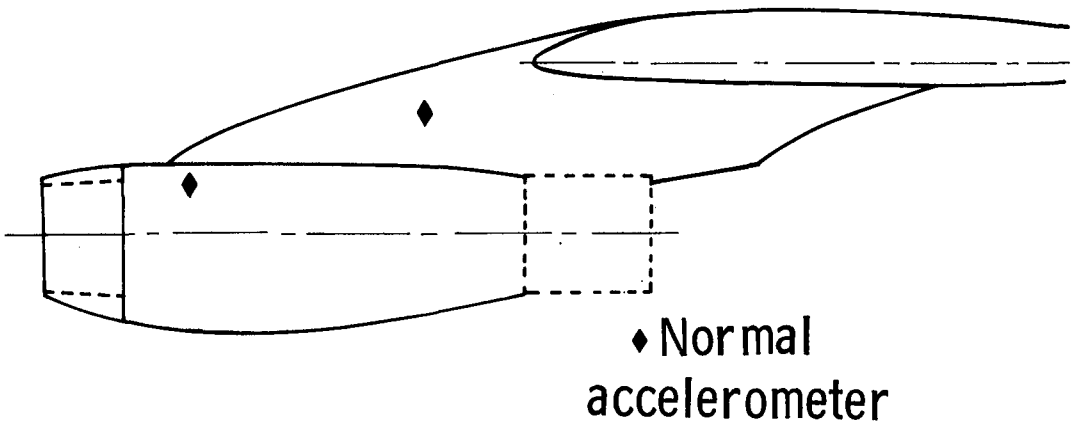

(c) Inboard nacelle (accelerometers only).

Figure 4. Concluded.

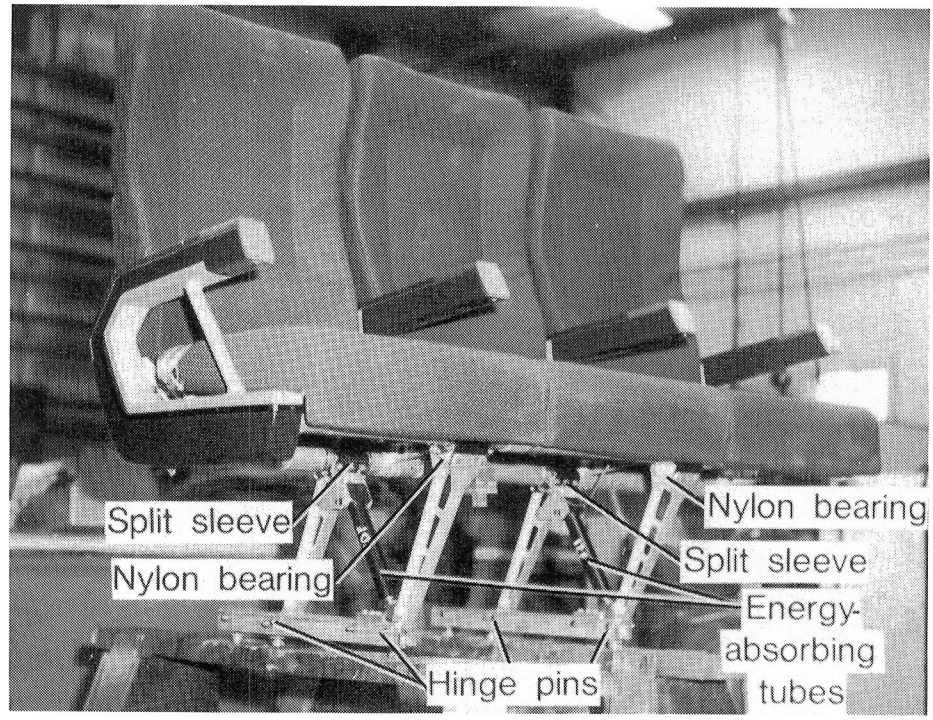

L-85-3878

Figure 5. NASA-modified Airest 2000 energy-absorbing seat.

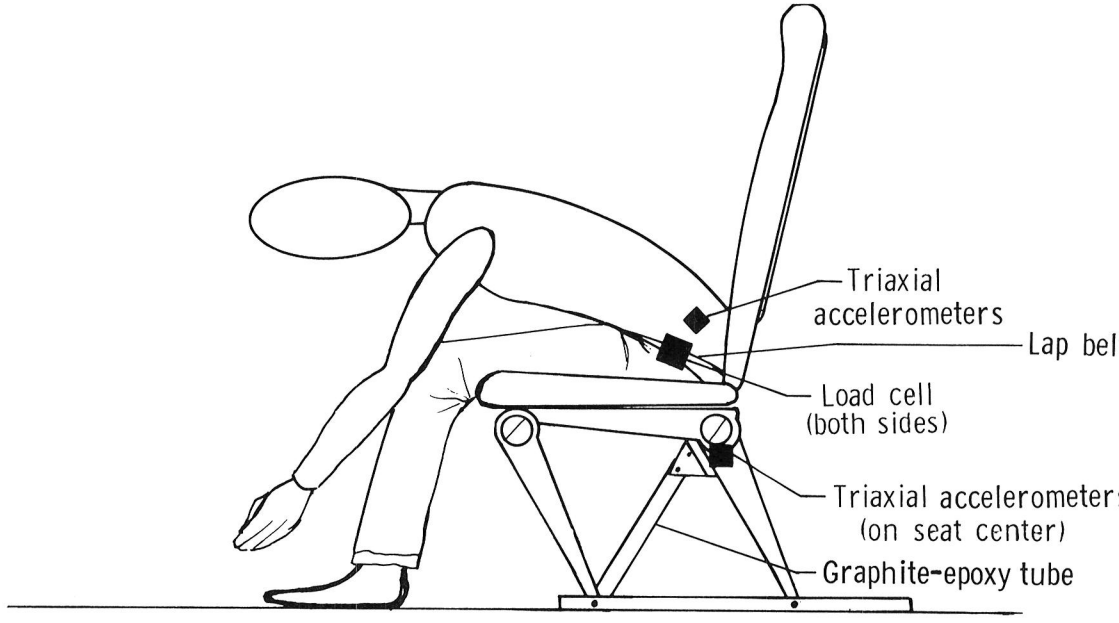

Figure 6. Instrumentation of NASA triple-seat and center-seated dummy.

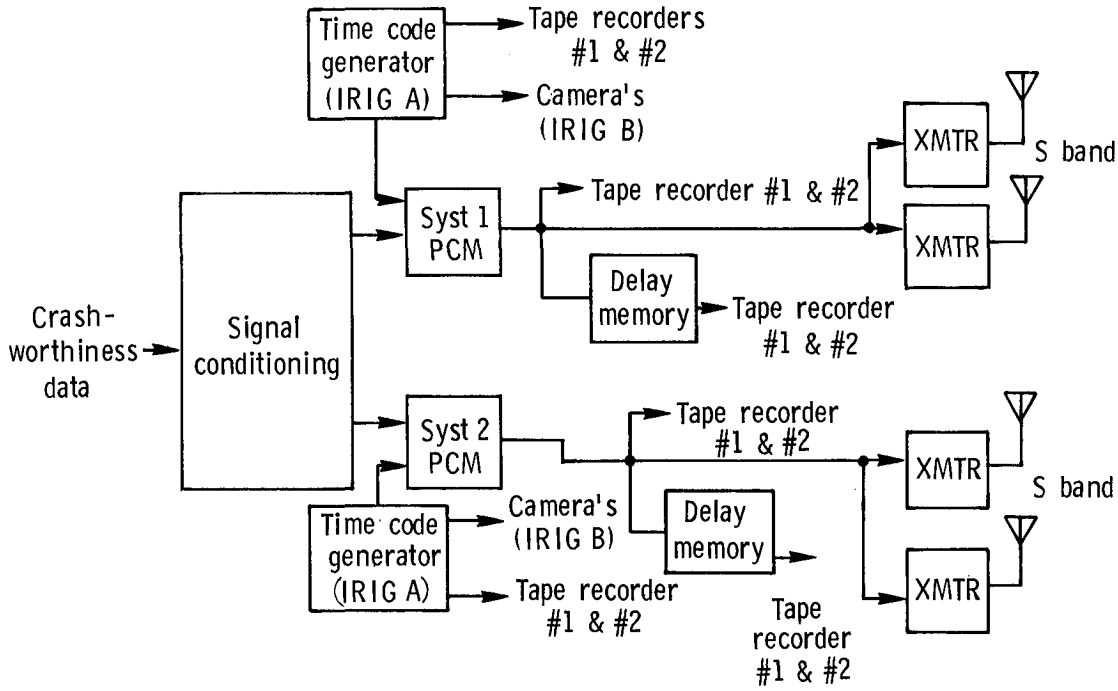

Figure 7. Block diagram of DAS.

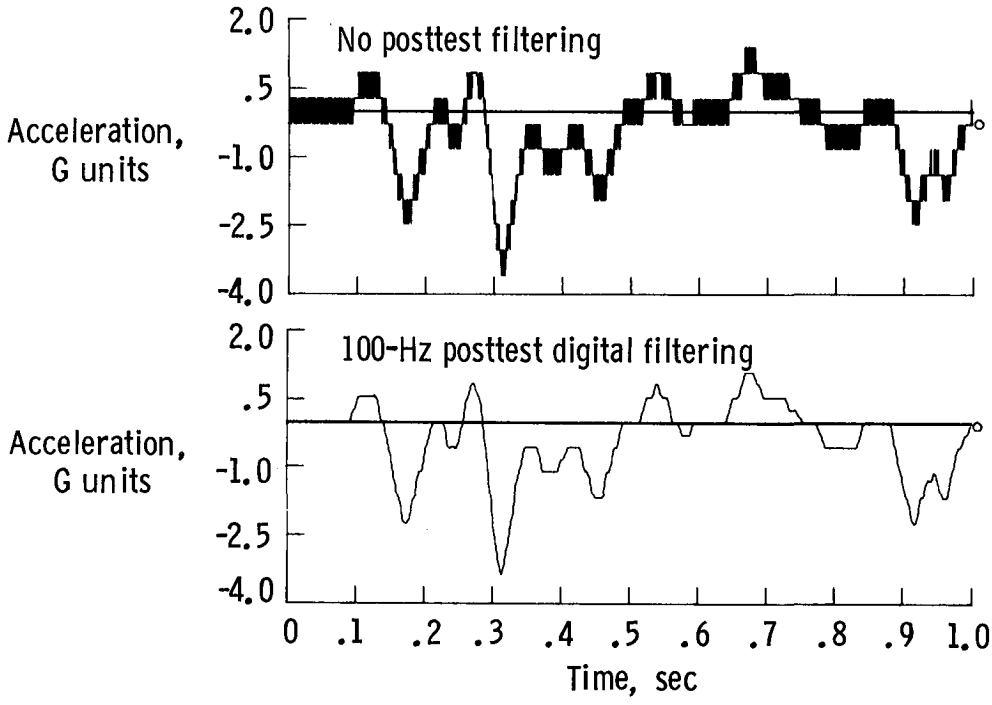

Figure 8. Data as recorded and digitally filtered.

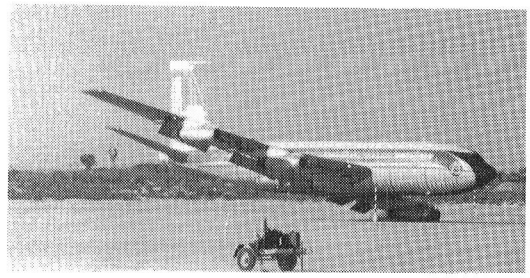

(a) Left-wing impact.

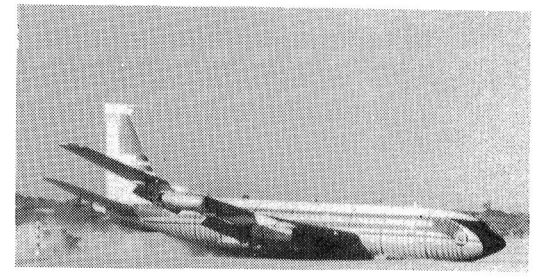

(b) Fuselage impact.

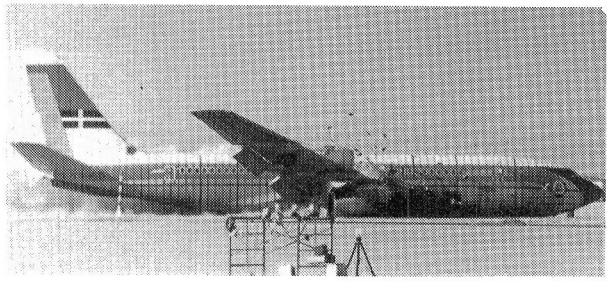

(c) Impact with wing openers.

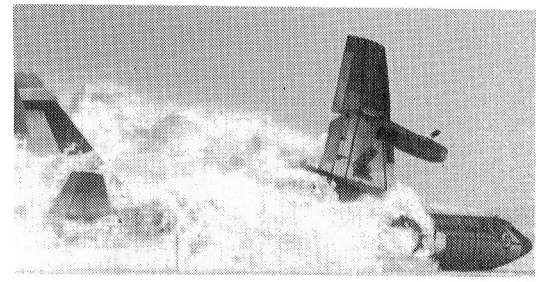

(d) Post-crash fire.

L-85-3877

Figure 9. CID impact sequence.

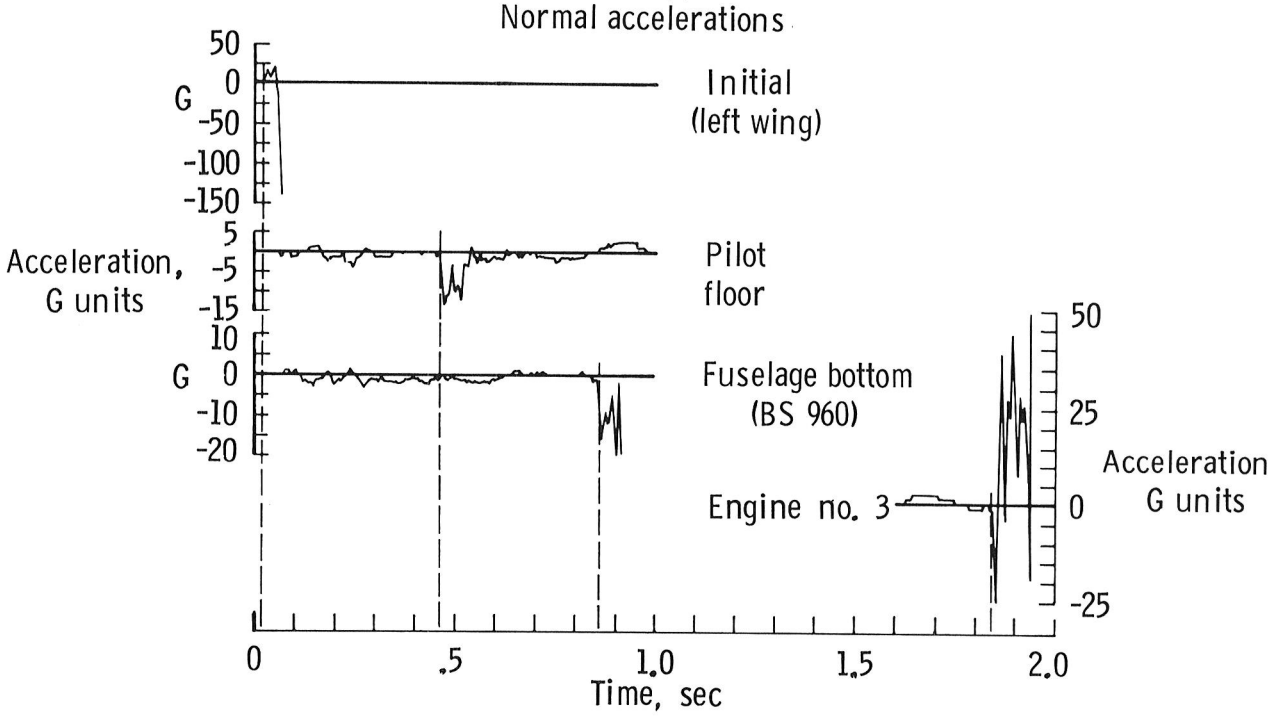

Figure 10. CID sequence of events.

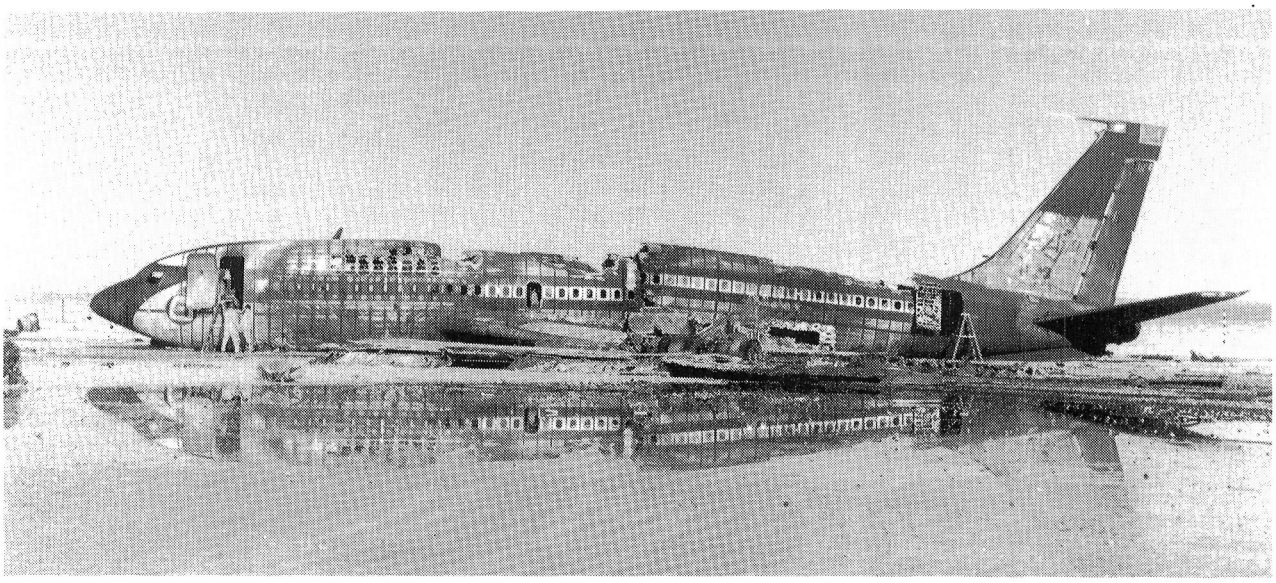

L-84-13,964

(a) Overall view.

L-86-319

(b) Interior aft view.

Figure 11. Post-CID damage.

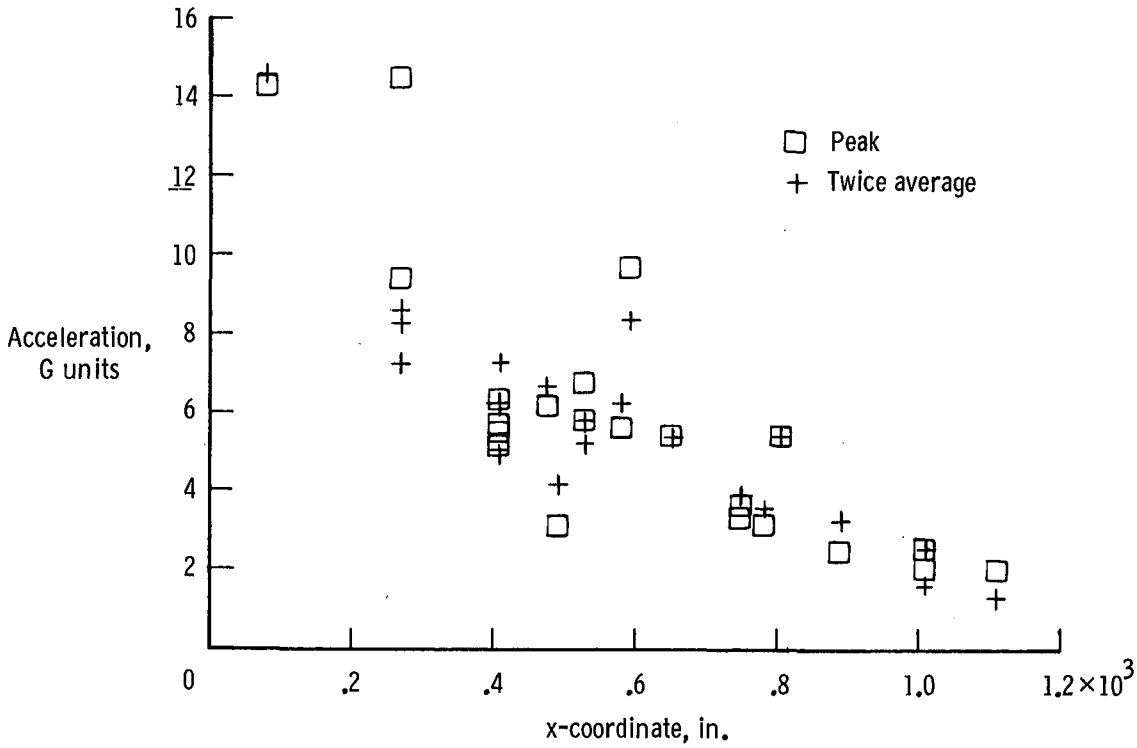

(a) Normal accelerations.

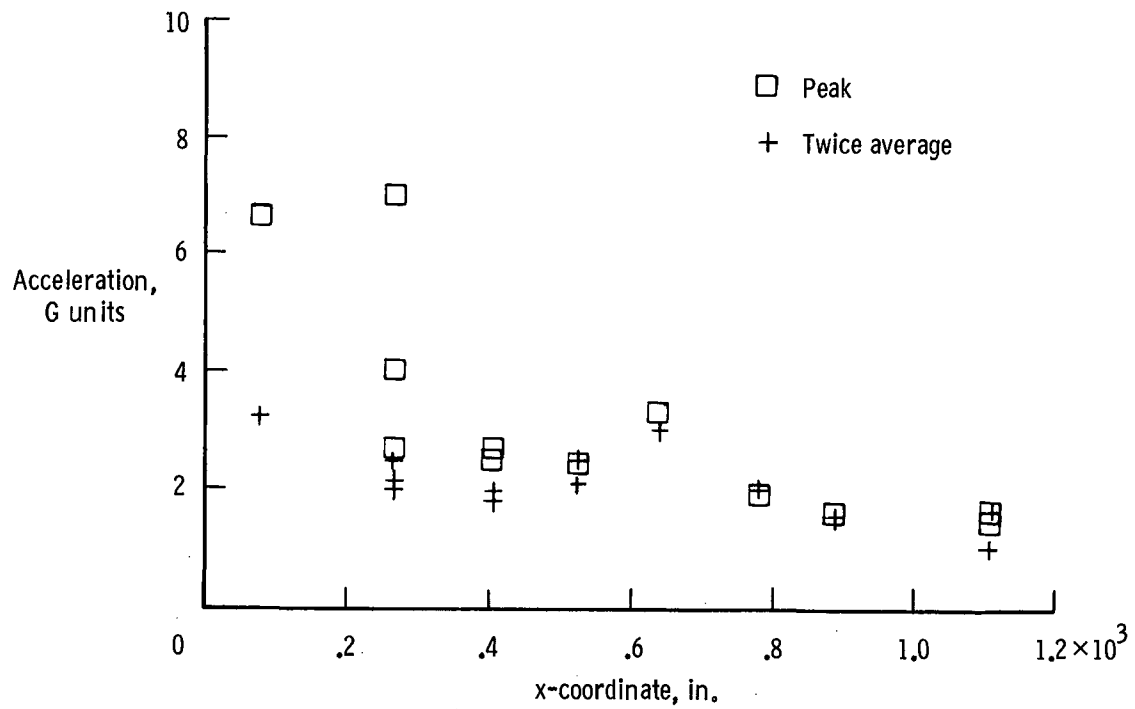

(b) Longitudinal accelerations.

Figure 12. Floor accelerations for fuselage impact. $T = 0.5$ sec.

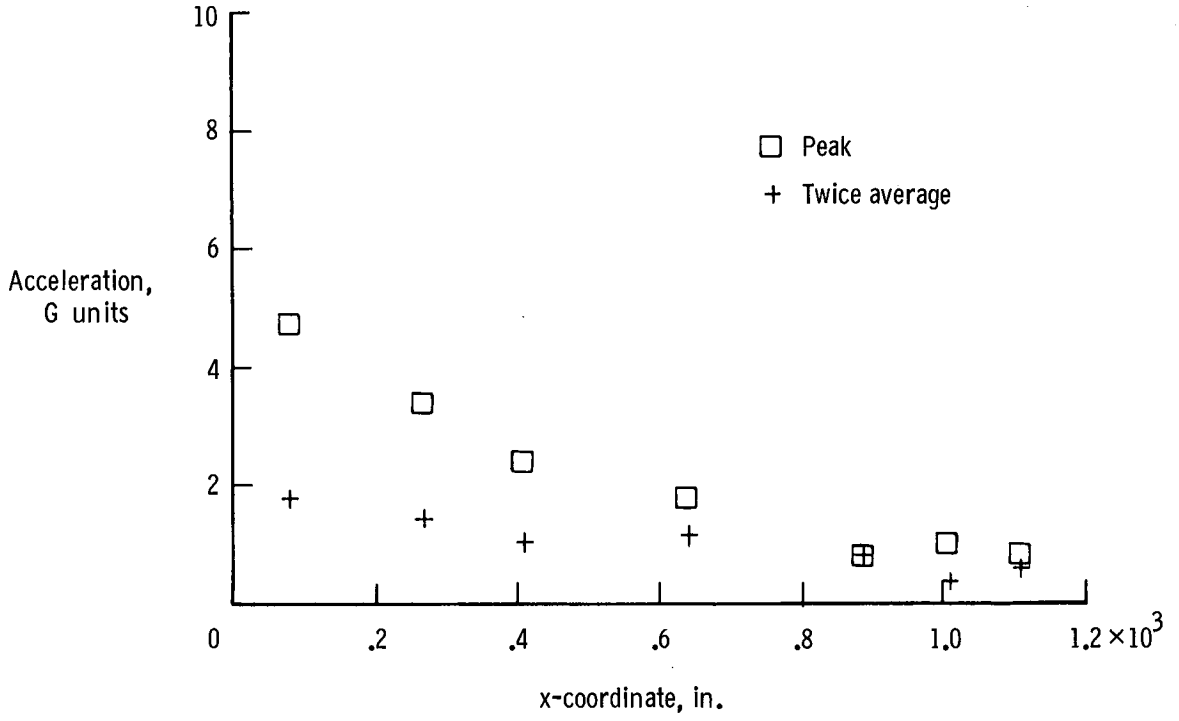

(c) Transverse accelerations.

Figure 12. Concluded.

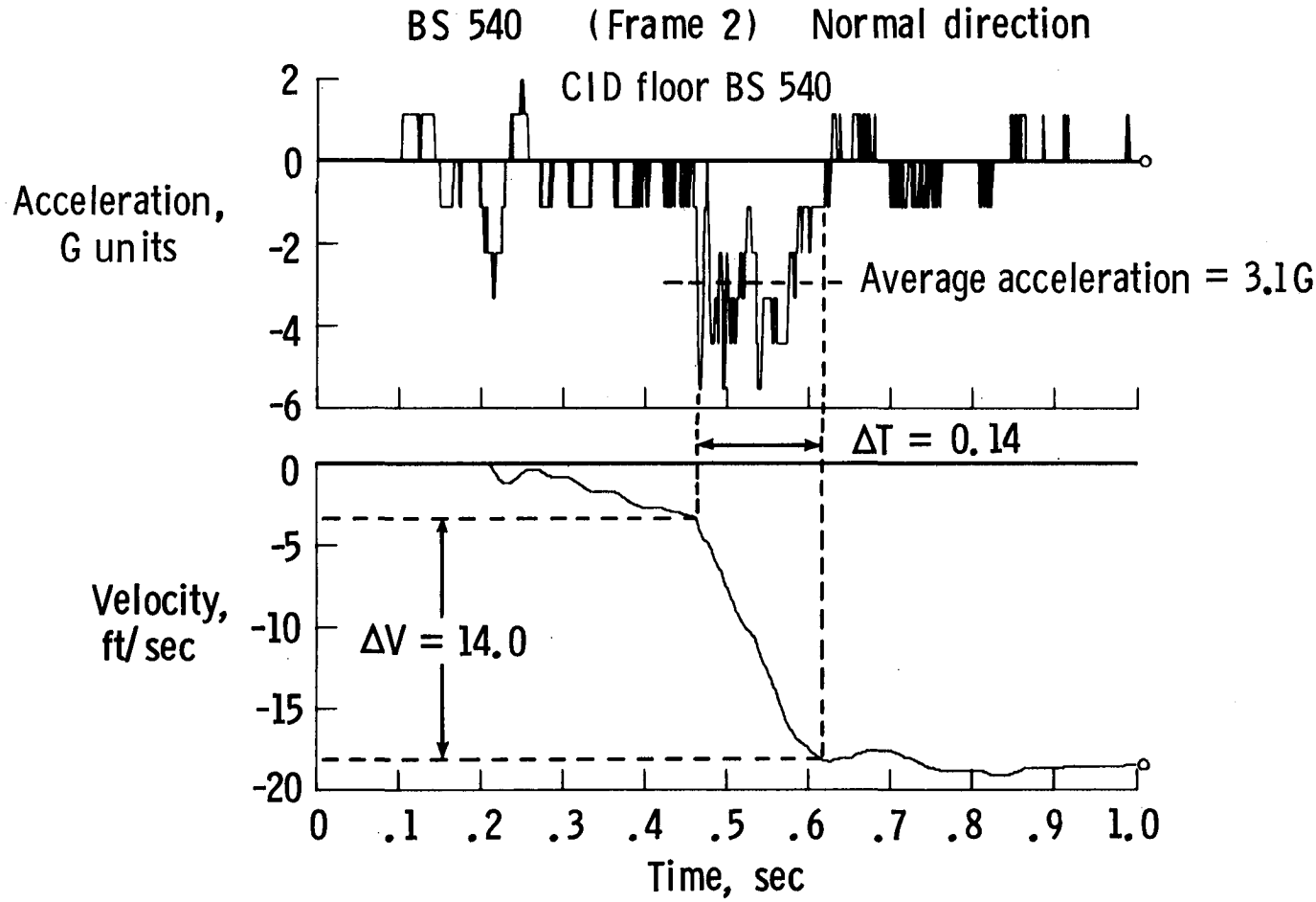

Figure 13. An example of acceleration, velocity change, and average acceleration for a typical data channel. The triangular equivalent pulse would have a peak acceleration of 6.2G (twice average).

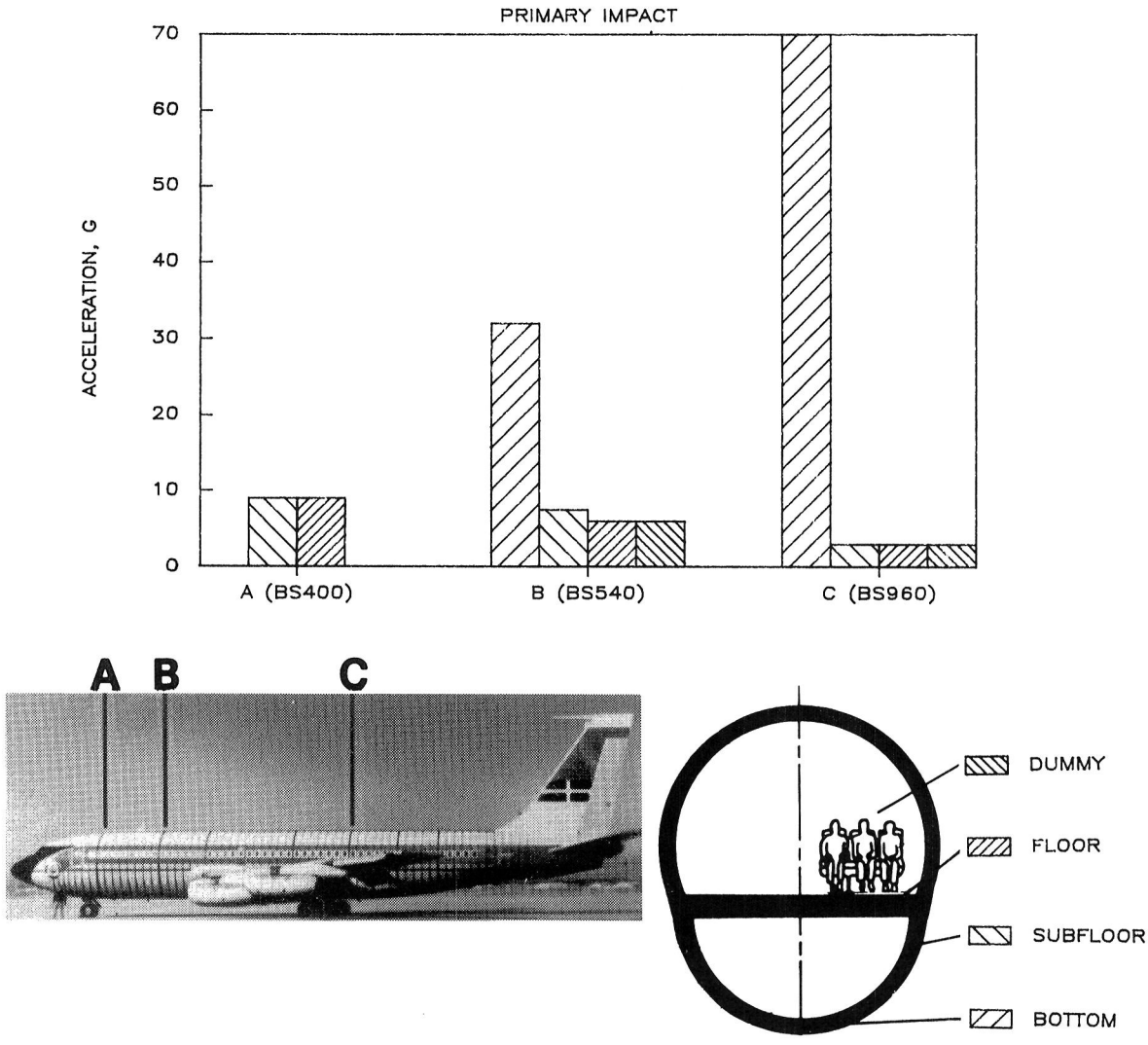

(a) Normal response.

Figure 14. Aircraft structural response.

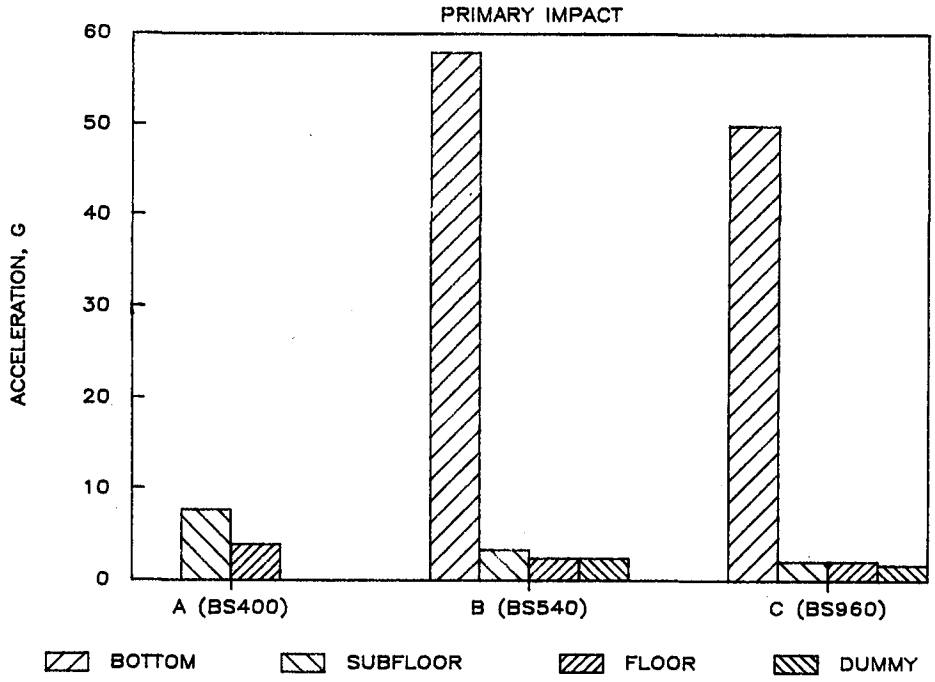

(b) Longitudinal response.

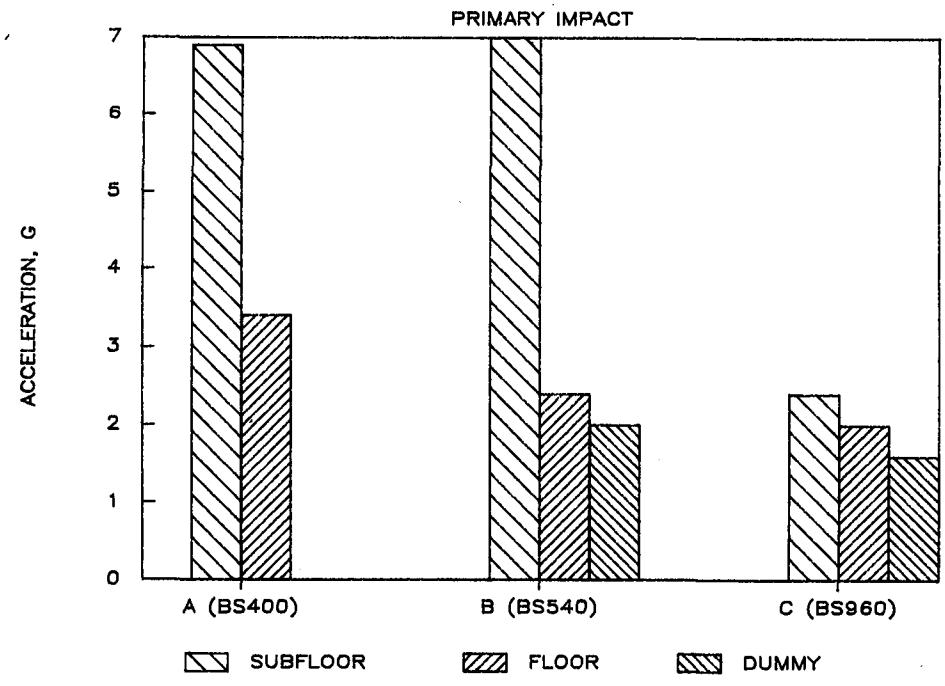

(c) Transverse response.

Figure 14. Concluded.

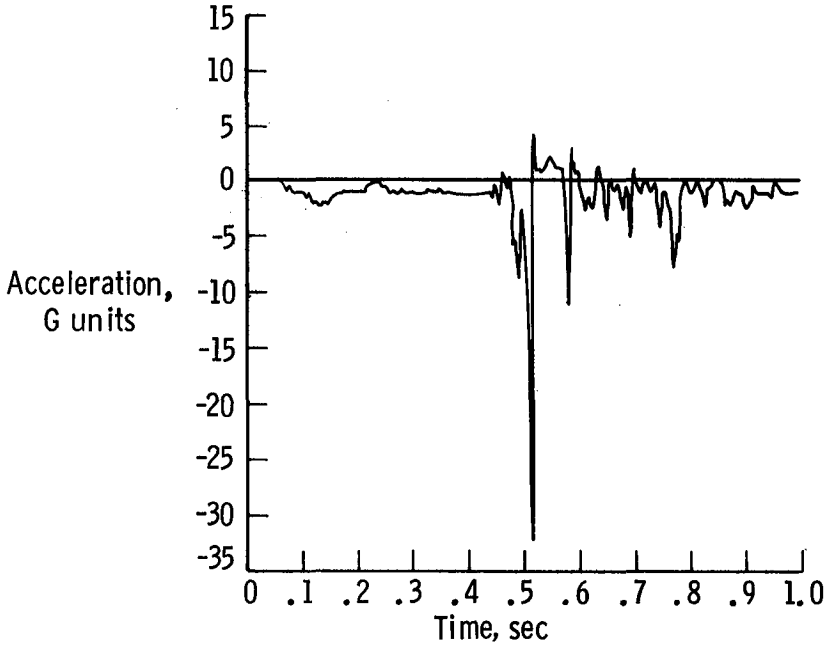

(a) Fuselage bottom.

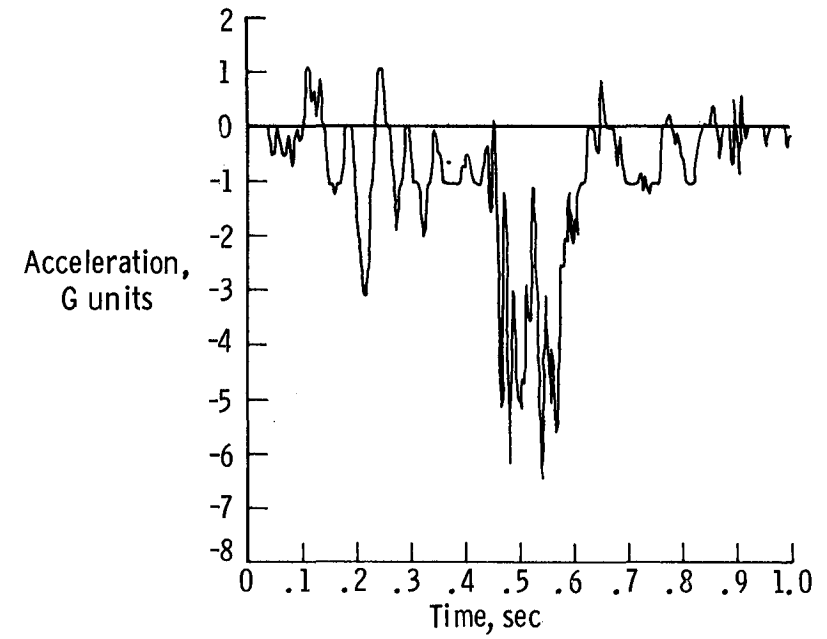

(b) Fuselage subfloor.

Figure 15. Peak normal acceleration at BS 540 during first second after impact.

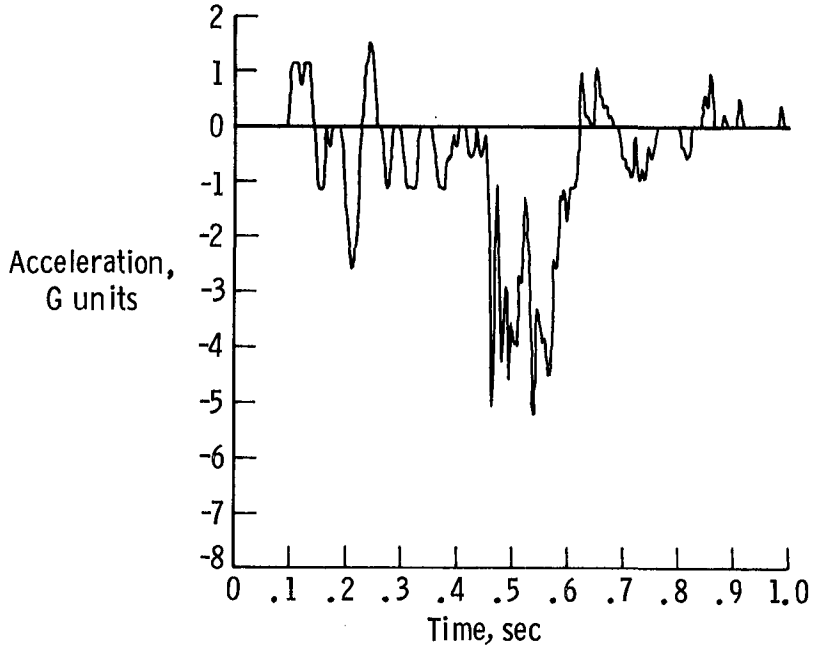

(c) Fuselage floor.

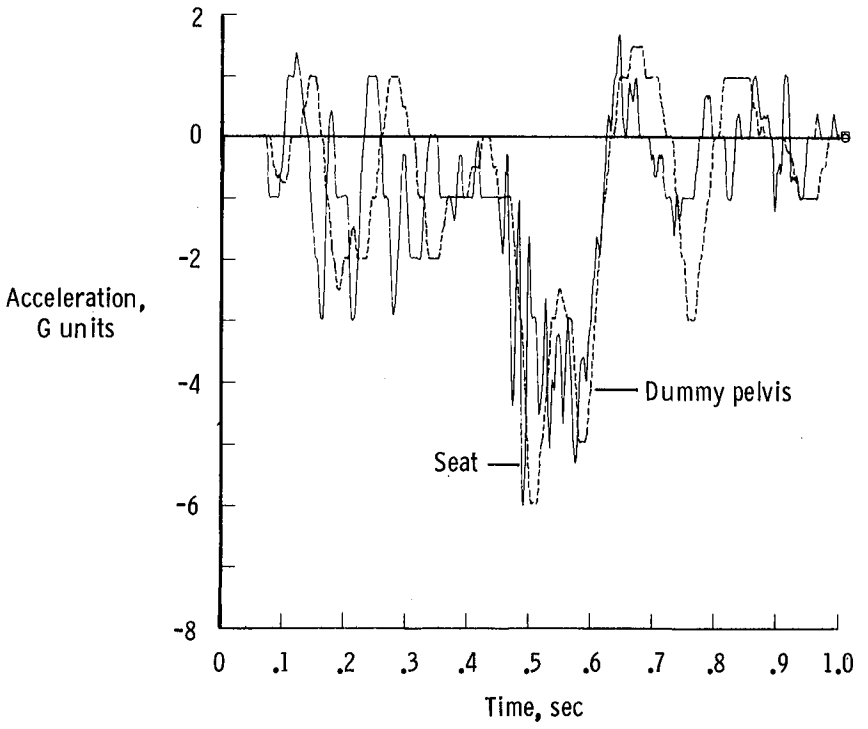

(d) Seat and dummy pelvis.

Figure 15. Concluded.

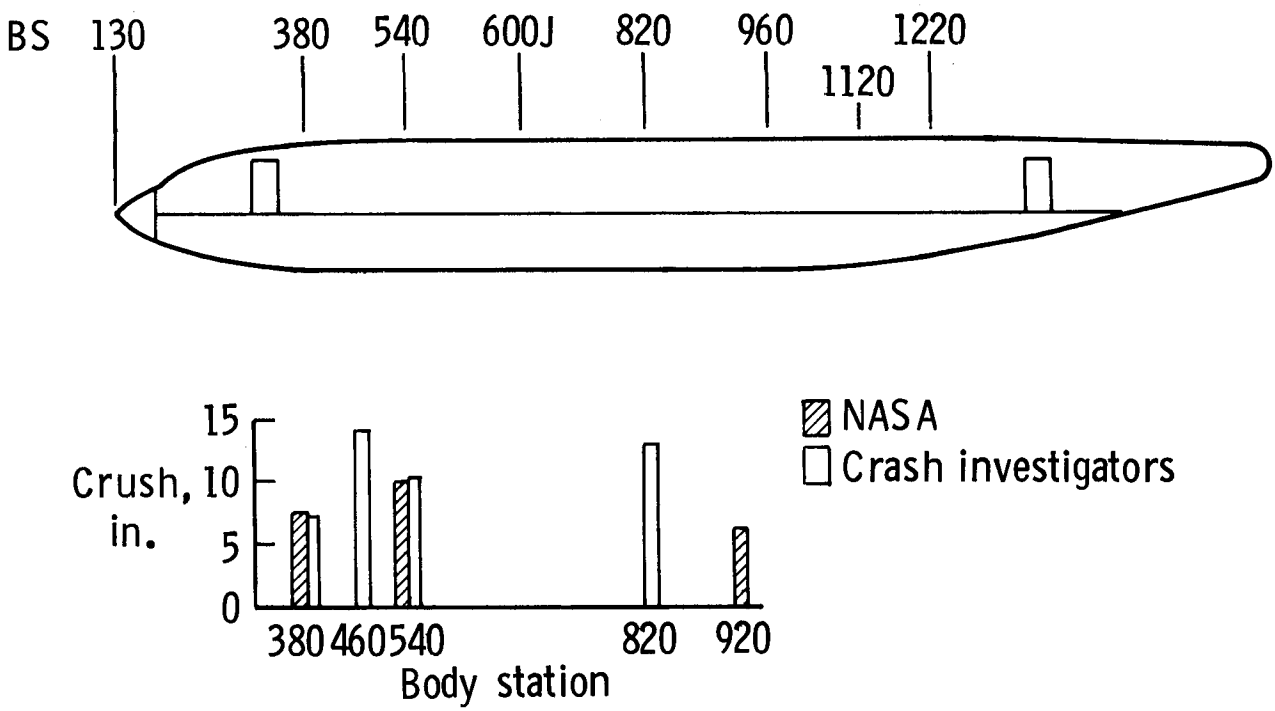

Figure 16. Fuselage crush.

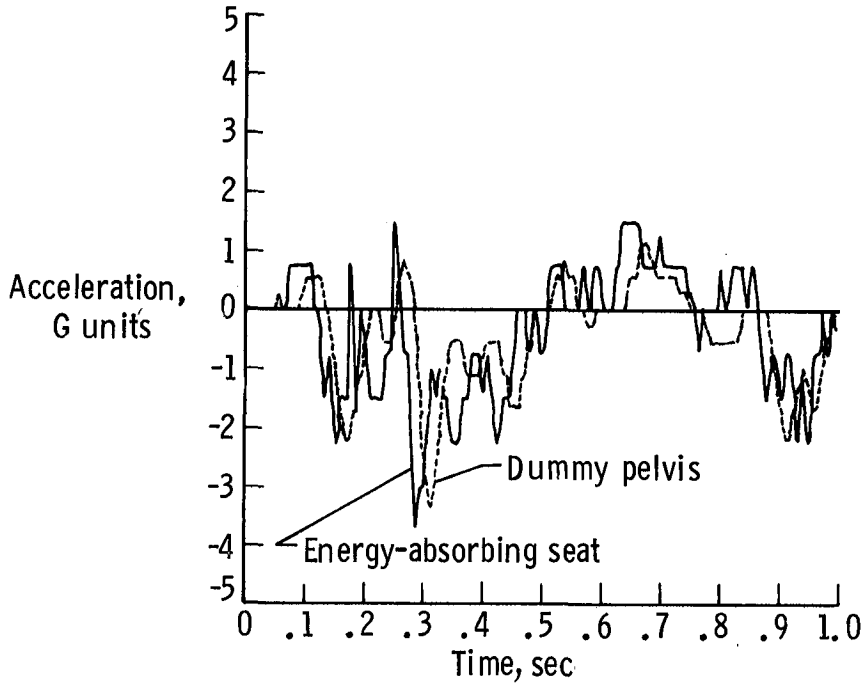

(a) NASA energy-absorbing seat.

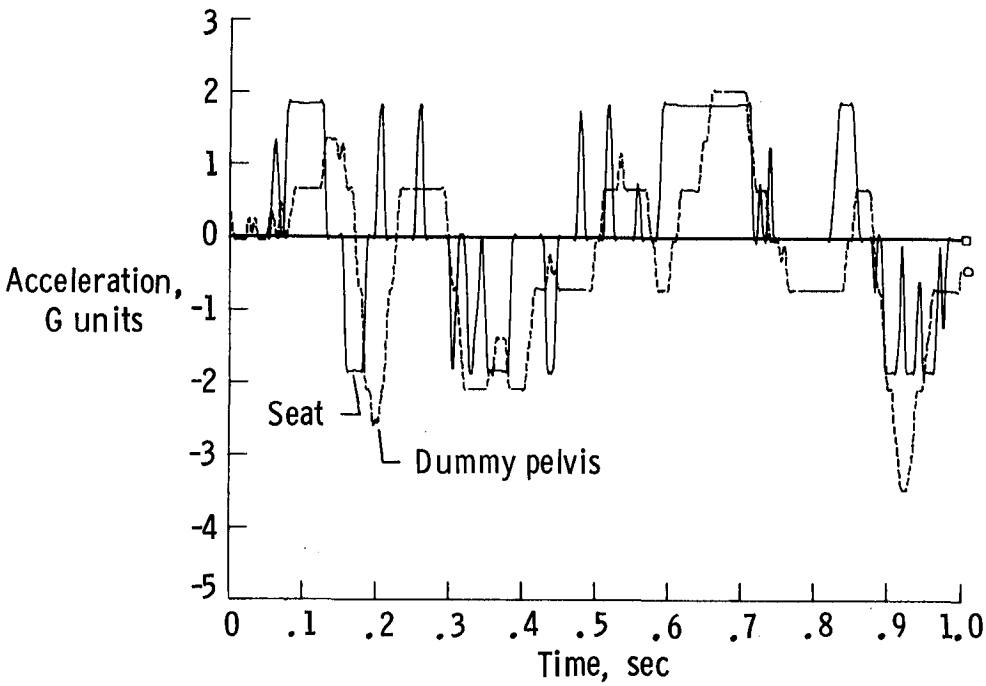

(b) Standard transport triple seat.

Figure 17. Seat and dummy normal accelerations during first second after impact.

Appendix A

Fuselage Accelerations, Loads, and Bending-Bridge Data

This appendix includes fuselage accelerations, loads measured in the links supporting an overhead storage bin experiment, and fuselage vertical bending moments for the first second after wing impact. For brevity a small number of data channels were omitted if redundant or if the traces contained obvious anomalies. Figure A1 shows the floor plan of the CID aircraft. In the longitudinal direction, the usual body station (BS) system was supplemented by an x-coordinate which was the distance in inches measured from the nose of the aircraft. The origin of the coordinate system was located at the aircraft nose ($x = 0$), centered laterally ($y = 0$) and with the floor level ($z = 0$). The positive X-axis was forward, positive Y-axis was out the right wing, and positive Z-axis was downward (fig. A2). The body stations were in inches; however, there were discontinuities depending on the particular model of airplane in each series. Table A1 gives the x-coordinate and the corresponding body station at typical fuselage locations.

Fuselage Acceleration Time Histories

The fuselage acceleration time histories are organized into three main groups: normal (Z-direction), longitudinal (X-direction), and transverse (Y-direction). The time histories within any main group have the same scale for the ordinate to make comparisons simple, and are ordered by body station starting with the nose of the aircraft and ending with the tail. The abscissa in each figure represents the time in seconds, with the origin taken to be the approximate time of left-wing impact with the ground (09:22:11 PST). Each time history spans 1 sec to cover the primary fuselage impact period. (The right-wing impact with the wing opener, which occurred approximately 1.8 sec after the left wing contacted the ground, is not covered in this report.) The label above each trace gives some or all of the following: the body station, a brief description of the structure on which the measurement was made, and the (x, y, z) coordinates of the transducer given in parentheses. The trace with the smallest body station (i.e., the smallest absolute value of x and thus closest to the nose) on a given page is at the bottom of the page, and the trace with largest body station (i.e., the largest absolute value of x and thus farthest from the nose) is at the top of the page. In all traces the accelerometer data were filtered after the test with a 100-Hz low-pass digital filter.

Fuselage Normal Acceleration Time Histories

Figures A3(a) to A3(i) show the normal (Z-direction) acceleration time histories for the first second after left-wing impact for 63 accelerometers located on fuselage structures. The accelerations in the interval from wing contact (0 sec) to about 0.46 sec were $5G$ or less and were due to crushing of the left wing. After wing contact, the aircraft, initially level, began to pitch forward. At 0.46 sec the forward fuselage impacted the ground near the nose wheel well rear bulkhead, just forward of BS 400. The highest floor accelerations are shown in figure A3(a) for locations on the left side near BS 400, with peak accelerations exceeding $15G$. The pilot floor at BS 228 showed a peak acceleration near $14G$ with a duration of nearly 0.08 sec. At BS 540 (see figs. A3(b) and A3(c)), the peak floor accelerations were less than $10G$, but with a longer duration (approaching 0.20 sec). Figure A3(c) shows a large peak acceleration ($30G$) of short duration for the accelerometer at the bottom of the frame at BS 540, which was the bottom accelerometer nearest the impact point. The accelerations continued to decrease rearward of BS 540 and the floor accelerations were typically $5G$ or below back to the tail. From 0.65 until 0.85 sec after initial impact, the accelerations were very low and oscillated about zero for most locations. At approximately 0.85 sec, the rear main landing gear bulkhead at BS 960 made ground contact (fig. A3(e)) and a small acceleration pulse was noticed for the rear fuselage locations from 0.85 until 1.00 sec. The output from the transducer at the bottom of the frame at BS 960 was not included because the accelerometer overloaded, producing a trace with a peak of over $90G$ and an erroneous pulse duration of 0.25 sec. For comparison, in vertical drop tests conducted at Langley (ref. 13) of a Boeing 707 center section (13 ft long, from BS 820 to 960) with impact velocity of 20 ft/sec, normal accelerations on this "rigid" lower bulkhead exceeded $70G$ with only 0.02 to 0.03 sec duration.

Fuselage Longitudinal Acceleration Time Histories

Figures A4(a) to A4(h) show the longitudinal (X-direction) acceleration time histories for the first second after left-wing impact for 55 accelerometers located on fuselage structures. The accelerations in the interval from wing contact (0 sec) to about 0.46 sec were all very low (below $2G$ at floor level in most locations) and were due to left-wing drag forces. At 0.46 sec the forward fuselage impacted the ground. The acceleration increase that occurred when the forward fuselage impacted is shown in the traces in figures A4(a) and A4(b) and is most apparent for the

trace labeled "BS 540 Bottom $(-410, 0, 61)$" in figure A4(b). This accelerometer, located on the bottom of the frame at BS 540, showed a very large spike ($50G$) near 0.50 sec. This acceleration was very localized, was of short duration, and was not transmitted into the surrounding structure, as can be seen by analyzing the other traces for BS 540 in figures A4(b) and A4(c). The longitudinal accelerations measured on the floor were all low, with peak values below $10G$ and with average accelerations over time in the $2G$ to $3G$ range. The trace for the bottom of the fuselage frame at BS 960 (the main landing gear bulkhead) in figure A4(e) is included to indicate rear-fuselage impact. However, this accelerometer was mounted on the very stiff center section designed to carry main landing gear loads. The velocity change obtained from integrating this acceleration was quite large, indicating that the transducer output was probably overloaded and not a valid output.

Fuselage Transverse Acceleration Time Histories

Figures A5(a) to A5(d) contain 29 acceleration time histories for the transverse (Y) direction. The initial acceleration pulse from 0.05 to 0.20 sec was due to the left-wing contact. For many locations, this pulse was the most significant when both duration and magnitude are considered. Since the airplane was yawed at impact, the transverse accelerations were larger than anticipated. However, the peak transverse acceleration was no more than $5G$ for many locations. The largest peak measured ($30G$) was at 0.86 sec (fig. A5(b)) for the bottom of the frame at BS 820. This is the location of the main landing gear wheel well forward bulkhead, a very rigid structural bulkhead.

Loads in Overhead-Bin Support Links

Figure A6 shows the load in pounds for two of three supporting links for the overhead-storage-bin experiment located at BS 540. Unfortunately, the strain gage on the third link was not operative. The loads were initially zeroed and the values shown are above and below the static value. As shown in figure A6, the load is oscillatory but does not exceed 100 lbf for the first second after wing impact. In addition to the links, a triaxial accelerometer was located on a fixed mass attached to the storage bin. Accelerations are shown in figures A3(b), A4(b), and A5(a).

Fuselage Vertical Bending-Bridge Data

Figure A7 shows the moment time histories of the eight bending bridges located on the fuselage at BS 410 to BS 1250. The bridges were located at critical areas such as production breaks, geometric transitional areas, and areas where maximum bending moments were expected. Each bending bridge was made with temperature-compensated strain gages in a four-arm bridge configuration. To measure the fuselage bending, two of the strain gages were bonded to the crown of the fuselage and two were bonded either in the vicinity of the floor or close to the bottom of the fuselage at six locations.

In the data reduction process, an initial static reading (prefire) was taken for each bending bridge shortly before CID take-off. This value was subtracted to give each bending moment a zero initial value with the aircraft sitting on the ground. Consequently, all bending-moment traces shown in this appendix are incremental moments above or below the static moment that existed with the fully loaded airplane on the ground prior to take-off.

The highest vertical bending moments were recorded at BS 1030, a slightly lower value at BS 600J-10 (i.e., 10 in. in front of BS 600J), and the smallest value at BS 410 near the nose. There is similarity in the shape of all traces (except for that from BS 410, which lost the signal after about 0.58 sec); this similarity indicates the validity of the bending-bridge data.

TABLE A1. RELATIONSHIP OF x-COORDINATE TO BODY STATION

x-coordinate, in.	Body station, in.	Location
0	130	Nose
−270	400	Frame 1
−410	540	Frame 2
−490	600G	
−510	600H	
−530	600J	Frame 3
−550	620	
−750	820	Frame 4 front bulkhead main landing gear
−890	960	Frame 5 rear bulkhead main landing gear
−1010	1120	Frame 6
−1110	1220	Frame 7
−1270	1380	Rear cabin attendant seat

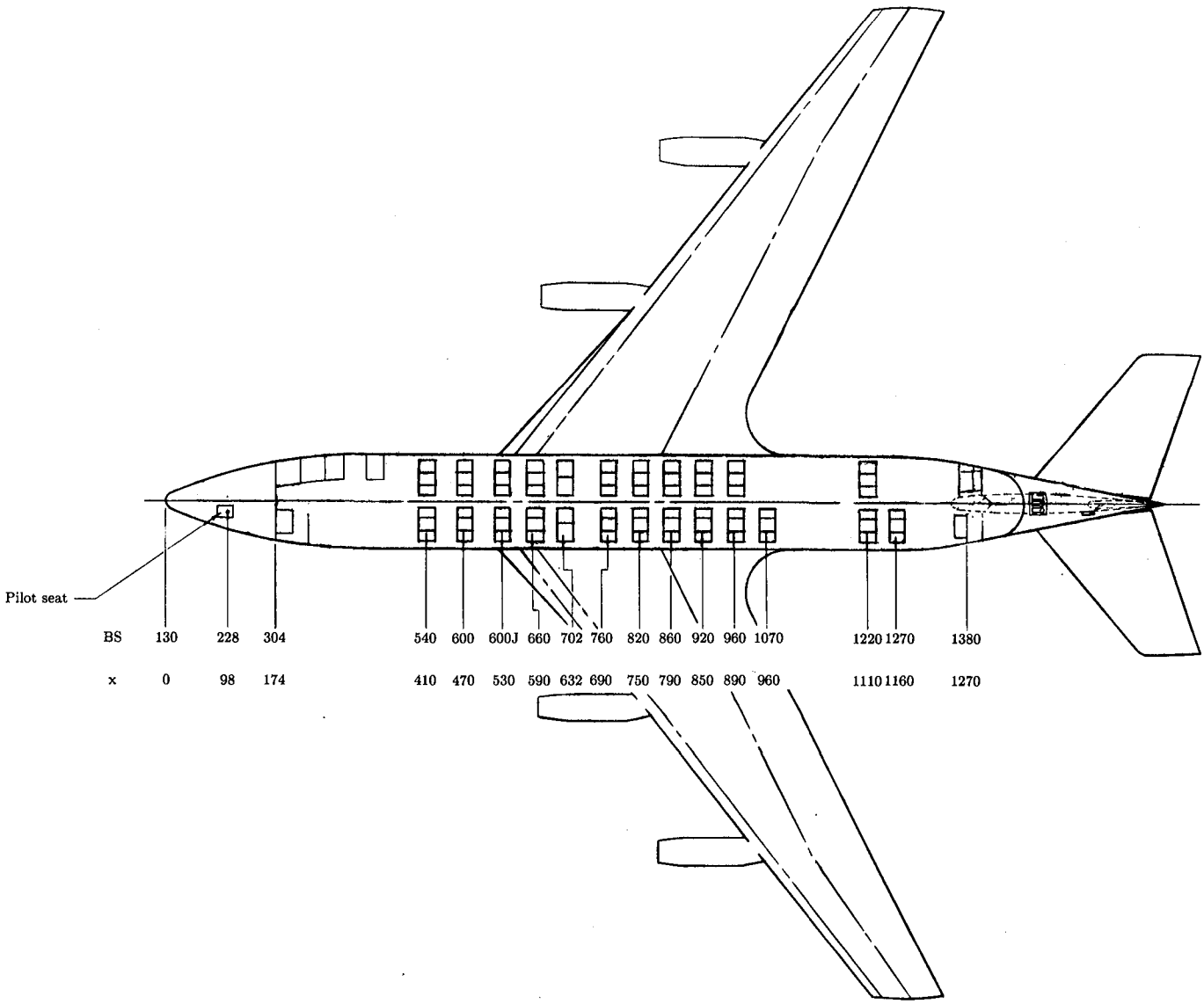

Figure A1. CID floor plan with x-coordinates and body stations (BS).

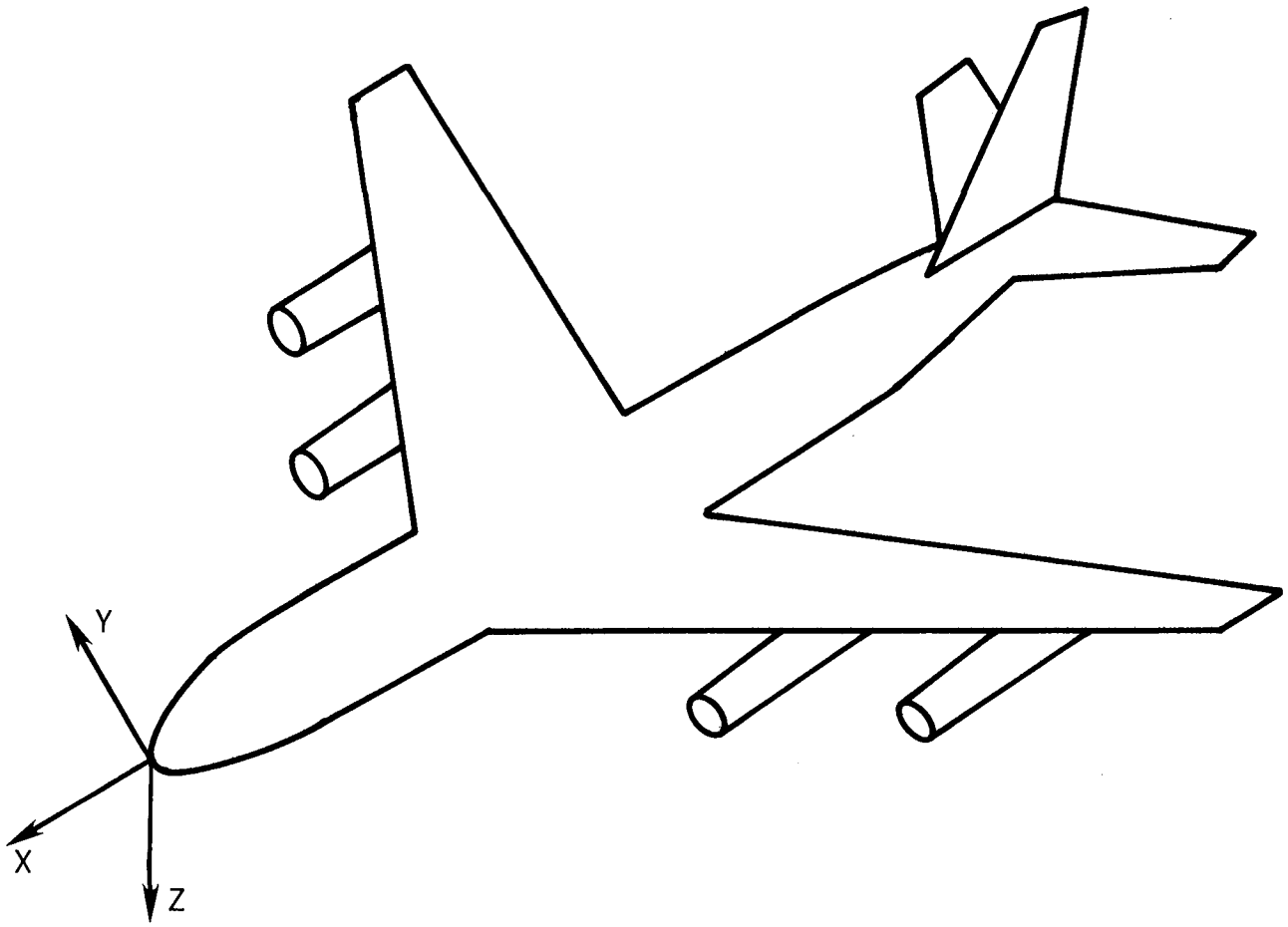

Figure A2. Origin and directions of coordinate axis system.

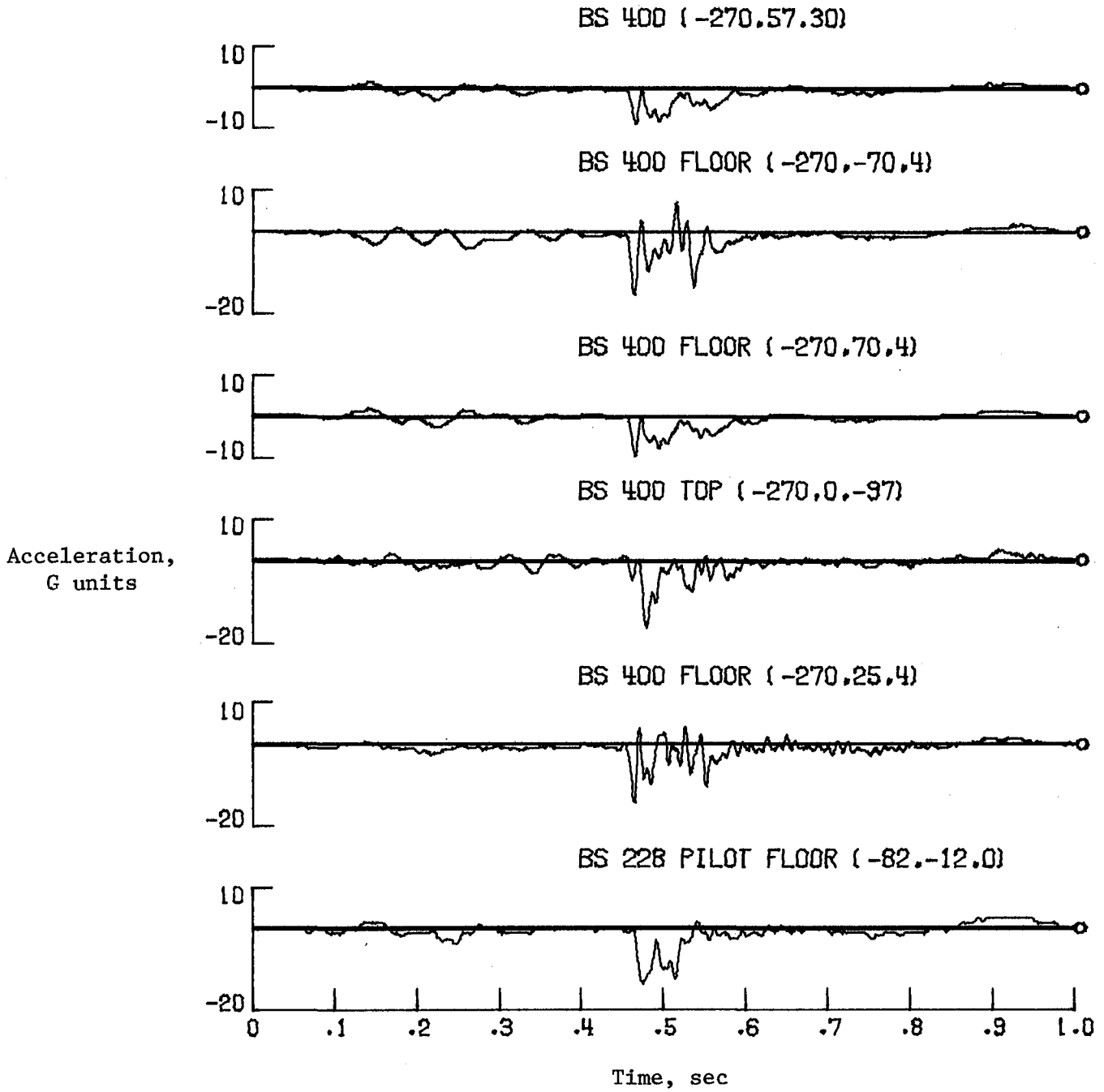

(a) BS 228 to 400.

Figure A3. Fuselage normal acceleration time histories.

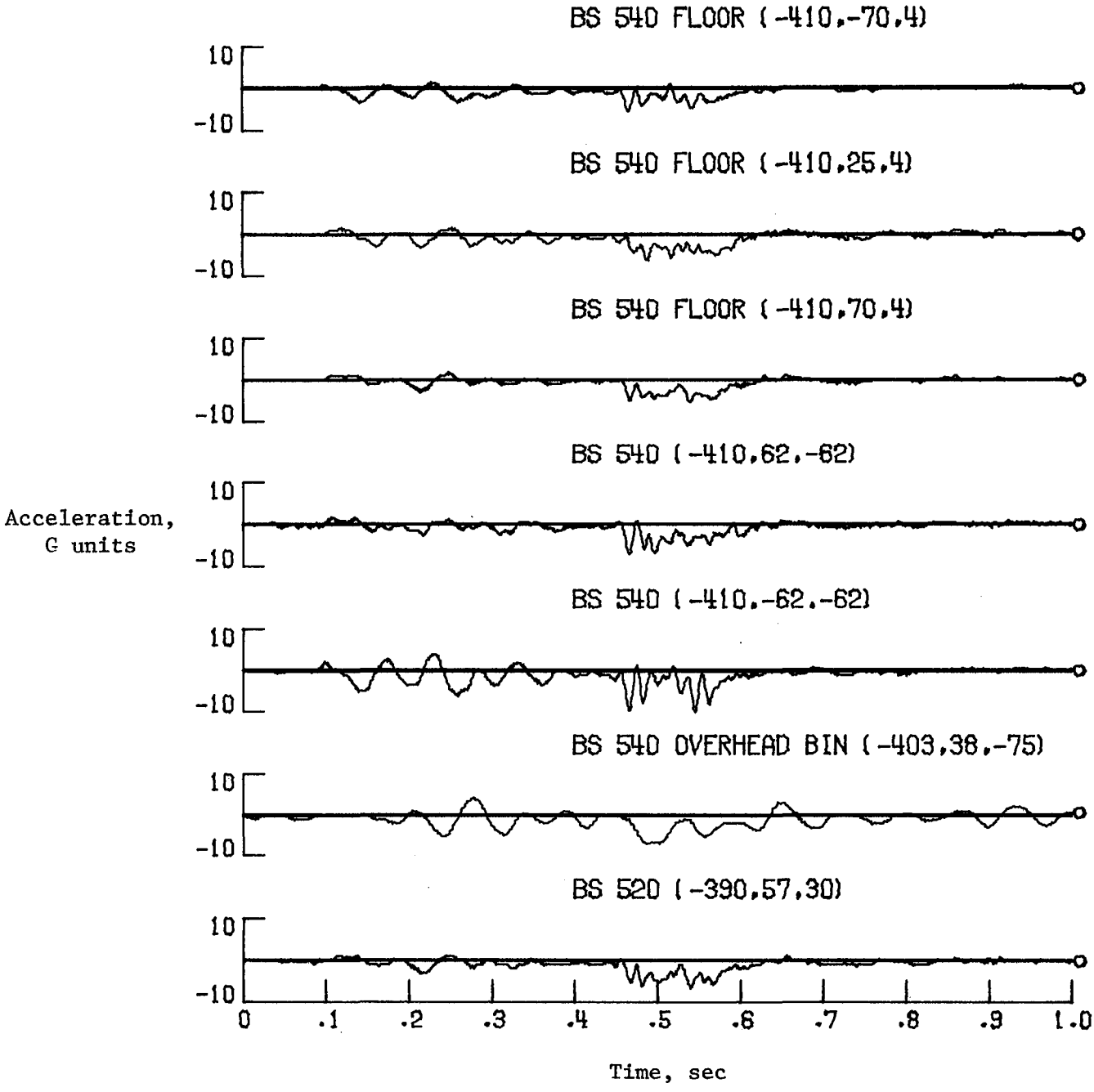

(b) BS 520 to 540.

Figure A3. Continued.

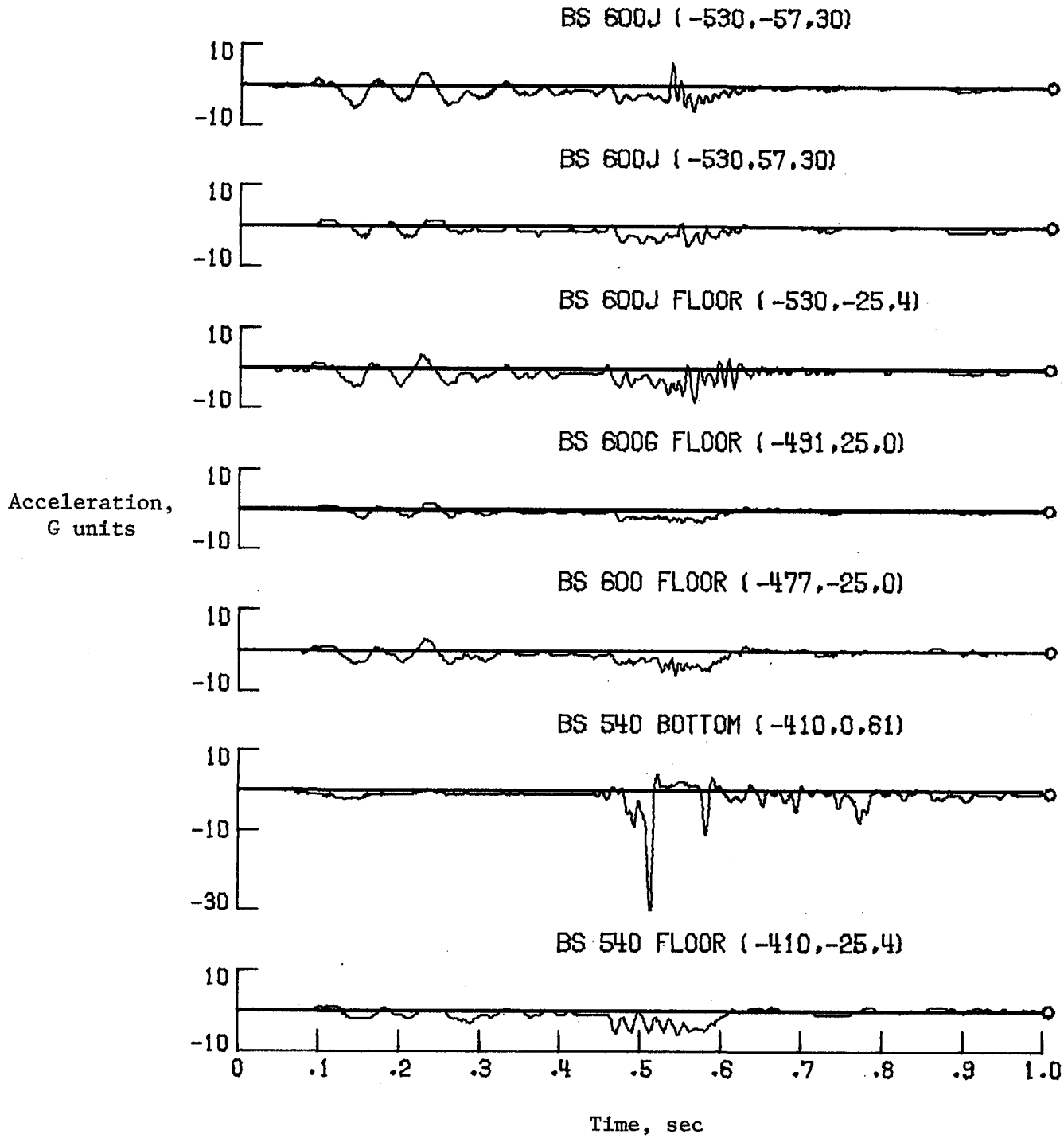

(c) BS 540 to 600J.

Figure A3. Continued.

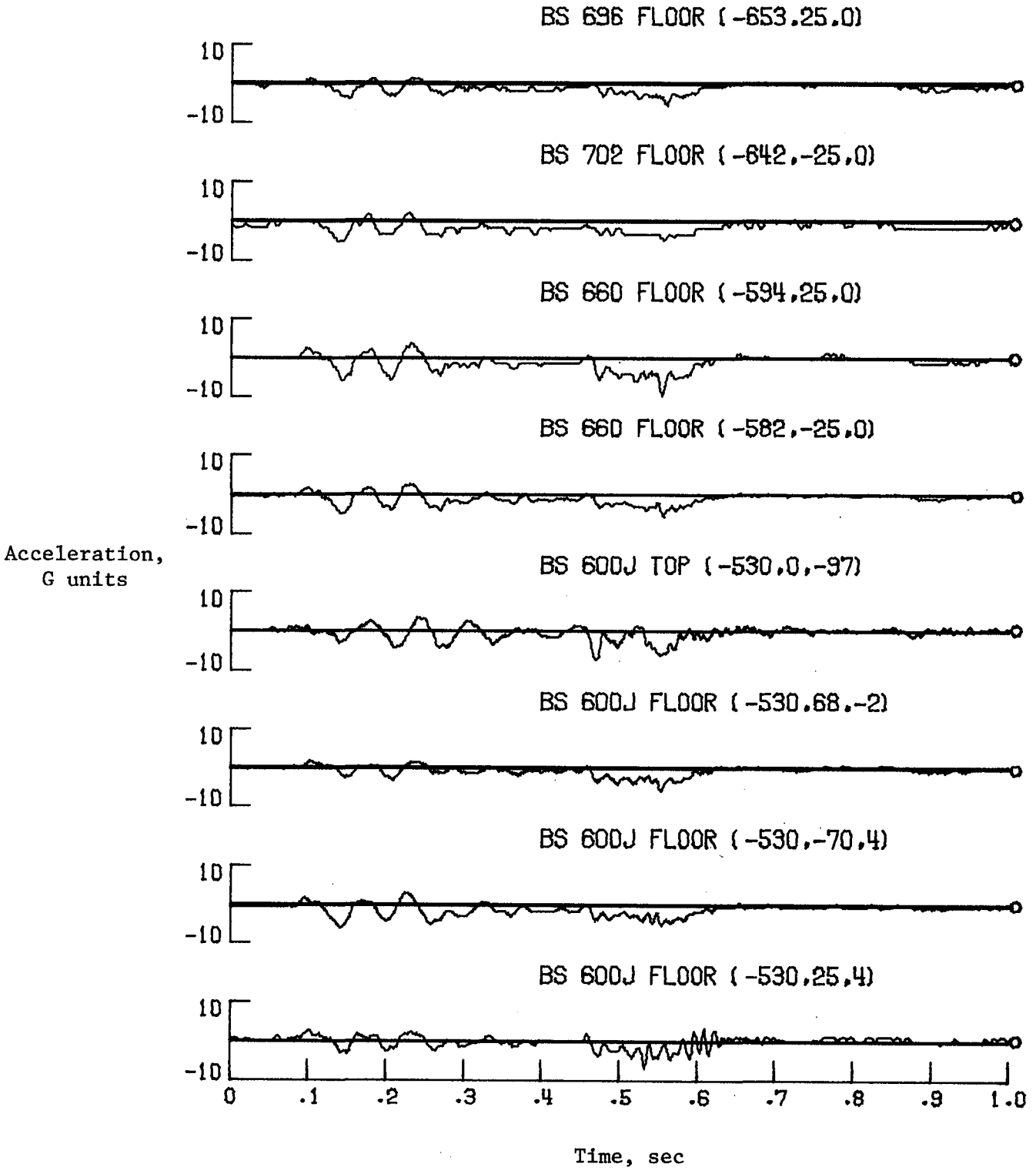

(d) BS 600J to 696.

Figure A3. Continued.

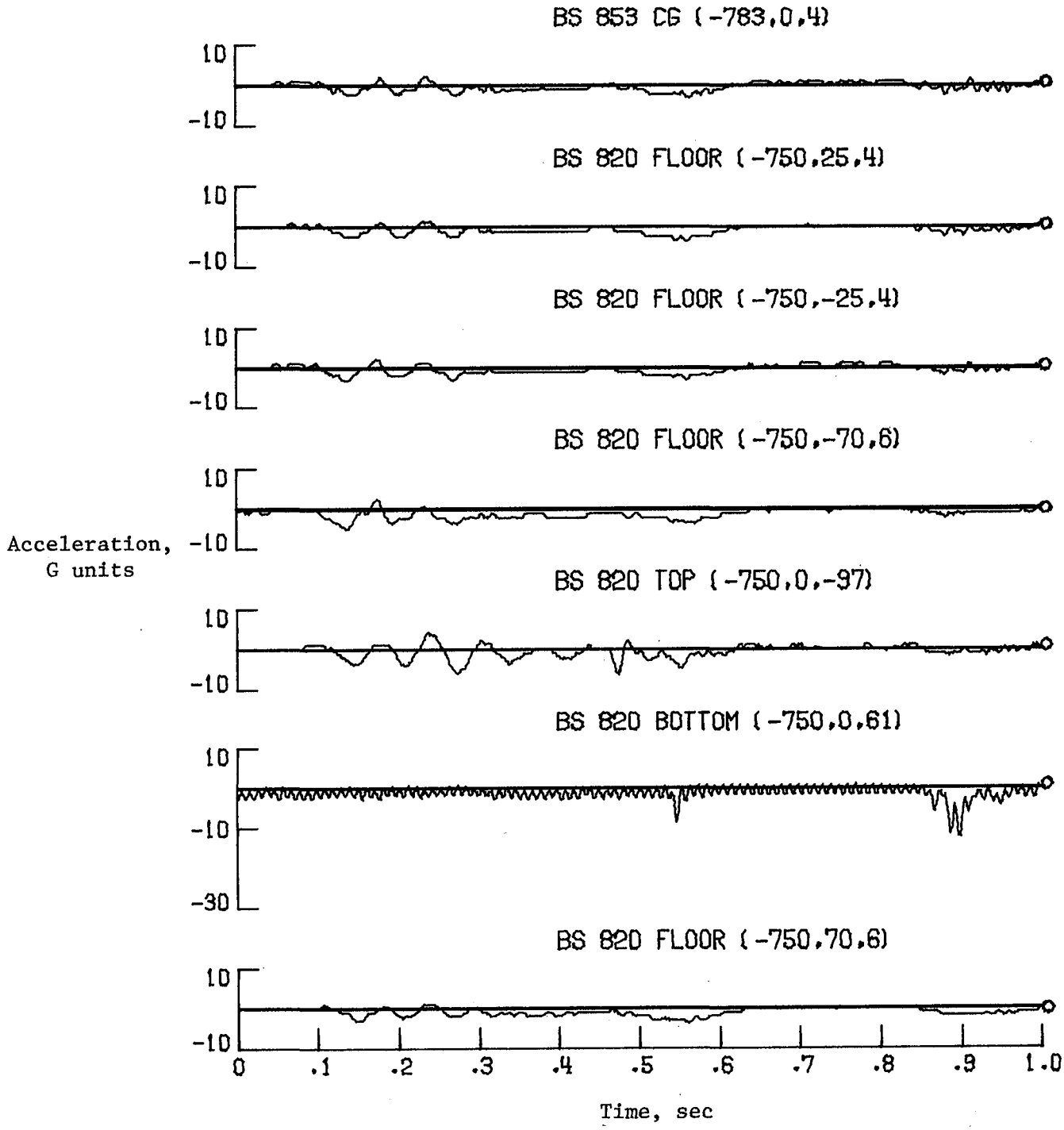

(e) BS 820 to 853.

Figure A3. Continued.

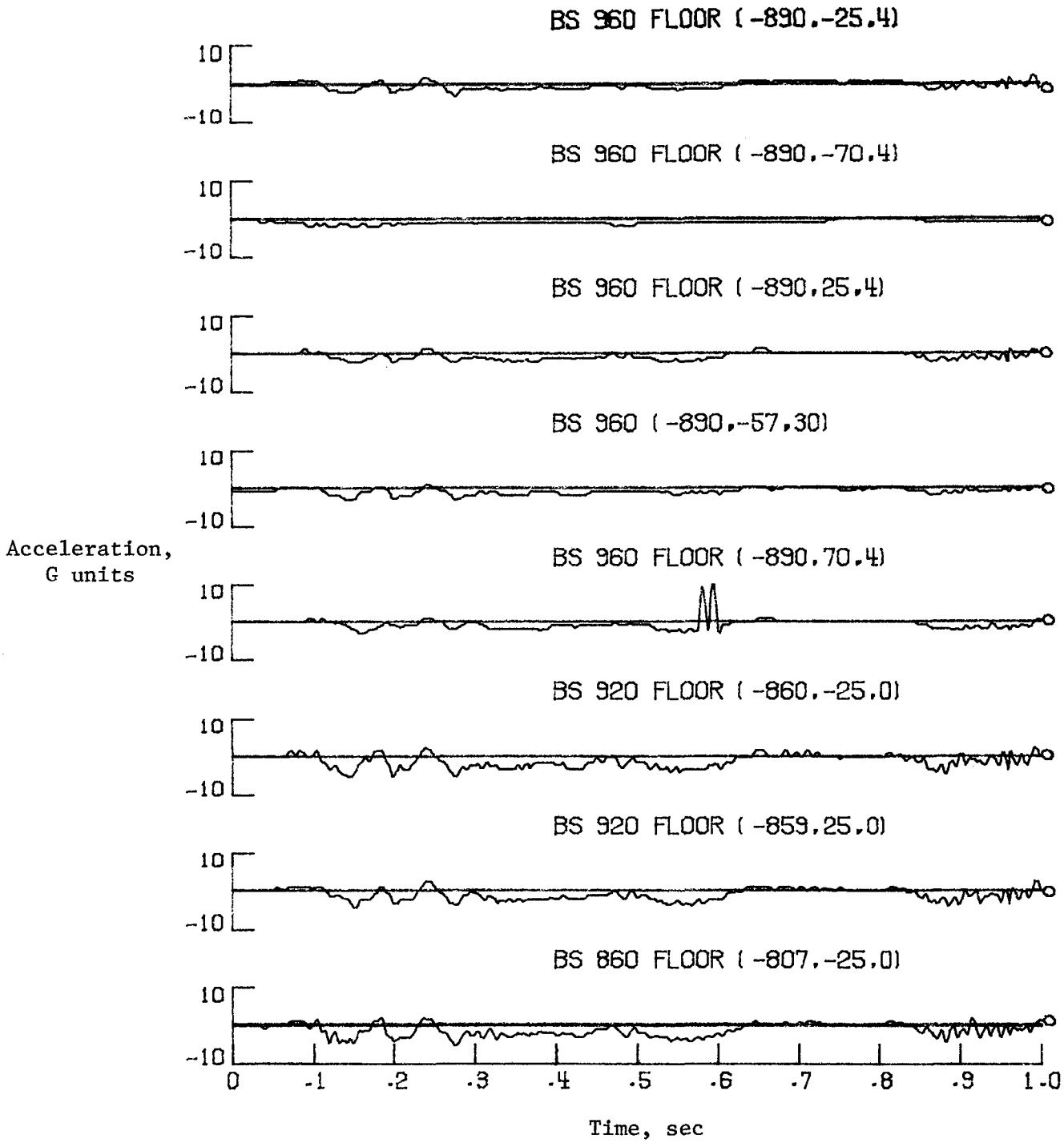

(f) BS 860 to 960.

Figure A3. Continued.

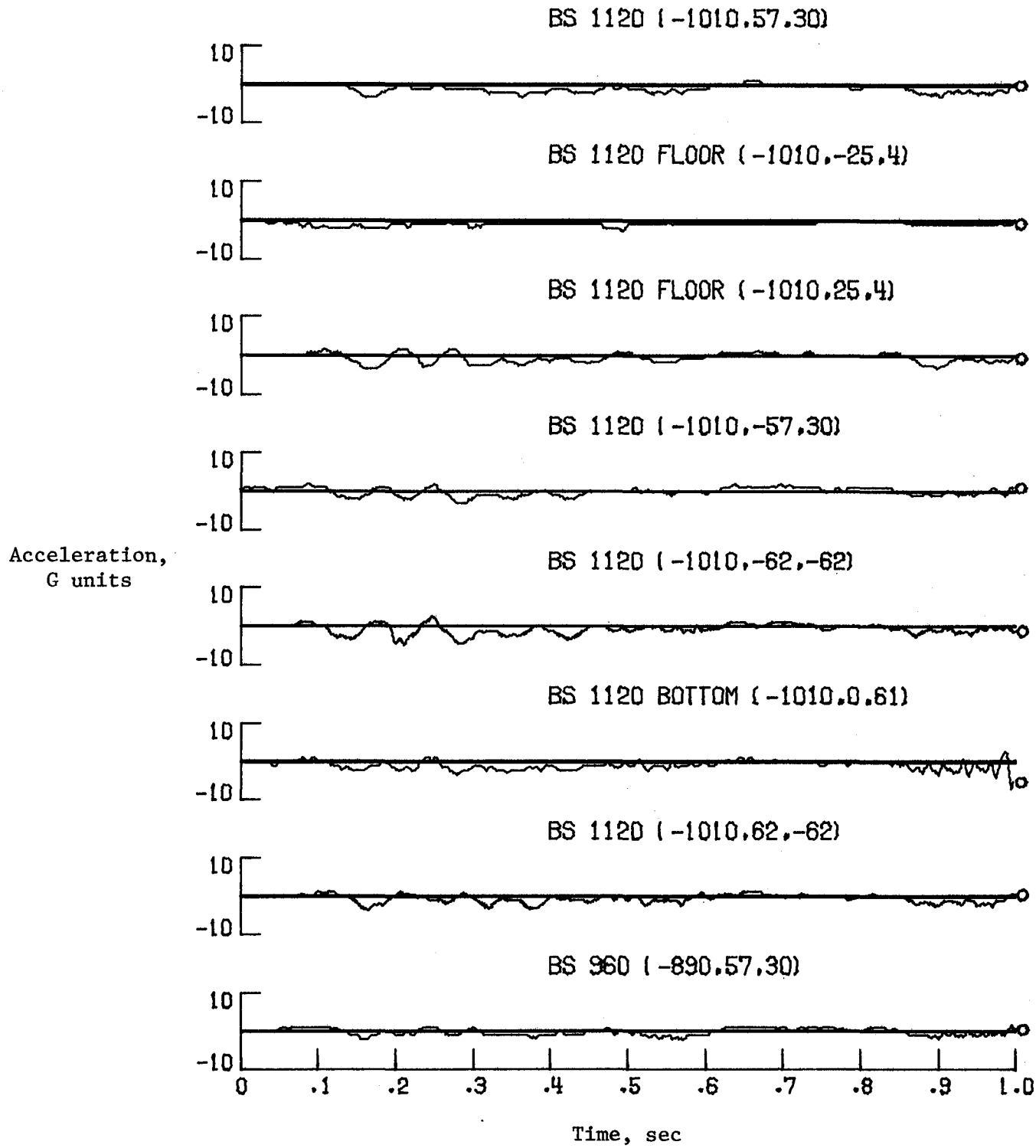

(g) BS 960 to 1120.

Figure A3. Continued.

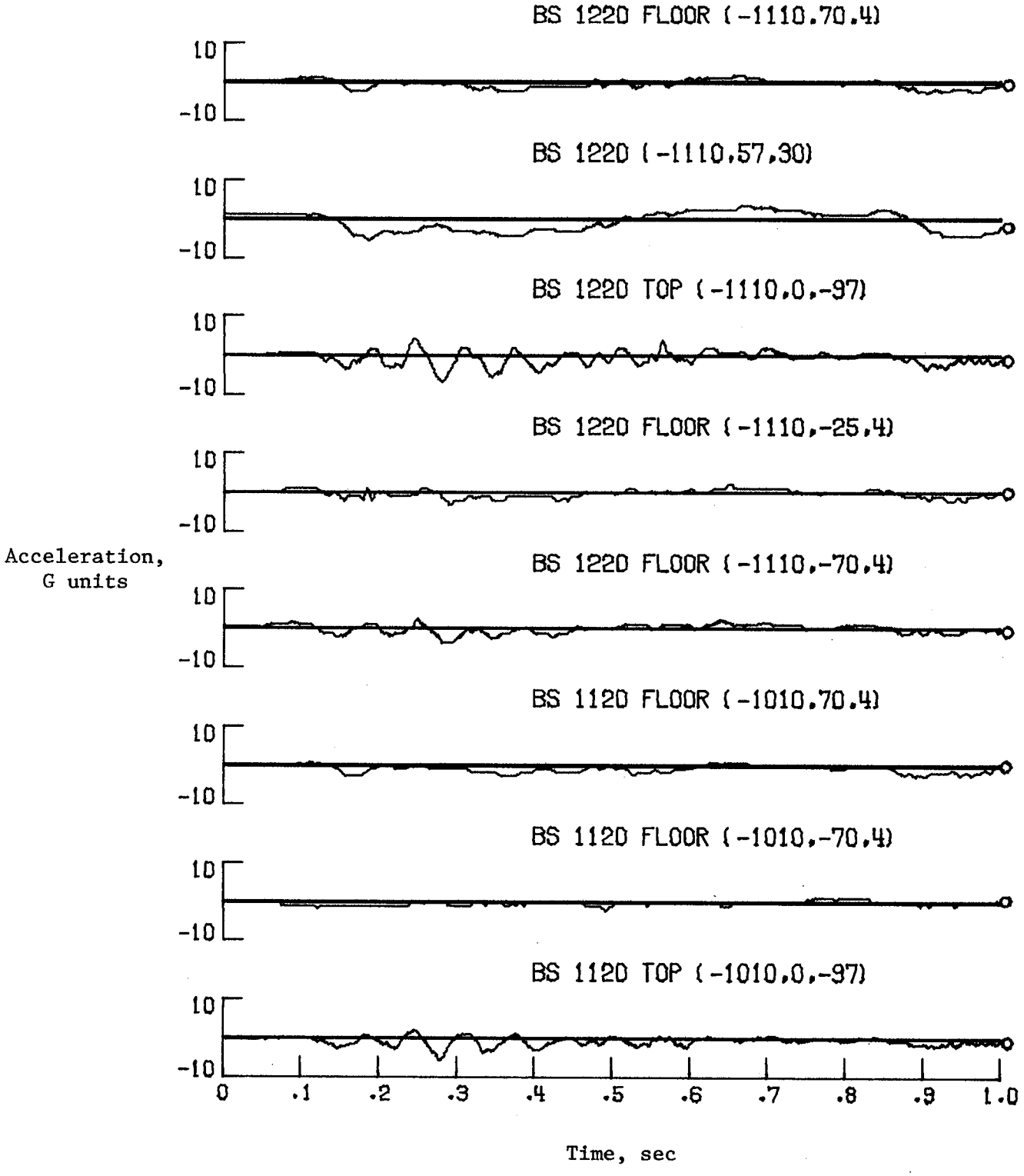

(h) BS 1120 to 1220.

Figure A3. Continued.

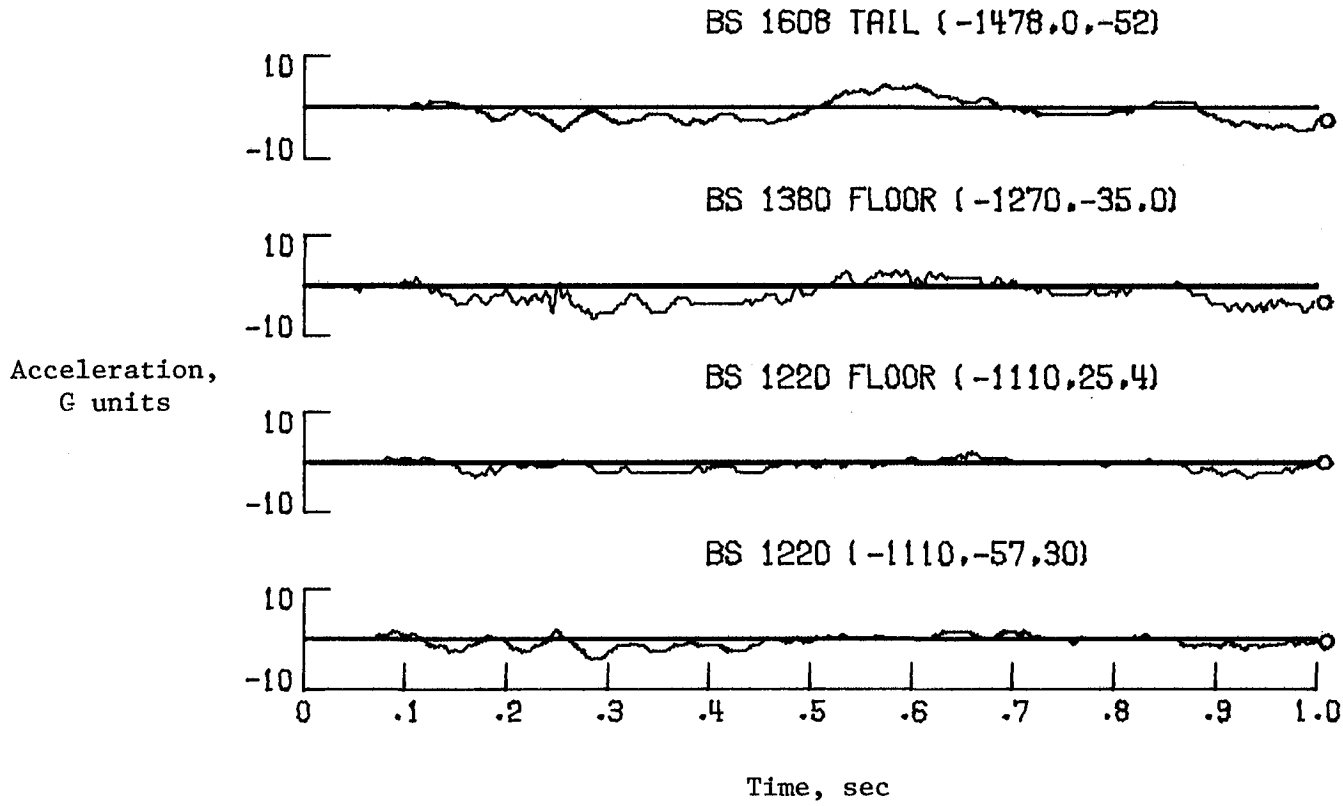

(i) BS 1220 to 1608.

Figure A3. Concluded.

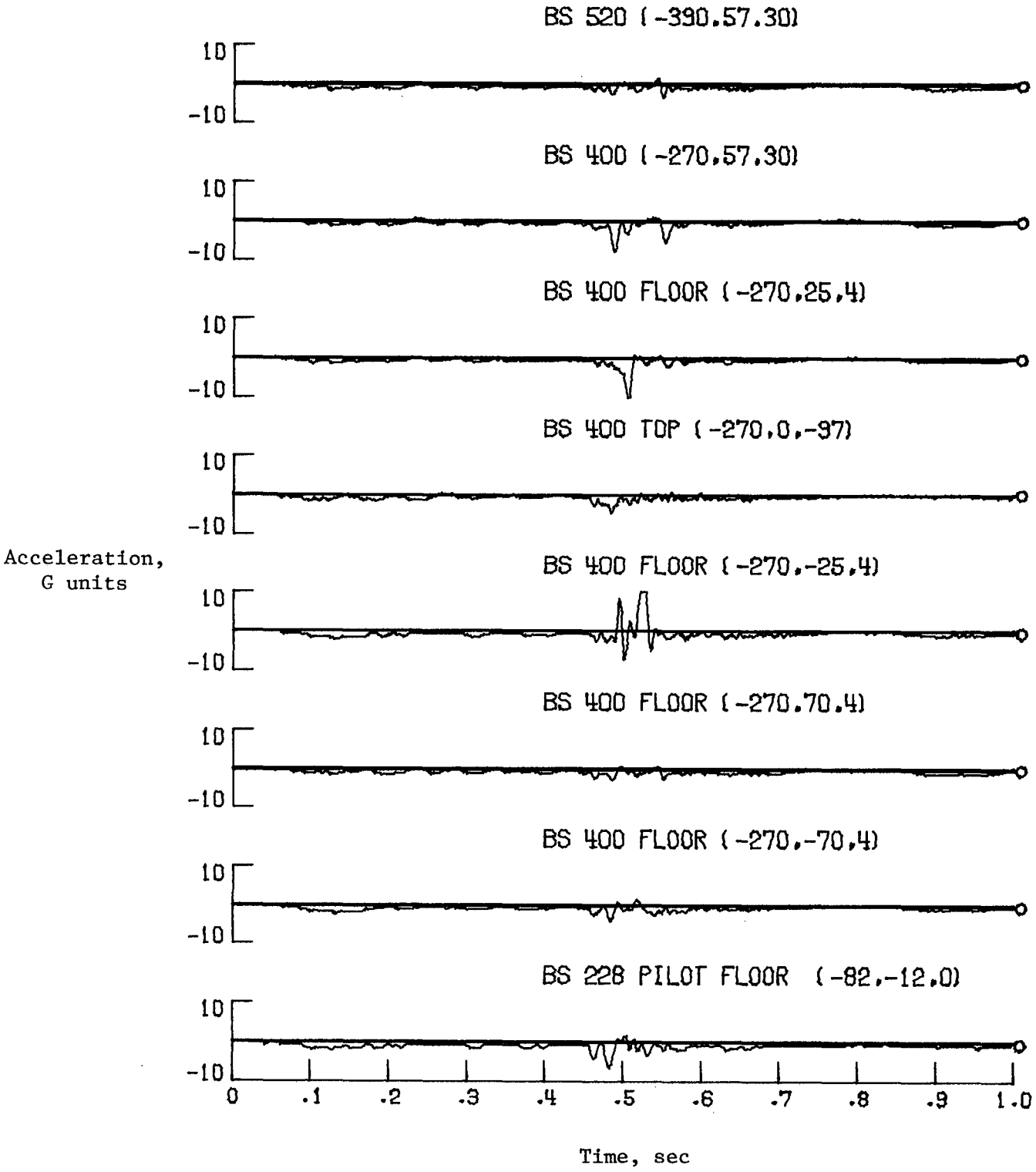

(a) BS 228 to 520.

Figure A4. Fuselage longitudinal acceleration time histories.

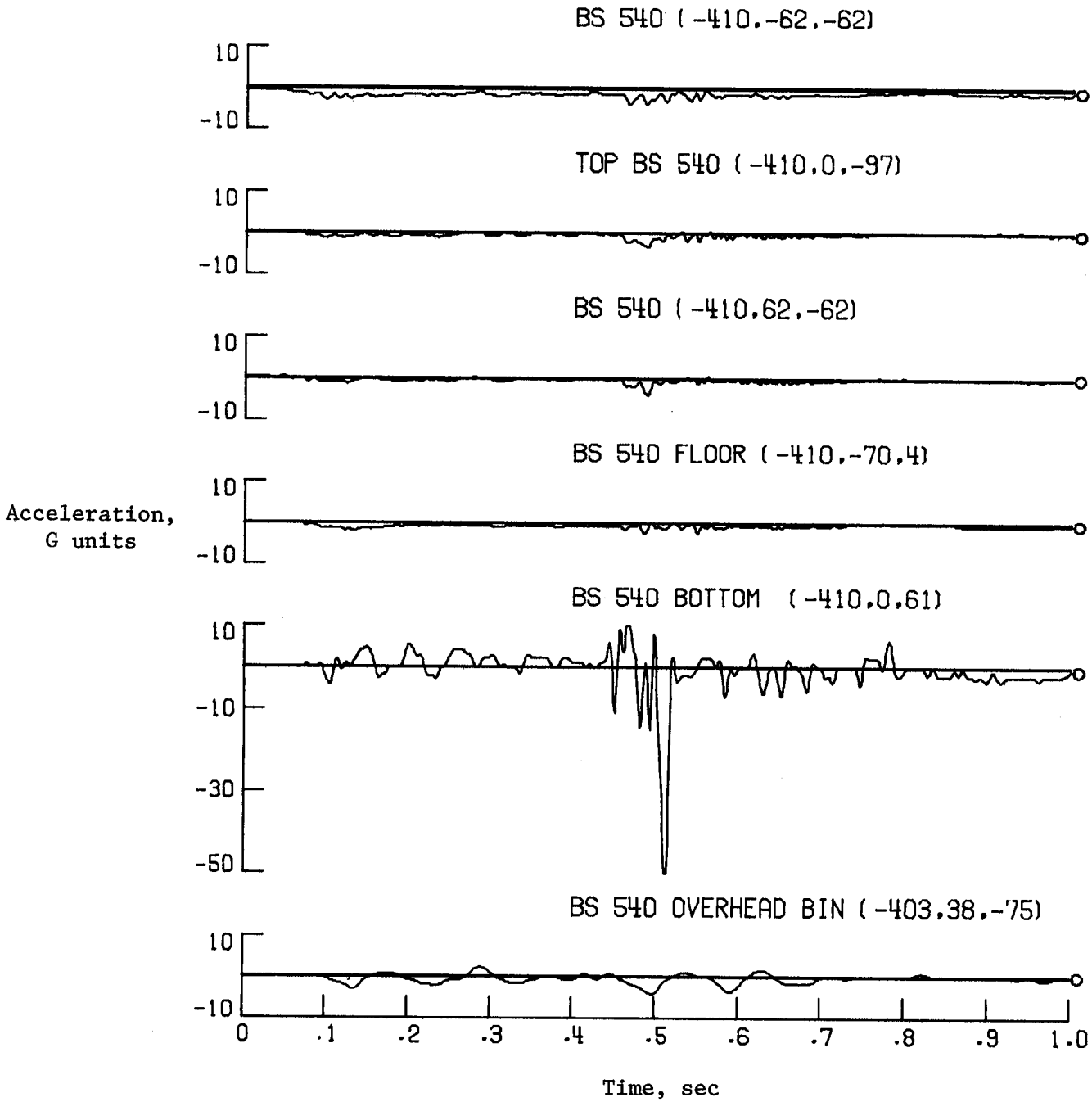

(b) BS 540.

Figure A4. Continued.

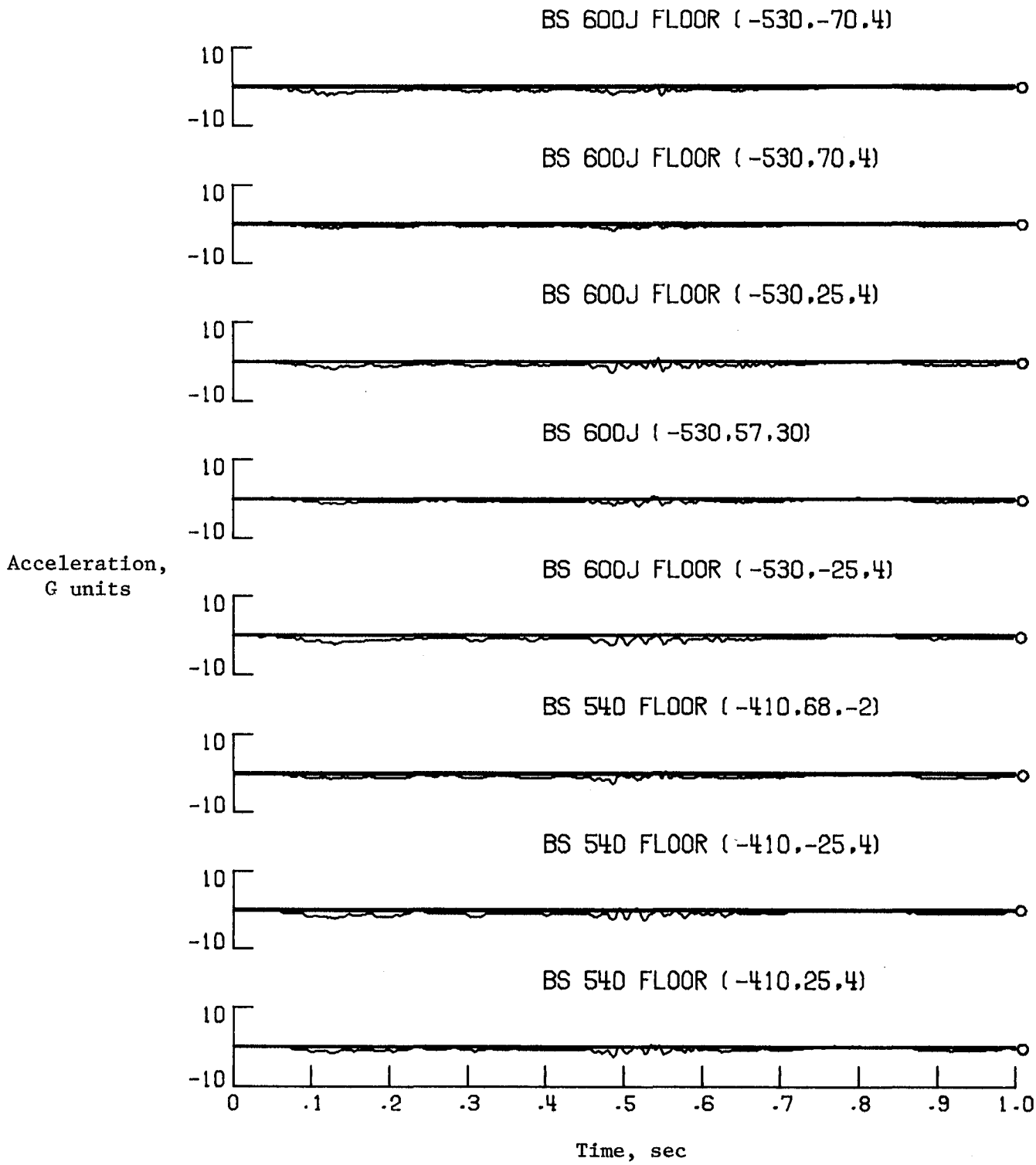

(c) BS 540 to 600J.

Figure A4. Continued.

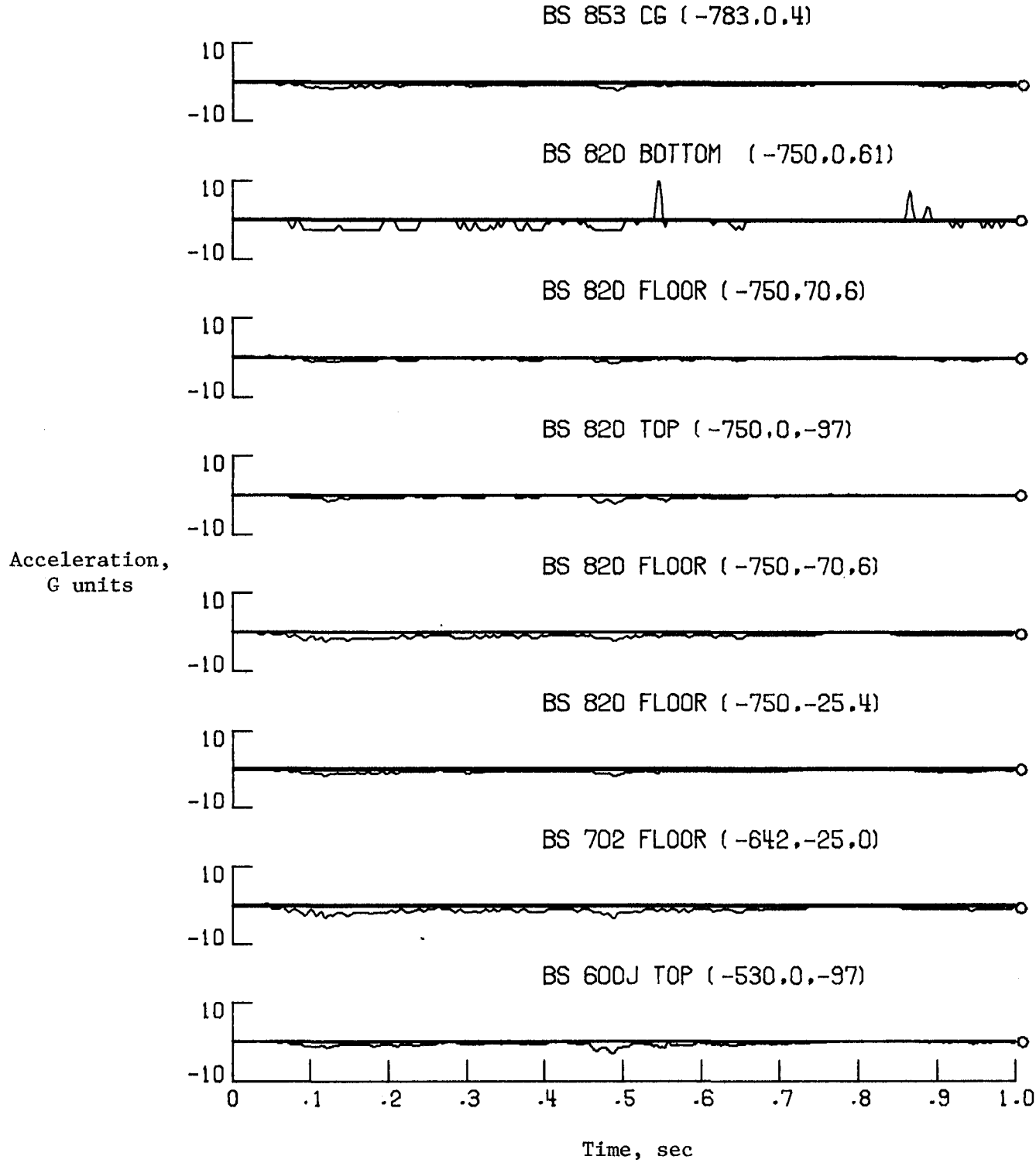

(d) BS 600J to 853.

Figure A4. Continued.

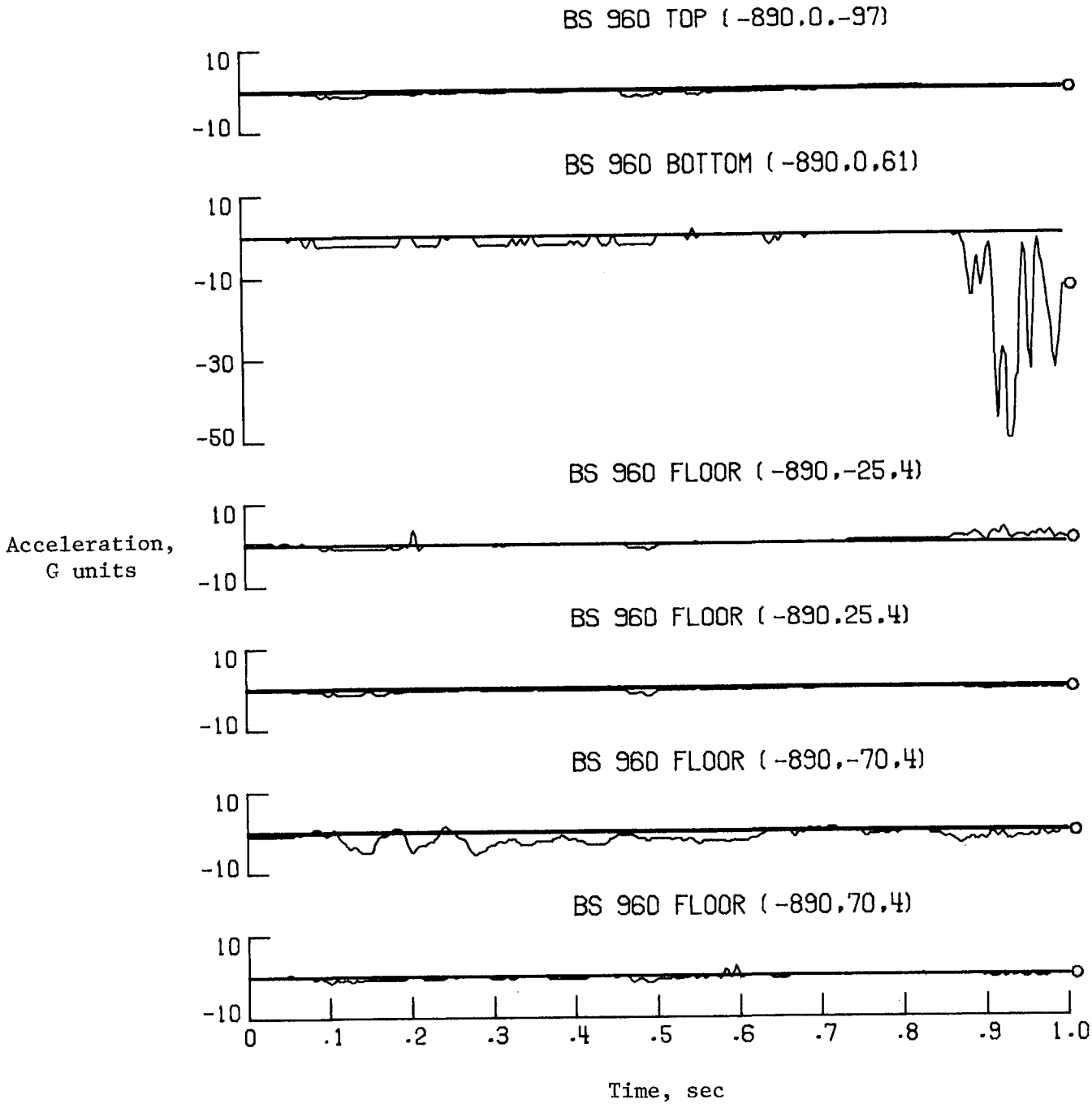

(e) BS 960.

Figure A4. Continued.

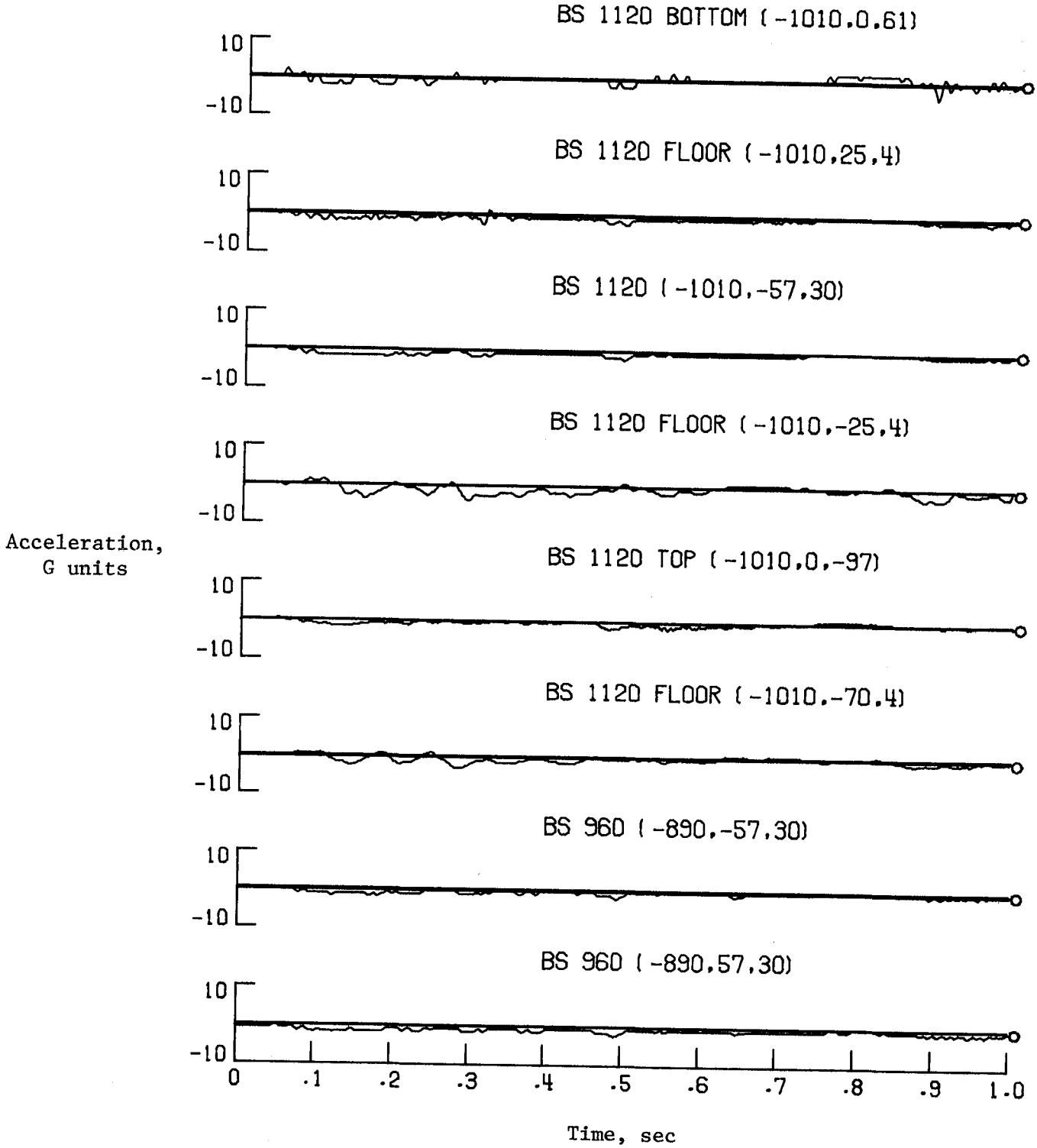

(f) BS 960 to 1120.

Figure A4. Continued.

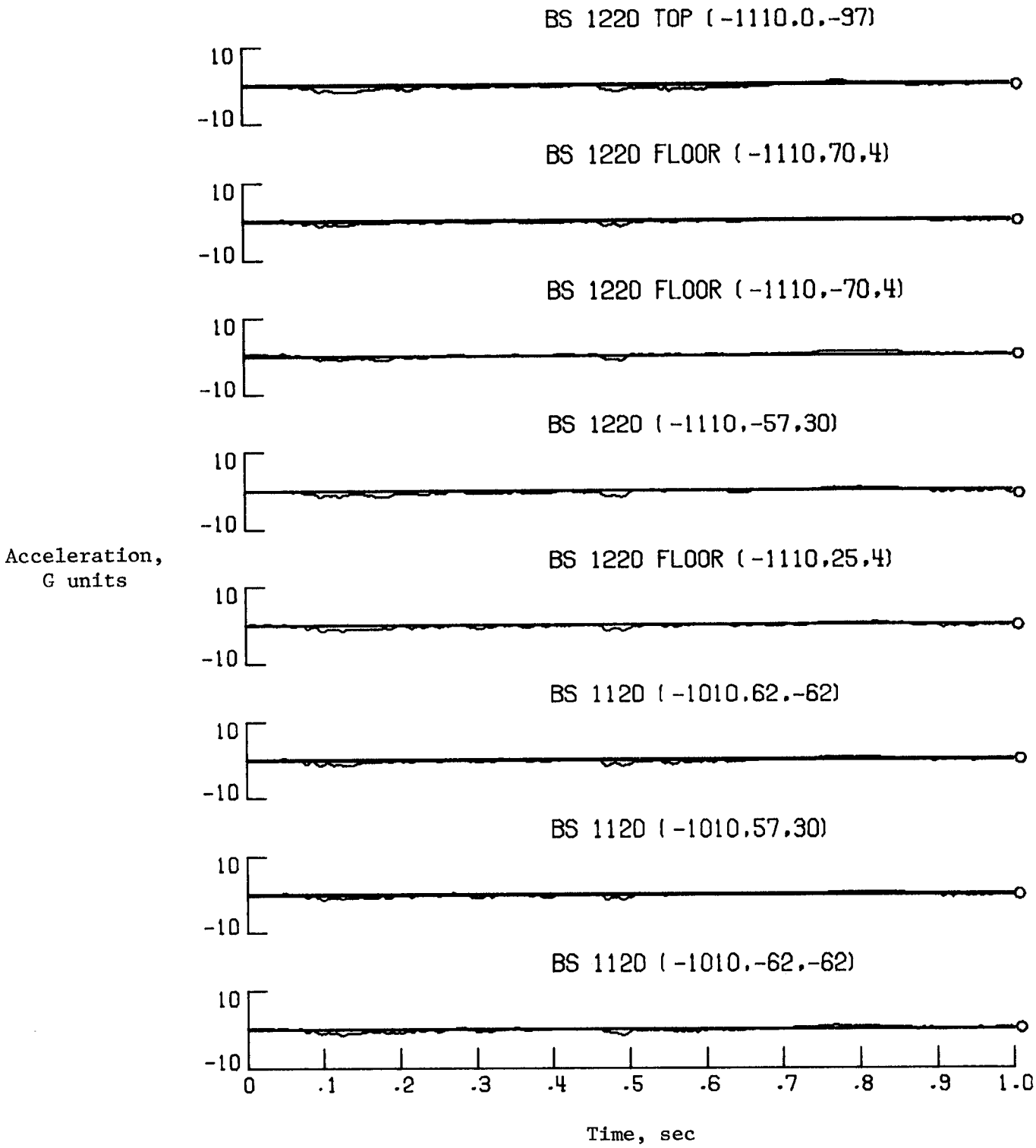

(g) BS 1120 to 1220.

Figure A4. Continued.

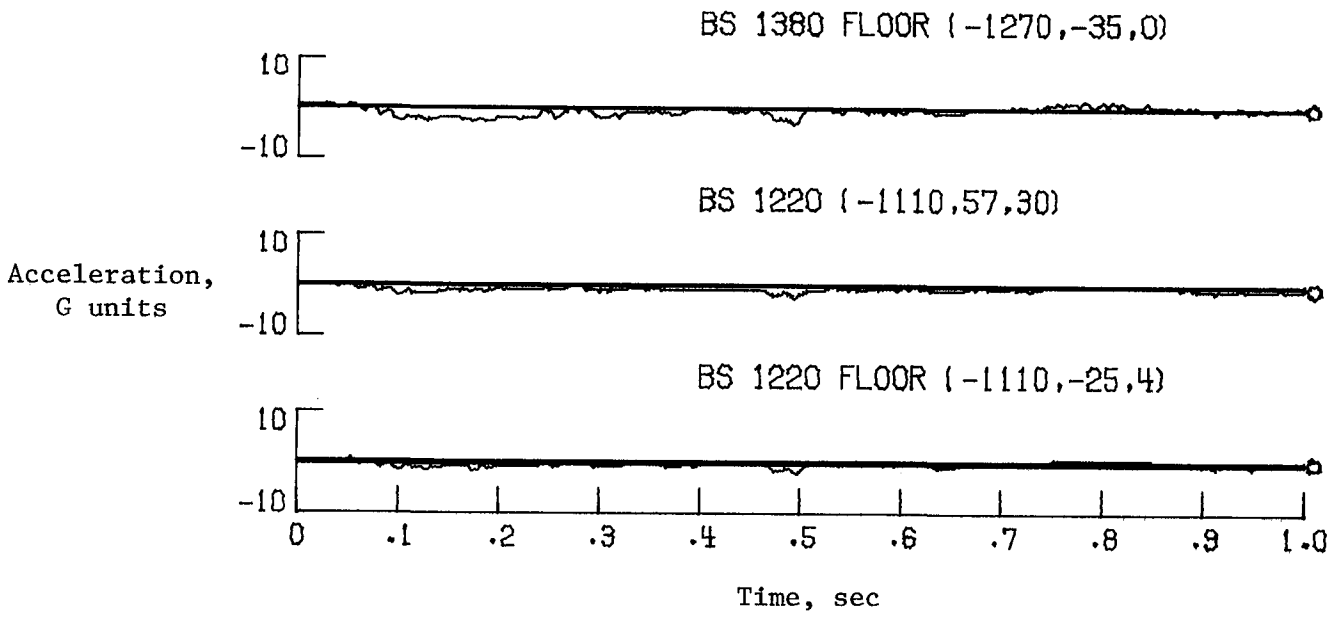

(h) BS 1220 to 1380.

Figure A4. Concluded.

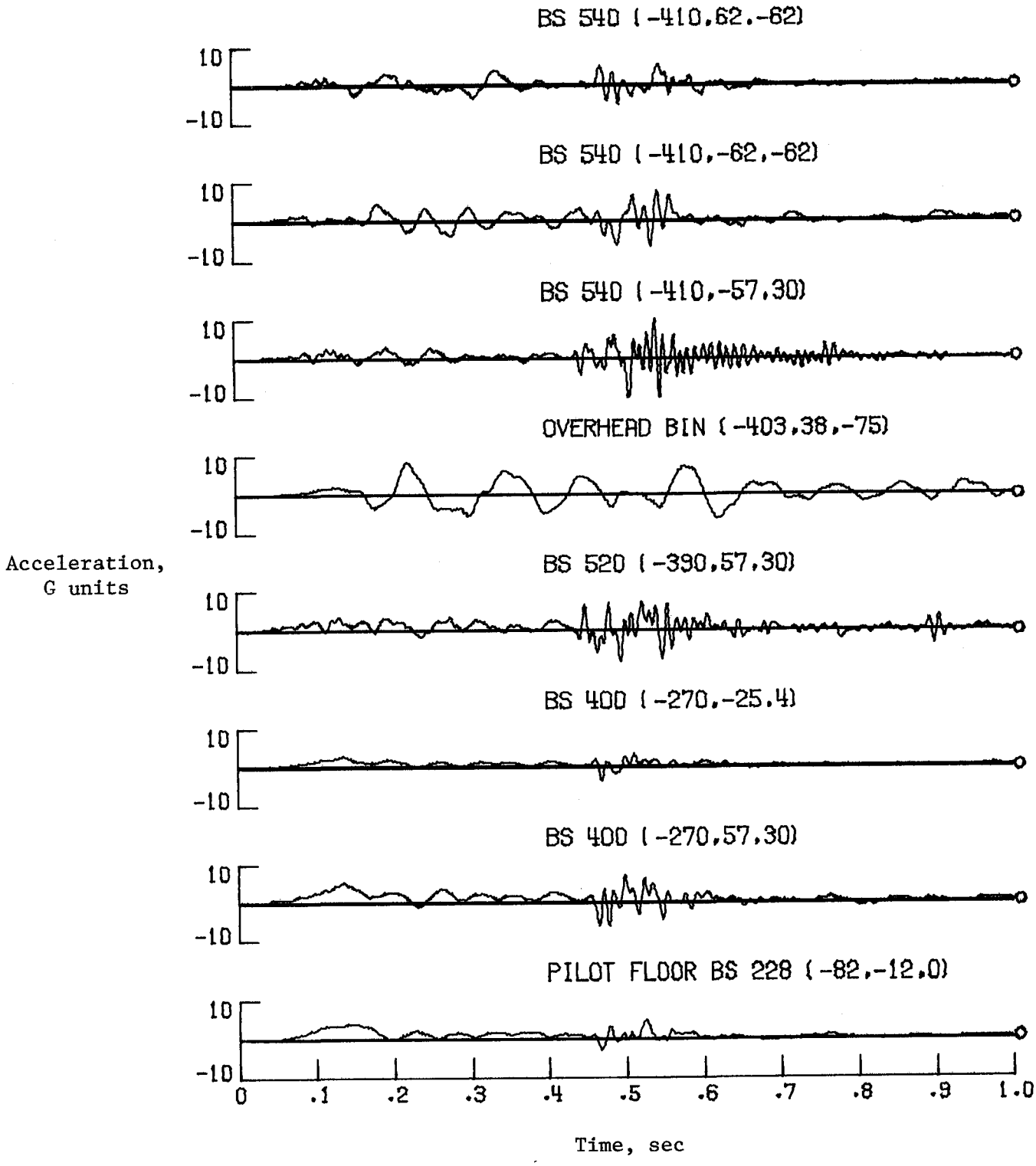

(a) BS 228 to 540.

Figure A5. Fuselage transverse acceleration time histories.

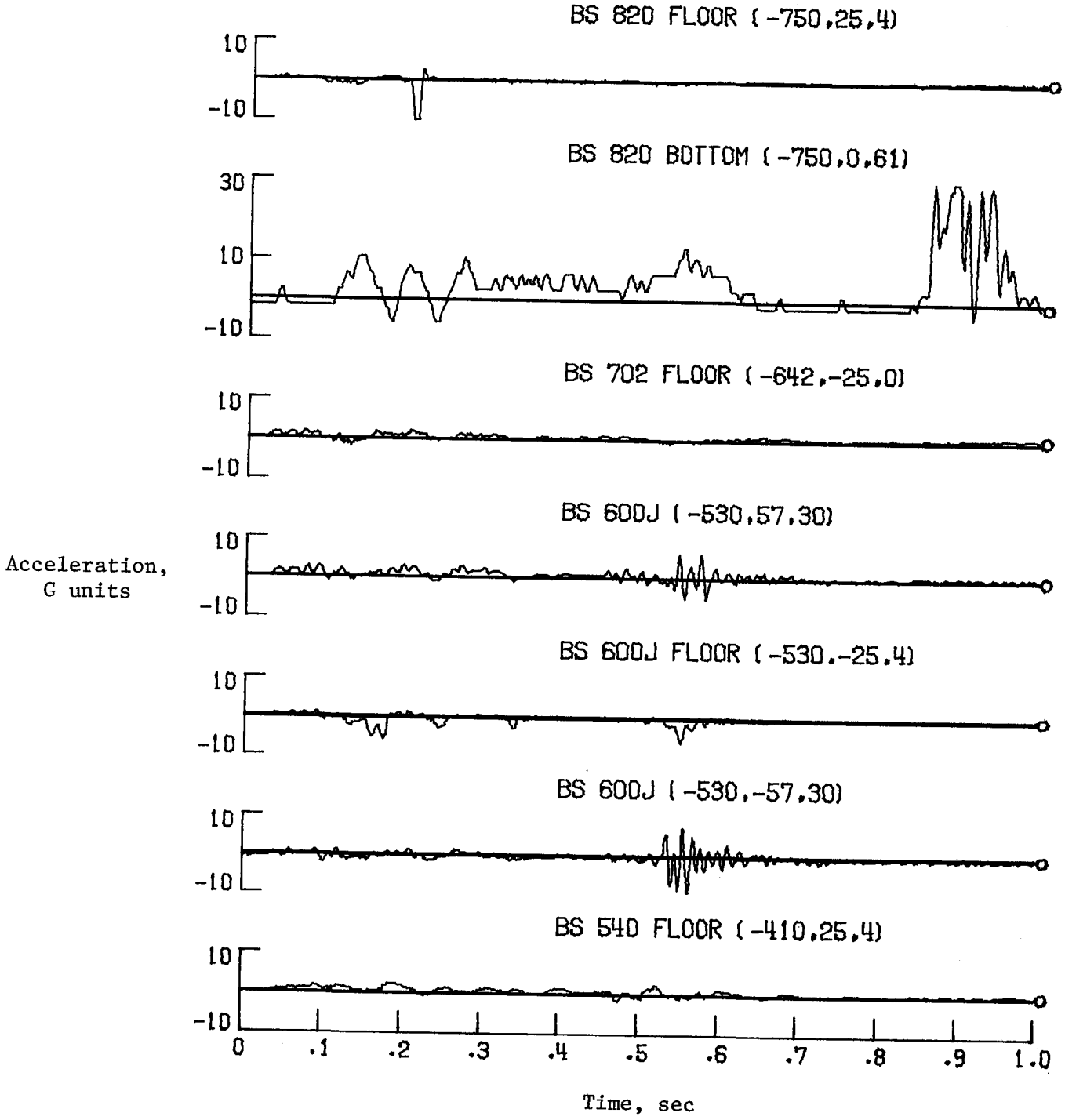

(b) BS 540 to 820.

Figure A5. Continued.

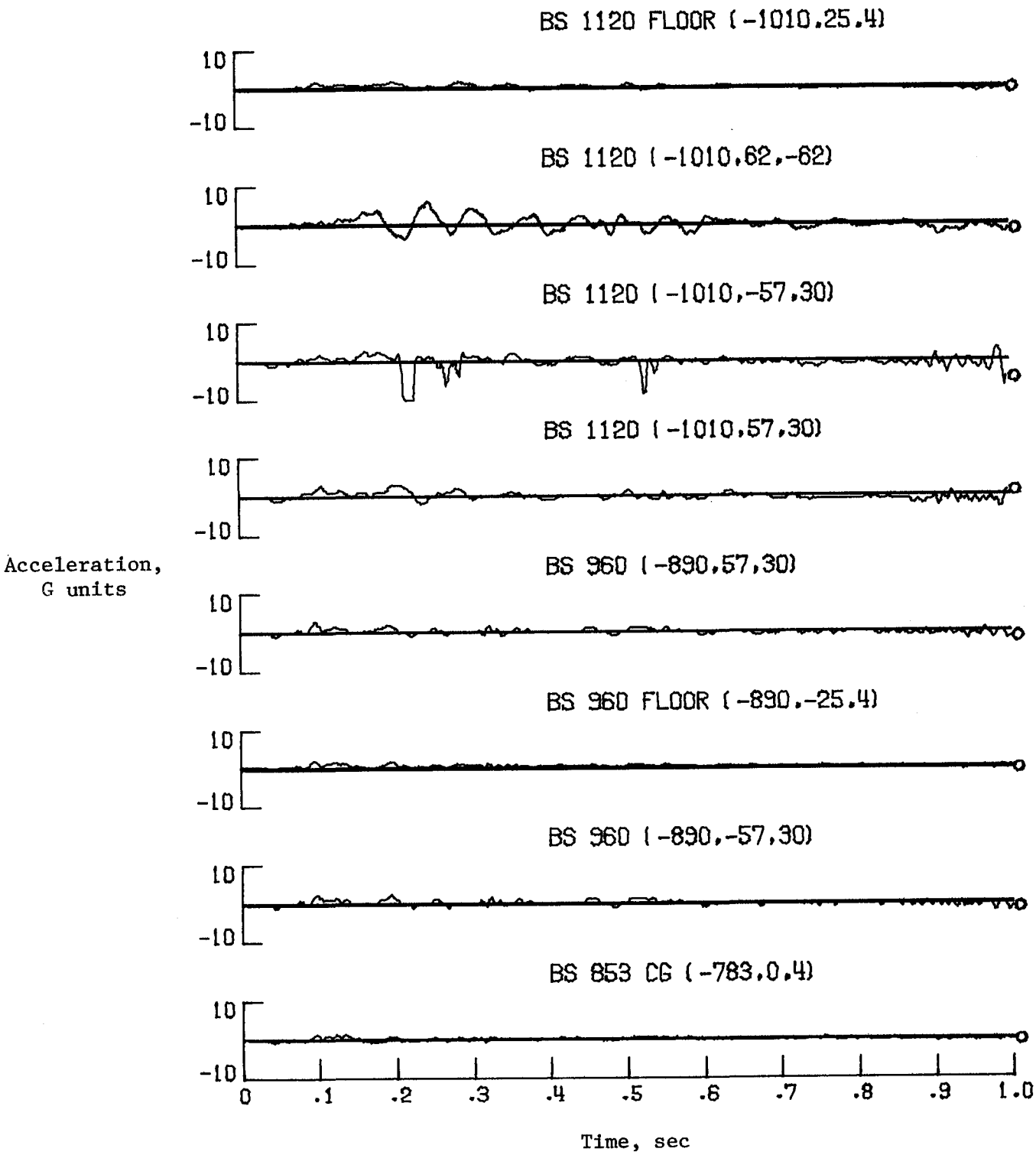

(c) BS 853 to 1120.

Figure A5. Continued.

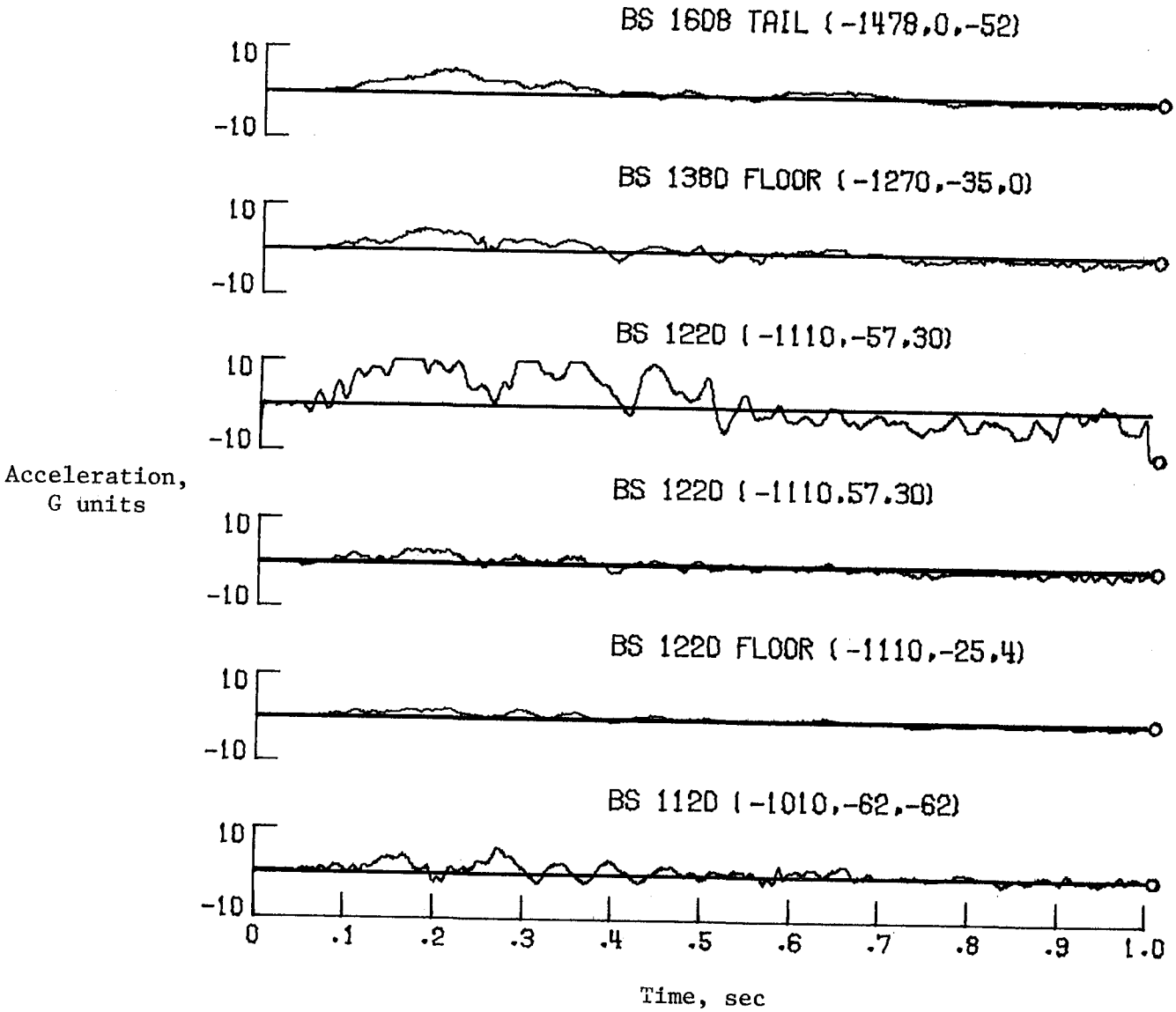

(d) BS 1120 to 1608.

Figure A5. Concluded.

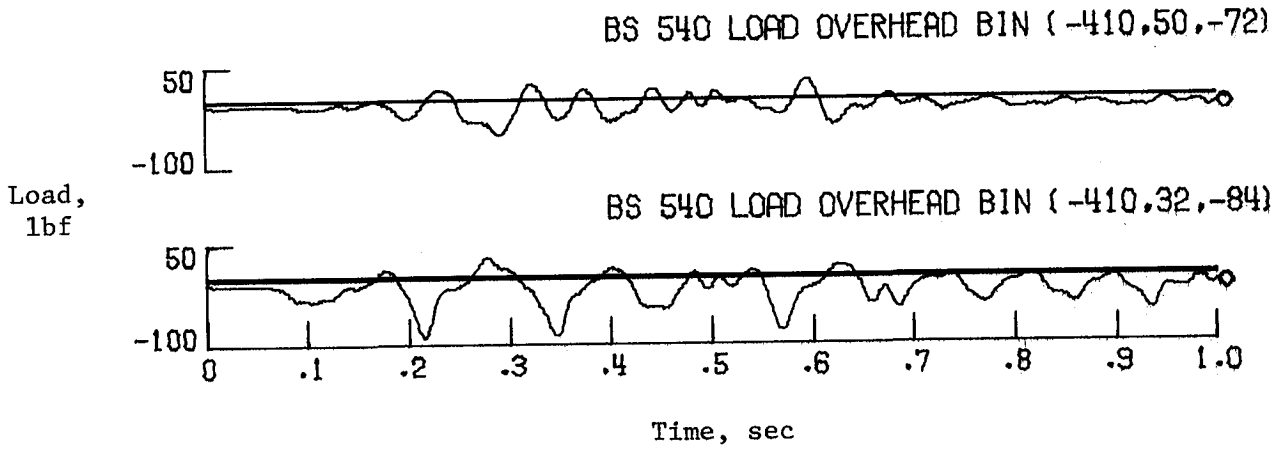

Figure A6. Loads in two links that support the overhead storage bin located at BS 540.

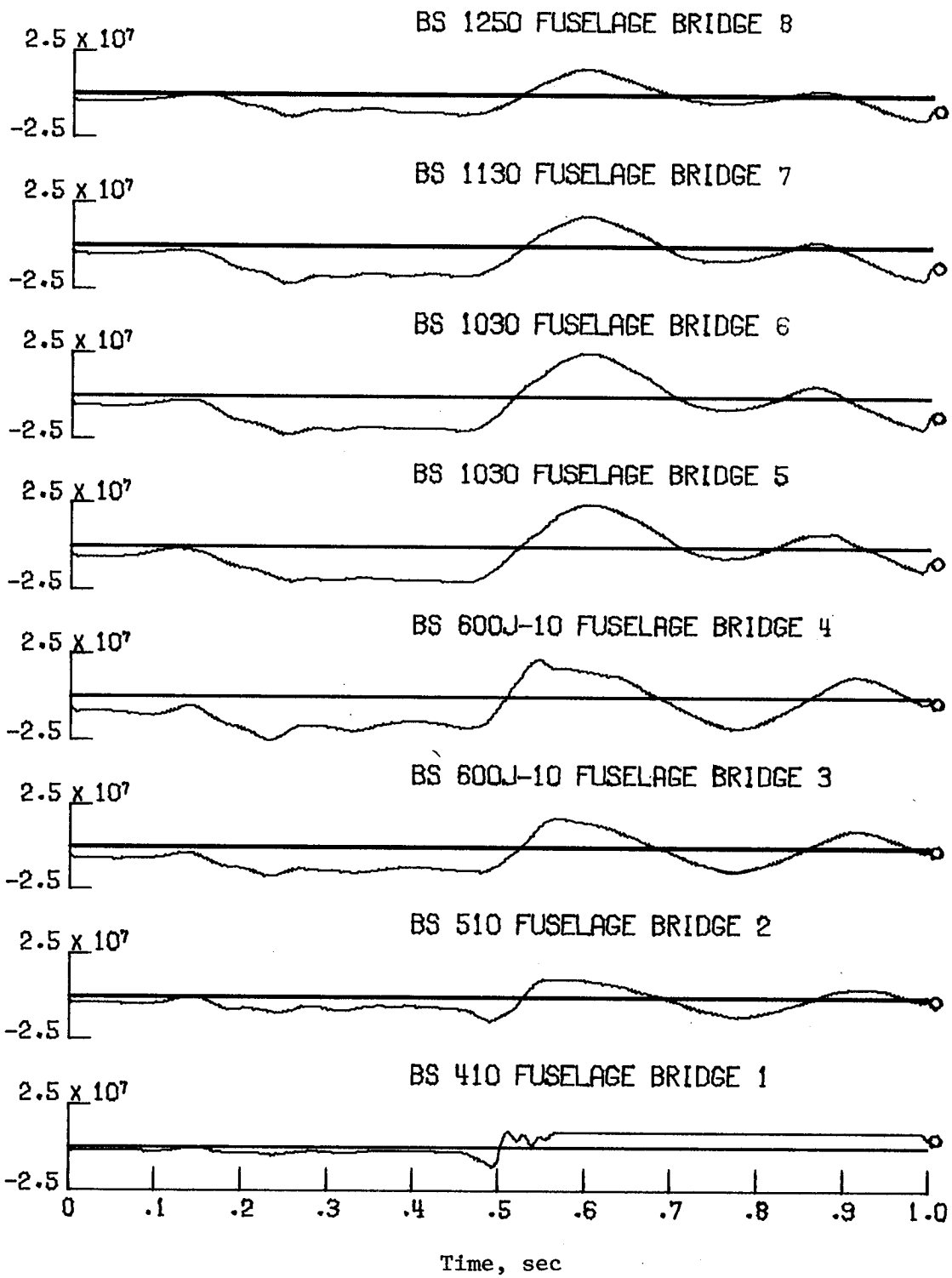

Figure A7. Fuselage vertical bending moment time histories.

Appendix B

Wing Accelerations and Vertical Bending Data

This appendix includes wing accelerations for the normal (Z-direction) and longitudinal (X-direction) aircraft body directions and wing vertical bending moments for the 1-sec period after initial left-wing impact with the ground. In the longitudinal direction, the usual body station system was supplemented by an x-coordinate, which was the distance in inches measured from the nose of the aircraft. The origin of the coordinate system was located at the aircraft nose, with positive X-axis forward, positive Y-axis out the right wing, and positive Z-axis downward. Figure B1 shows the accelerometer locations for the left wing. The right wing was instrumented similarly. The time histories for wing acceleration data and wing vertical bending data are given in figures B2 to B4. The abscissa in each figure represents the time in seconds, with the origin taken to be the approximate time of left-wing impact with the ground (09:22:11 PST). Each time history spans 1 sec to cover the primary fuselage impact period. The label above each trace gives some or all of the following: the body station, a brief description of the structure on which the measurement was made, and the (x, y, z) coordinates of the transducer given in parentheses. All accelerations and bending-bridge data were filtered after the test with 100- and 50-Hz low-pass digital filters, respectively.

Wing Normal Accelerations

Figures B2(a) to B2(c) show 14 wing normal (Z-direction) acceleration time histories. Several of the wing accelerations went off the scale but are still included for completeness. The maximum acceleration range was approximately $\pm 150G$ in the normal direction and $\pm 100G$ in the longitudinal direction. The left outboard engine (No. 1) contacted the ground first. No accelerometer was located on the No. 1 engine or pylon. The accelerometer nearest to the initial impact point was located at BS 1020 on the front left-wing spar. (See fig. B2(b).) This trace shows a peak acceleration that exceeded $150G$ at a time near 0.08 sec. Shortly afterwards, just before 0.1 sec, the left-wing tip registered a peak of $130G$ (fig. B2(c)), and at 0.12 sec the No. 2 engine lower pylon accelerometer showed a peak near $150G$ and then went off the scale (fig. B2(a)). The last acceleration to go off the scale was for the accelerometer located on the front spar behind the No. 2 engine (fig. B2(a)). The No. 2 engine upper pylon accelerometer registered a maximum acceleration of only $50G$. The other wing accelerometers on the left wing all were well below $50G$. All the right-wing accelerometers showed relatively low levels.

Wing Longitudinal Accelerations

There were only four longitudinal accelerometers located on the wings. They were located on the front spar directly behind each engine. Both traces from accelerometers on the left wing go off the scale. The accelerations for the No. 1 engine at BS 1020 (see fig. B3) peaked first at the maximum range of $100G$ and went off the scale. The left-wing accelerometer behind the No. 2 engine went off the scale just after 0.2 sec. The right-wing accelerometers in comparison showed very low levels.

Wing Vertical Bending-Moment Data

Figure B4 shows the wing vertical bending-bridge traces. Two bridges were located on each wing, an "inner" bridge located near the wing root and an "outer" bridge located on the wing between the two engines. Each bridge consisted of four strain gages, two on the front spar and two on the rear spar. The bridges were calibrated in units of inch-pounds. The values shown are incremental values above the initial zero taken with the aircraft fueled just before takeoff. The four traces shown in figure B4 unfortunately go beyond the maximum range, and all saturate at approximately 0.3 sec after left-wing impact. At 0.1 sec, the left inner bridge showed the highest value (-3.5×10^7 in-lbf) and the right outer bridge showed the lowest value (-0.8×10^7 in-lbf).

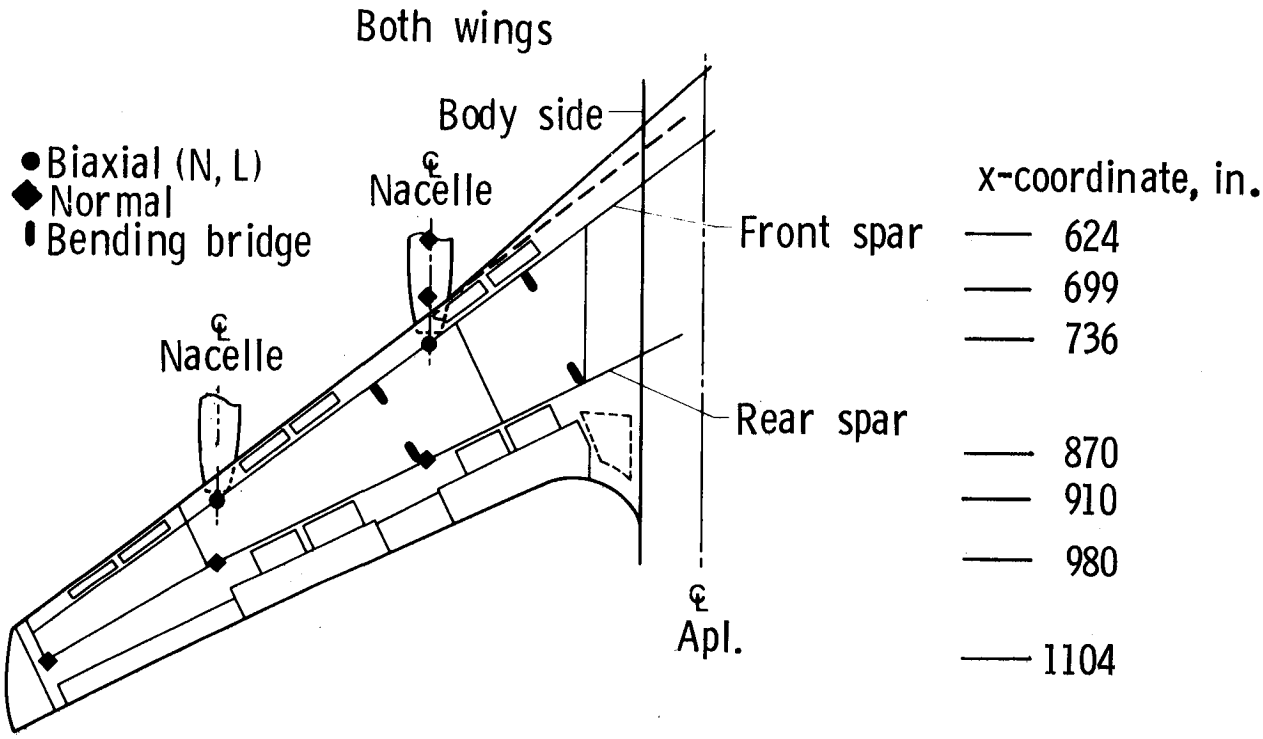

Figure B1. Wing accelerometer and strain-gage locations.

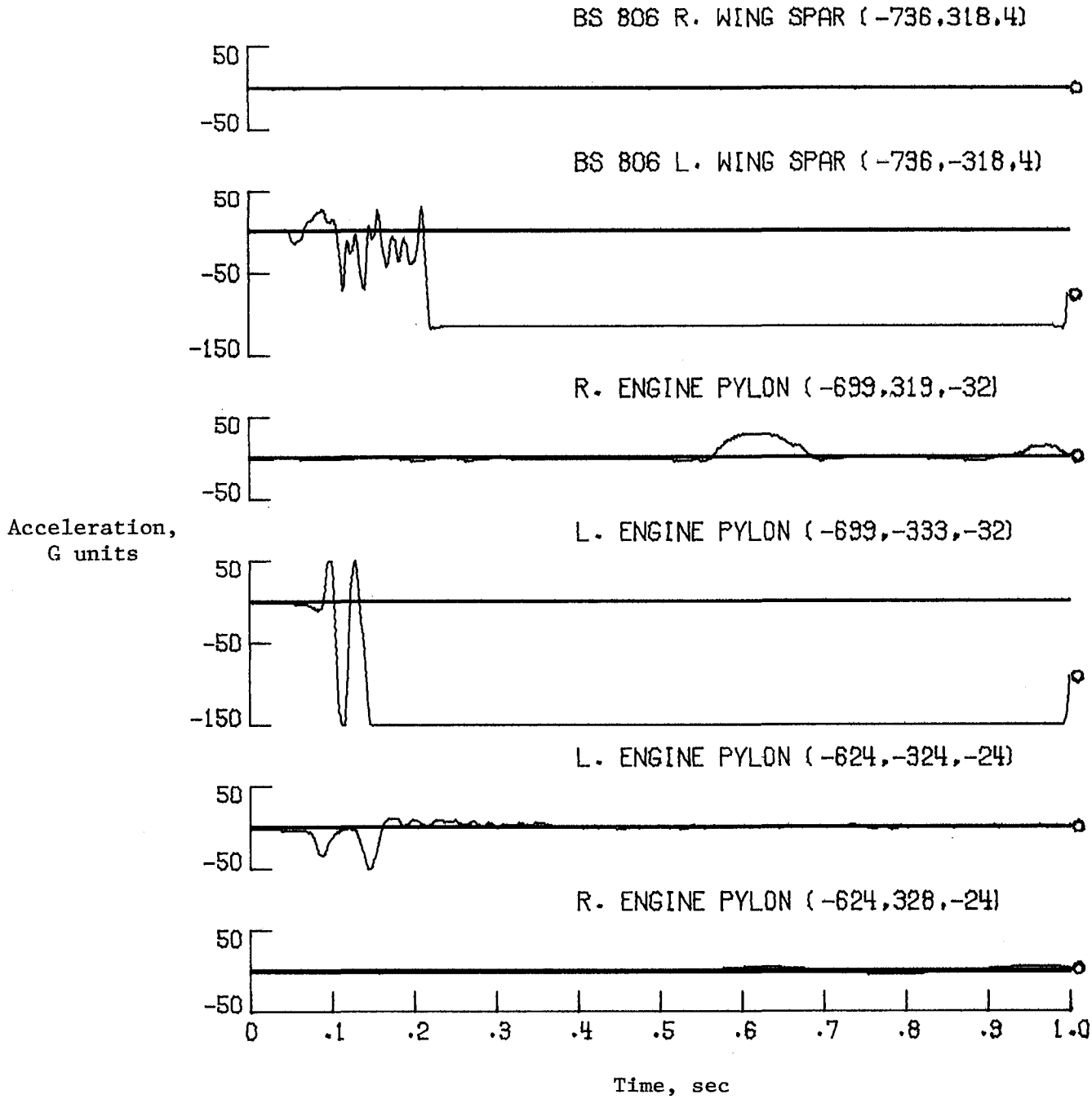

(a) Engine pylon and wing spar locations.

Figure B2. Wing normal acceleration time histories.

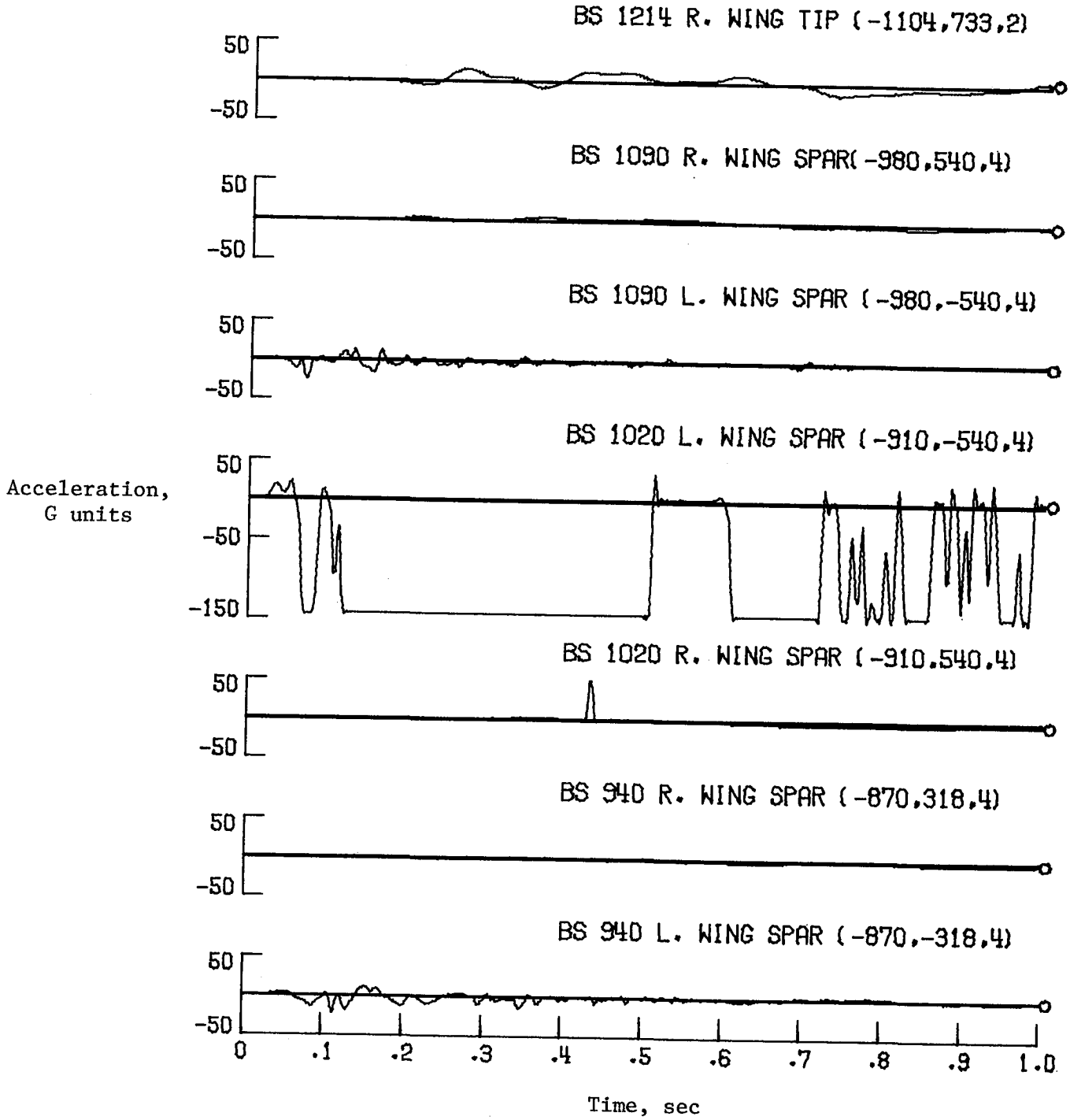

(b) Wing spar and wing tip locations.

Figure B2. Continued.

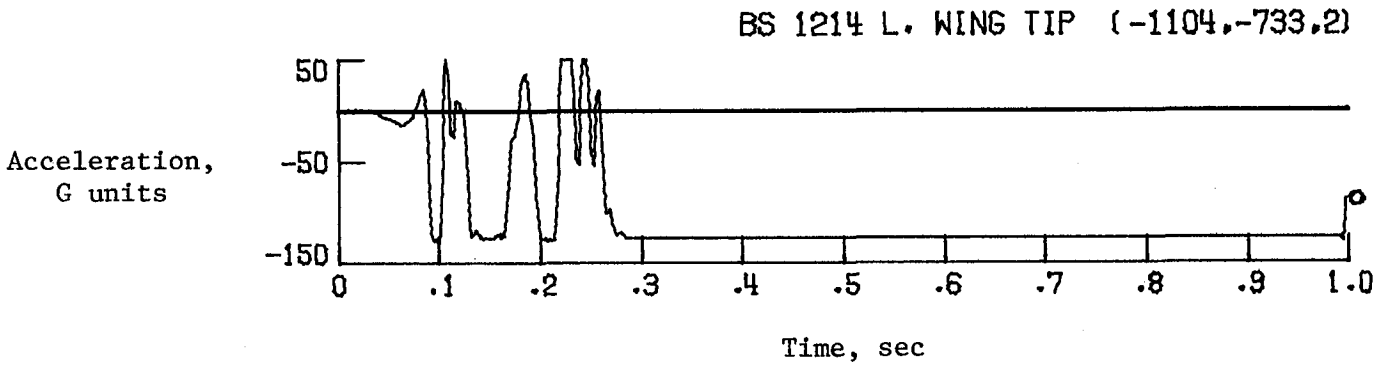

(c) Wing tip location.

Figure B2. Concluded.

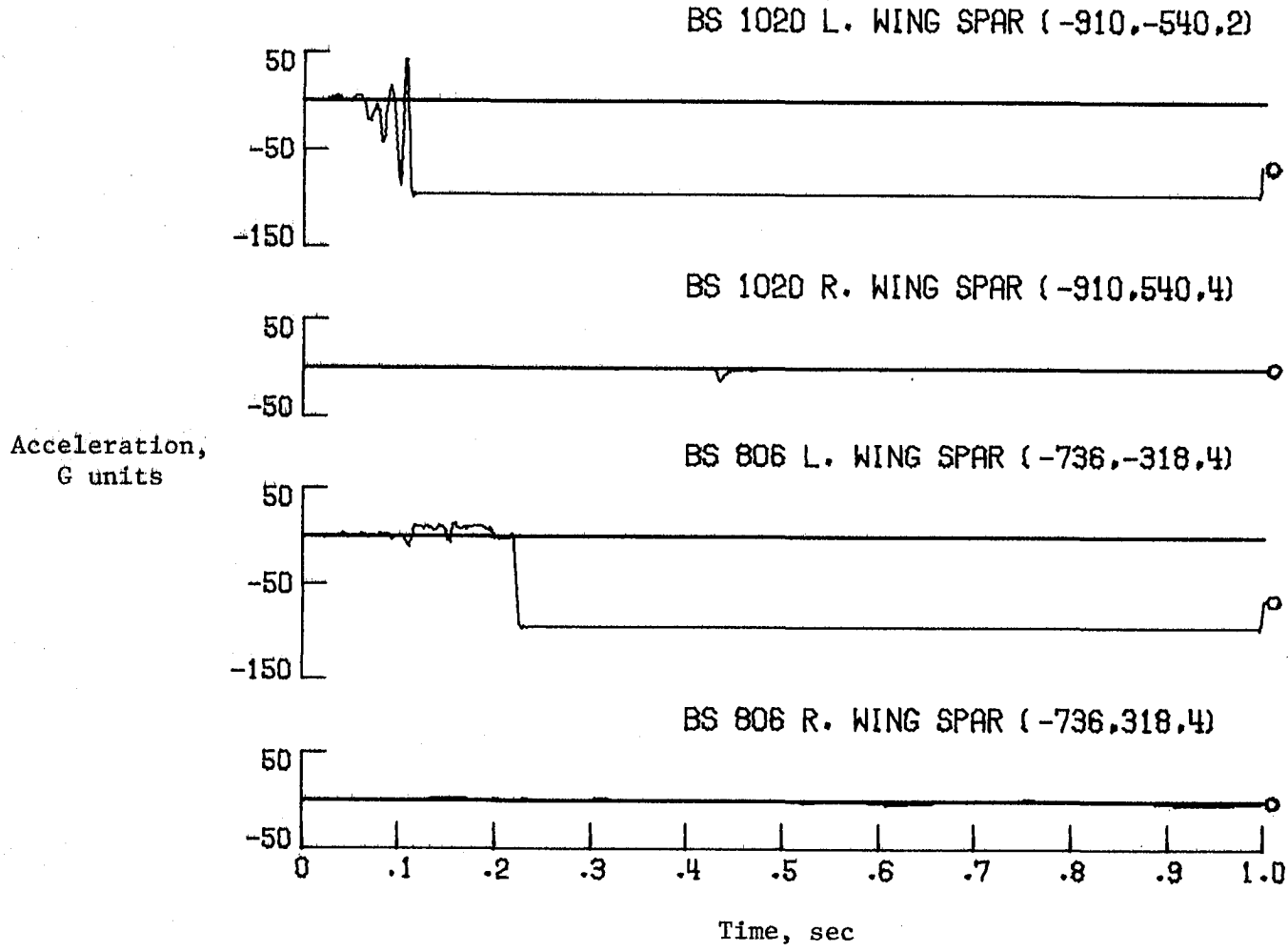

Figure B3. Wing spar longitudinal acceleration time histories.

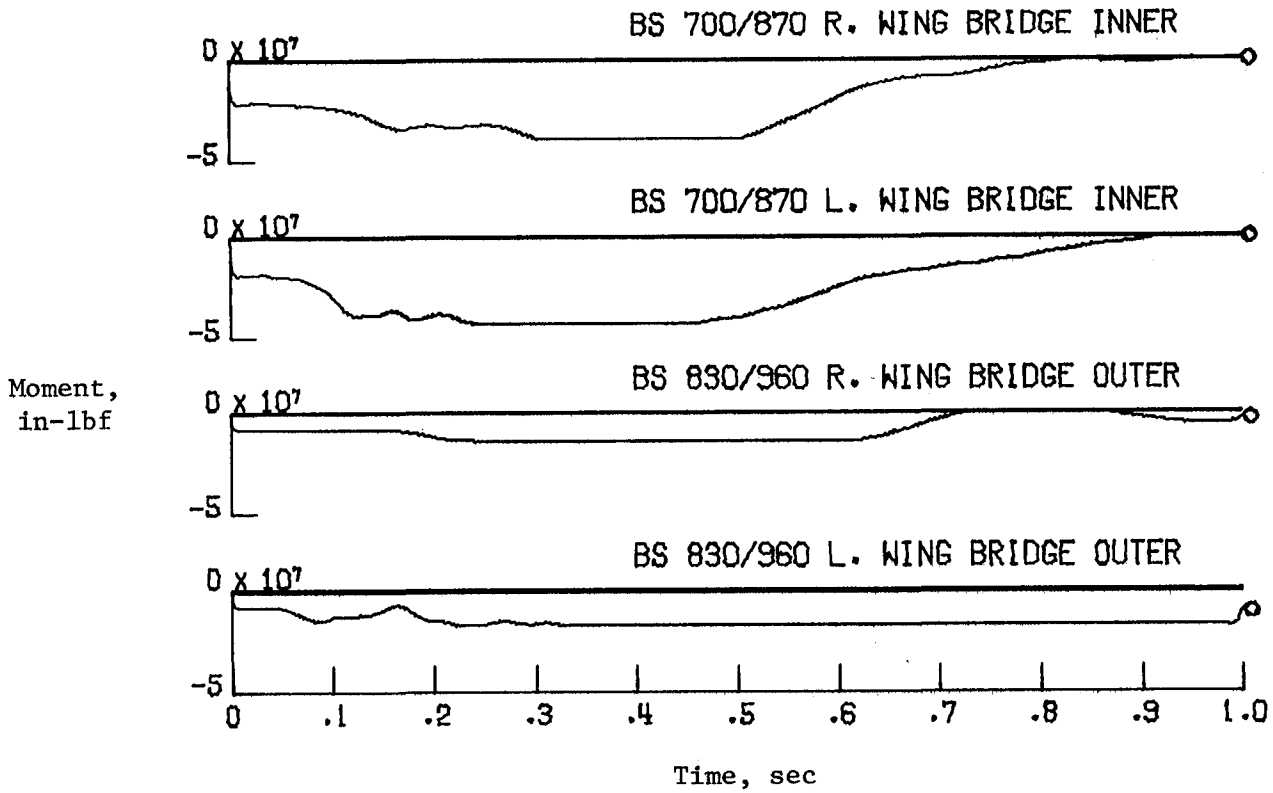

Figure B4. Wing vertical bending moments.

Appendix C

Seat and Anthropomorphic-Dummy Accelerations and Loads

Included in this appendix are seat and anthropomorphic-dummy accelerations and restraint (i.e., lap-belt and shoulder-harness) loads for the first second after initial left-wing impact with the ground. In the longitudinal direction, the usual body station system was supplemented by an x-coordinate, which was the distance in inches measured from the nose of the aircraft. The origin of the coordinate system used to locate transducers of seats and dummies was located at the aircraft nose, with positive X-axis (longitudinal) forward, positive Y-axis (transverse) out the right wing, and positive Z-axis (normal) downward. For the dummy accelerations, the accelerometer directions were in the dummy axis system (x_d, y_d, and z_d) and were only approximately along the aircraft X-, Y-, and Z-directions. In the case of the NASA dummies, which were bent over in a crash position, the upper torsos were rotated so that the dummy z_d-direction was approximately aligned with the aircraft X-axis. Table C1 includes a list of the seat experiments in the CID consisting of seat location (row and side), body station, seat type, and number of occupants in each seat. The seats were arranged in 16 widely spaced rows (see fig. C1) starting with the pilot seat (row 1) and ending with a two-place attendants' seat located on the rear bulkhead at BS 1380 (row 16). Each plot is labeled with the seat or dummy row number, the side of the airplane (for example, seat 3L is in the third row on the left side of the aircraft), body station, and the coordinate location of the transducer. There were 27 seats aboard with a capacity of 75 occupants. The seats were arranged in widely spaced rows so that one seat experiment would not interfere with any other seat in case a failure occurred. Of the 73 dummies placed onboard, only 17 were of anthropomorphic research quality (with 13 instrumented). Dummy instrumentation consisted of accelerometers, which could be located in the pelvis (PEL), chest (CHST), and head cavities (HEAD), and of restraint load cells used to measure lap-belt and shoulder-harness loads (where applicable). The minimum dummy instrumentation was three accelerometers located in the pelvis and two lap-belt load cells. All dummies were in a seated, upright position except for the dummies in the NASA triple seats, which were bent over and tied in a crash position. All accelerations and loads were filtered after the test with 100- and 50-Hz low-pass digital filters, respectively.

Seat and Dummy Normal Accelerations

The 39 normal (Z-direction) acceleration time histories measured on the seats (aircraft axis system) and in the dummies (dummy axis system) are presented in figure C2. The pilot received the greatest normal acceleration, with a nearly triangular acceleration pulse (fig. C2(a)). When integrated, the peak pelvis acceleration of 18.3G (base duration of about 0.075 sec) gives a velocity change over 17 ft/sec. This was the largest measured dummy or seat normal acceleration and it occurred at the time of forward-fuselage ground impact (0.46 sec). From human tolerance studies, a triangular pulse of 18.3G and 0.075 sec duration is survivable, with only a small probability of any spinal injury (for a healthy, young adult). The pilot seat normal acceleration is also shown in figure C2(a) and was less than 14G. Normal accelerations of seats and dummies from the third row back to the tail of the airplane were all well under 10G. The accelerations of the seats and dummies because of the main gear bulkhead impact (BS 820 to 960) at approximately 0.85 sec are indicated by small pulses that are only apparent for the seats and dummies located rear of BS 600J. The dummy normal acceleration from left-wing impact (occurring just after time 0 sec), forward-fuselage impact at 0.46 sec, and landing gear bulkhead impact at 0.85 sec were comparable for locations to the rear of BS 820.

Seat and Dummy Longitudinal Accelerations

Seat and dummy longitudinal accelerations for the first second after left-wing impact from 48 transducers are presented in figure C3. For the longitudinal direction, the pilot-seat trace (fig. C3(a)) has the highest peak acceleration of 10G at 0.48 sec, slightly after the time of first fuselage impact. The pilot pelvis trace (fig. C3(a)) responds very little at the time of forward-fuselage impact, showing very small acceleration. From an examination of the traces, the seat and dummy accelerations overall were quite low in the longitudinal direction and in many cases did not exceed 2G or 3G. The head accelerations for dummies in seats 5L and 7L were higher than seat or torso accelerations and peaked at 5G (figs. C3(b) and C3(c)). The trace for seat 6R (fig. C3(c)) is included, but it is very suspect at the time of forward-fuselage impact (0.46 sec) and definitely goes bad at 0.60 sec. From human tolerance studies for seated subjects, these accelerations are very mild. In the high-speed motion pictures, the dummies did not exhibit large displacements, and dummies with a lap belt only did not "jackknife"

over the belt over the entire time period from initial impact to rest.

Seat and Dummy Transverse Accelerations

The transverse acceleration time histories are given in figure C4 for 36 seat and dummy locations. The ordinate ranges from $-2G$ to $5G$ and all transverse accelerations were within this range. The maximum transverse acceleration occurred early, at the time of left-wing impact and wing crushing. This acceleration was greatest in the crew area (fig. C4(a) traces for the pilot) and in the rear of the aircraft (fig. C4(e) traces for dummy in seat 16L); it measured approximately $4G$ in both locations. Although the aircraft was rolled and yawed at impact, the transverse accelerations were quite low, and in many locations the peak was only approximately $2G$.

Lap-Belt and Shoulder-Harness Loads

Since the longitudinal accelerations were quite low, one would not expect to find large lap-belt or shoulder-harness loads. Figure C5, which illustrates 29 load time histories for the dummy restraints, confirms this hypothesis. Only the pilot dummy and a rear attendant dummy (labeled 16L) had instrumented shoulder harnesses. The maximum measured load in a lap belt or shoulder harness for the primary impact was approximately 275 lbf and occurred in the left side of the pilot dummy lap belt and shoulder harness (fig. C5(a)), in the right side of the rear attendant dummy (16L) lap belt, and in the left side of the rear attendant dummy shoulder harness (fig. C5(d)). Most of the load cells measured less than 100 lbf of restraint tension.

TABLE C1. SEAT LOCATION AND DESCRIPTION

Seat (a)	Body station	Seat type	Occupants
1L	228	Pilot	1
2L	304	Flight attendant	2
3R	540	Triple, standard passenger	3
3L	540	↓	3
4R	600	↓	3
4L	600	↓	3
5R	600J	↓	3
5L	600J	↓	3
6R	660	↓	3
6L	660	↓	3
7L	702	Aft-facing triple, passenger	2
7R	702	Aft-facing triple, passenger	2
8R	760	Triple, standard passenger	3
8L	760	Aft-facing triple, passenger	3
9R	820	Triple, standard passenger	3
9L	820	↓	3
10R	860	↓	3
10L	860	↓	3
11R	920	↓	3
11L	920	↓	3
12R	960	↓	3
12L	960	↓	3
13L	1070	Composite triple, passenger	3
14L	1220	NASA energy absorbing	3
14R	1220	NASA standard	3
15L	1270	French seat	1
16L	1380	Flight attendant	2

[a]Row number and right (R) or left (L) side of aircraft indicated.

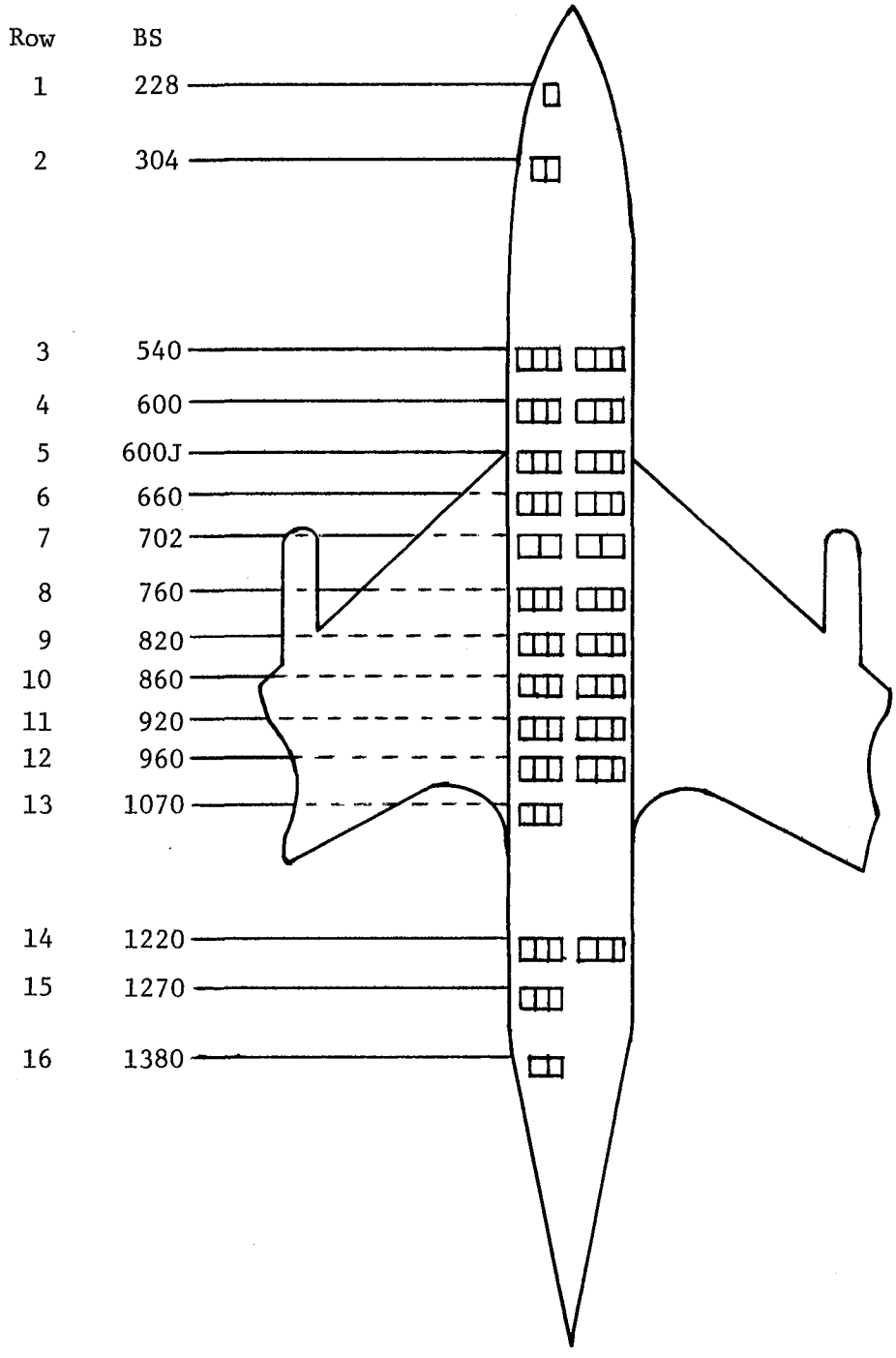

Figure C1. Seat locations for CID.

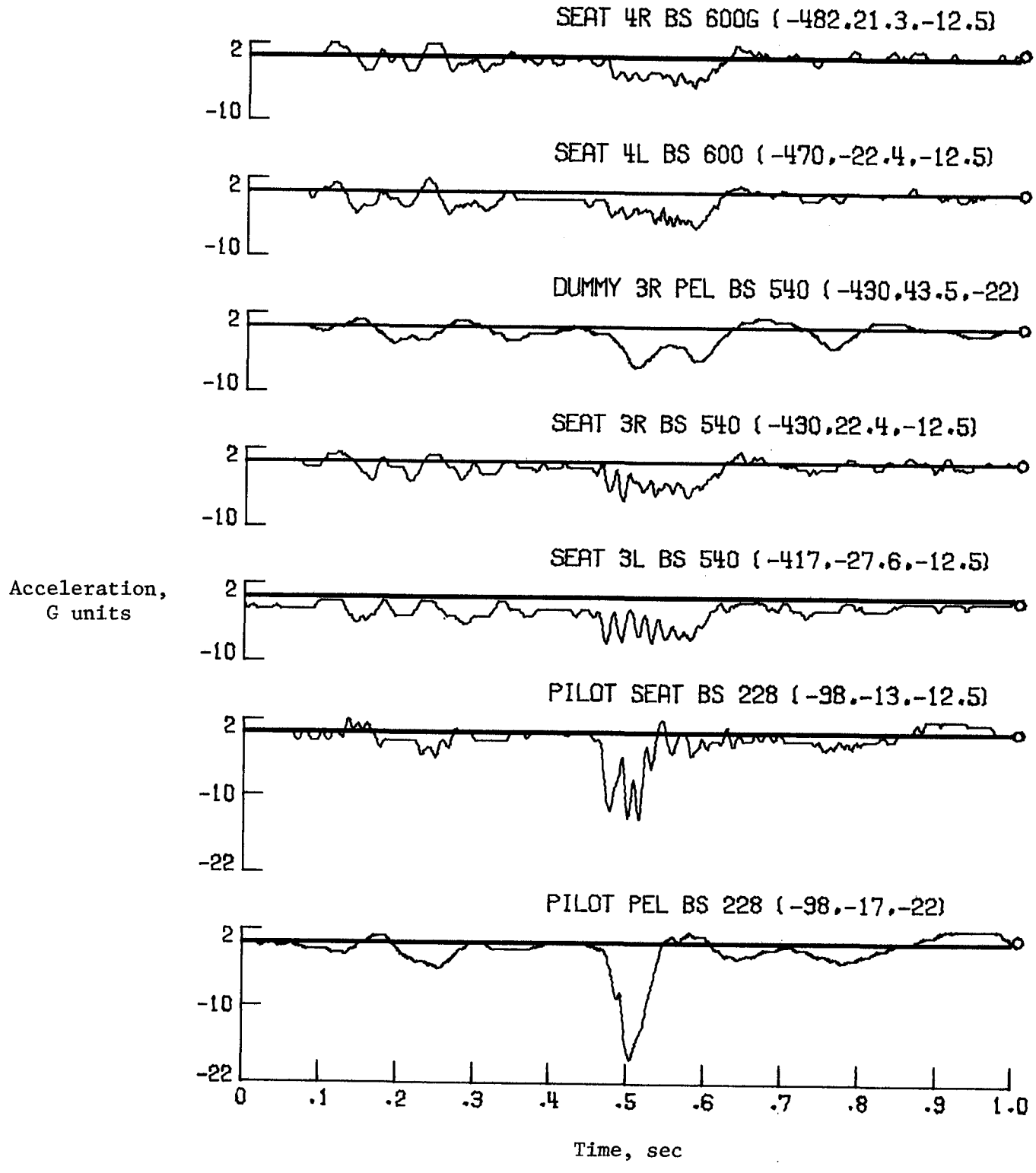

(a) BS 228 to 600G.

Figure C2. Seat and dummy normal acceleration time histories.

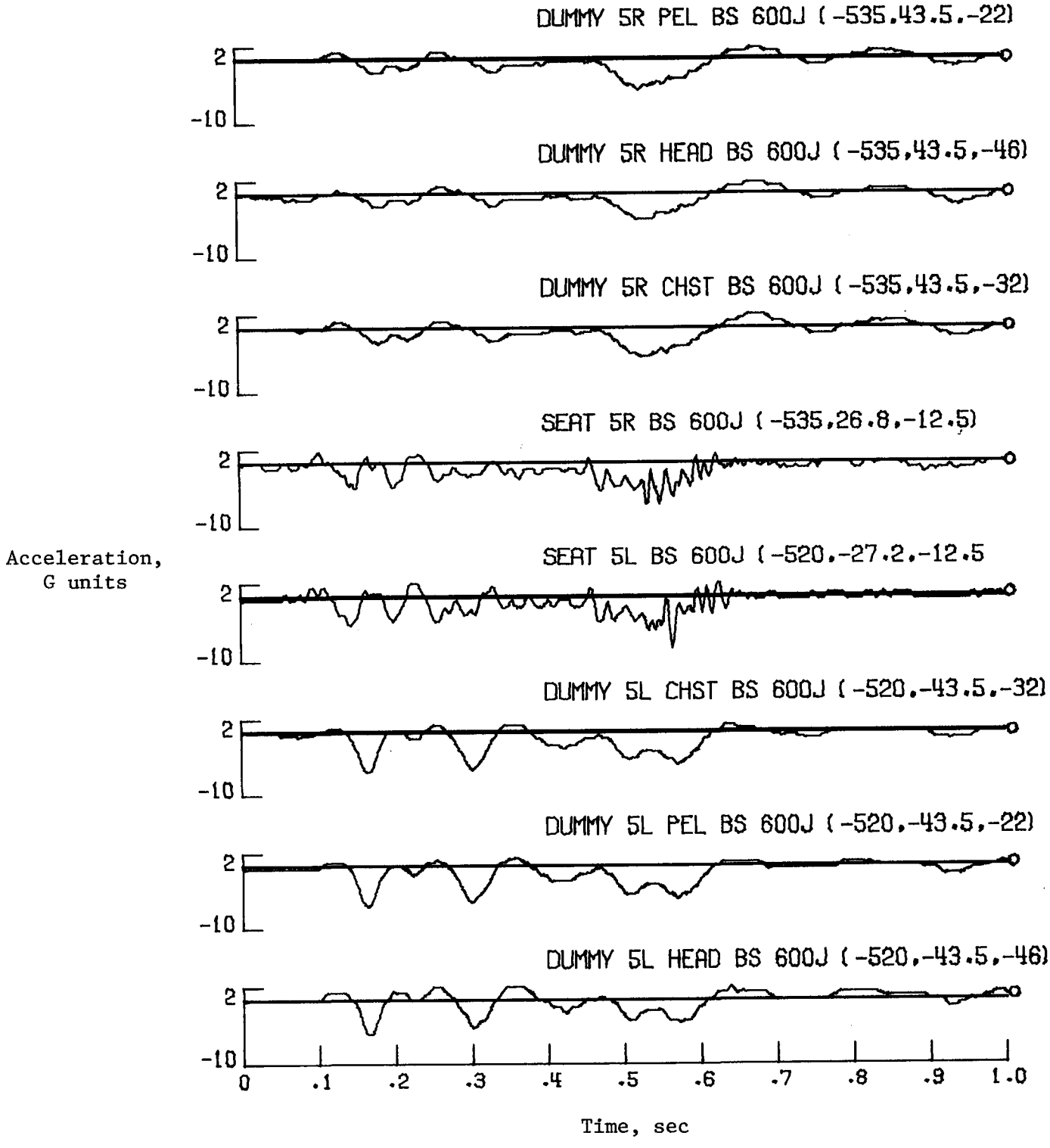

(b) BS 600J.

Figure C2. Continued.

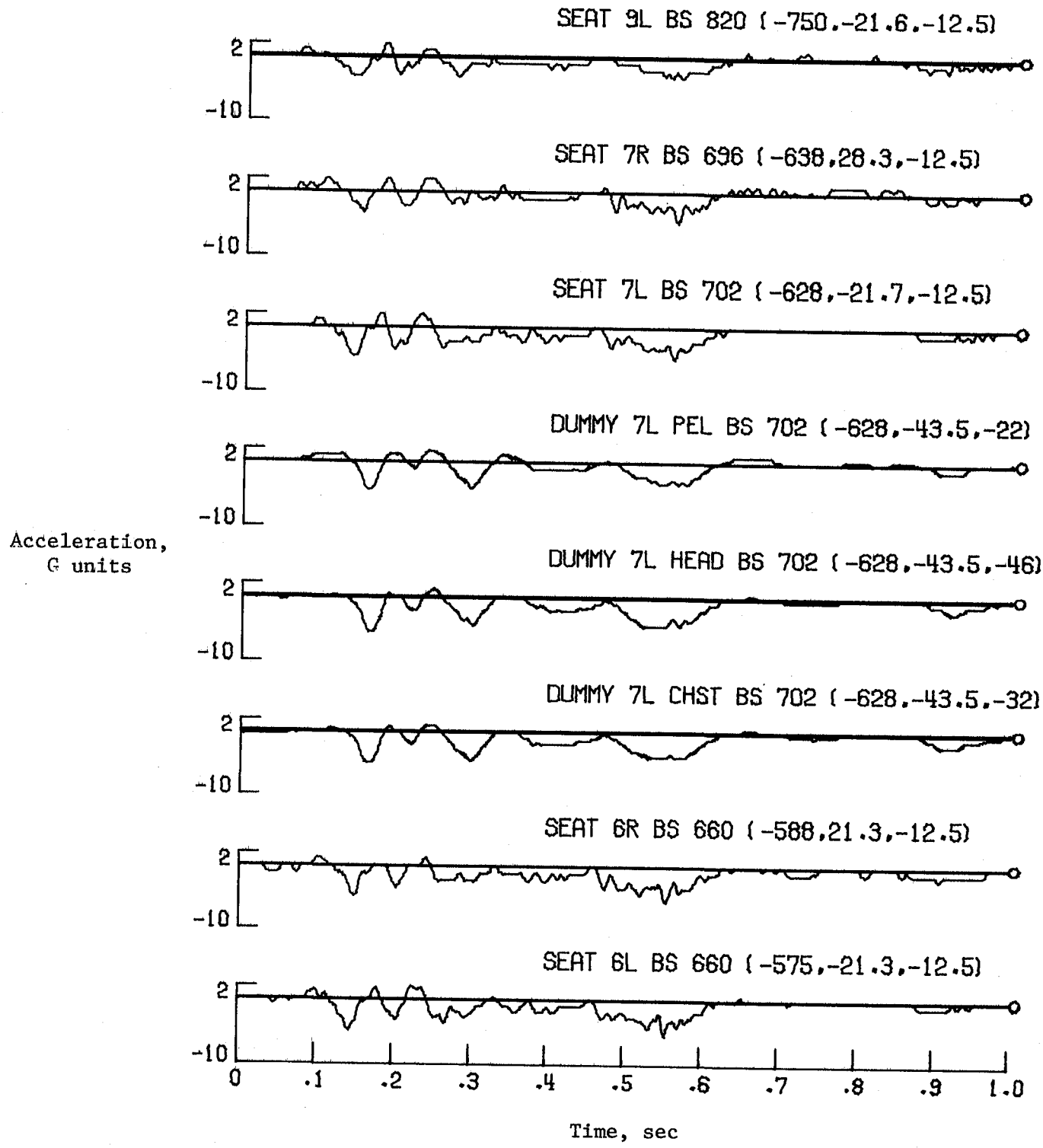

(c) BS 660 to 820.

Figure C2. Continued.

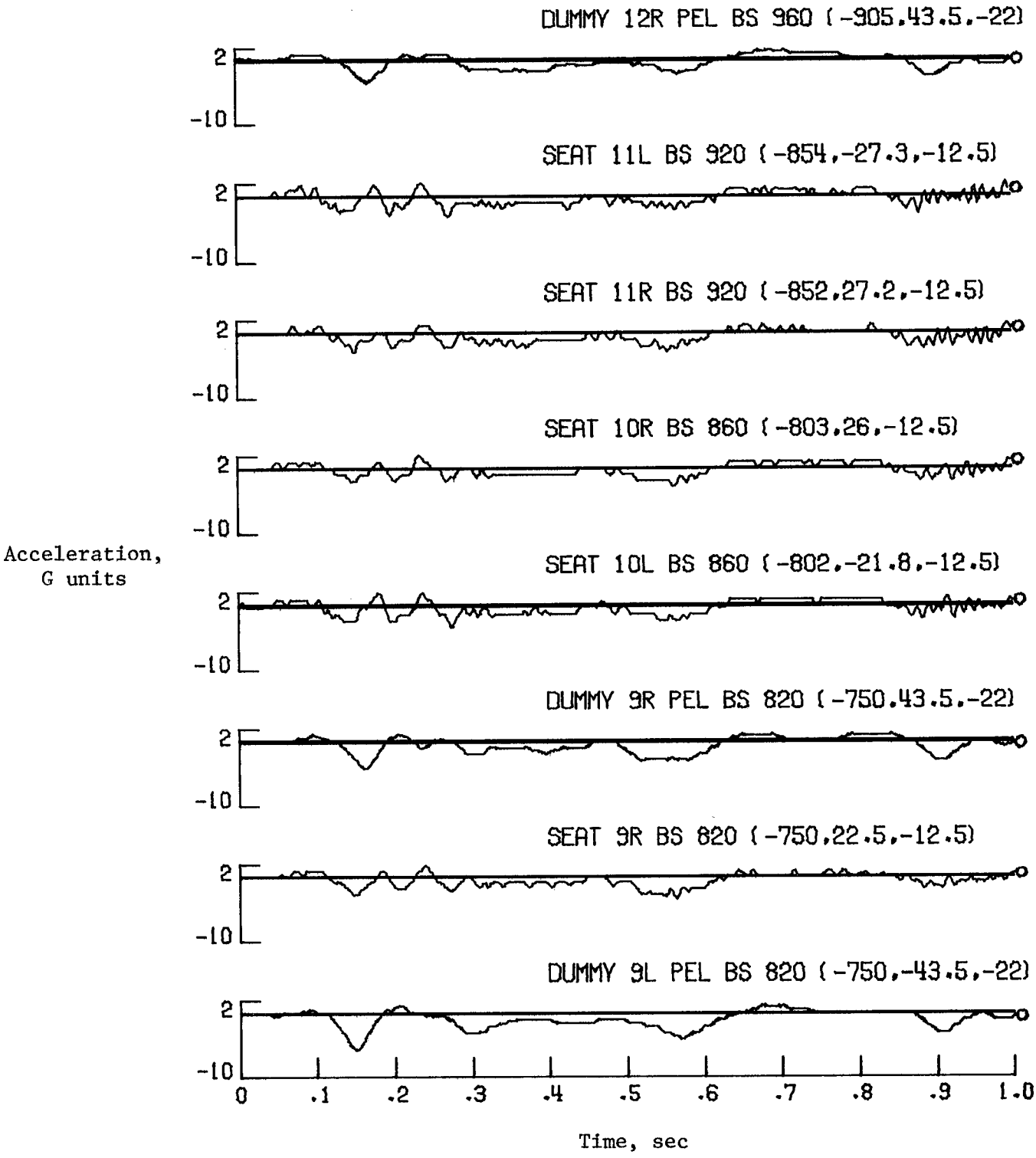

(d) BS 820 to 960.

Figure C2. Continued.

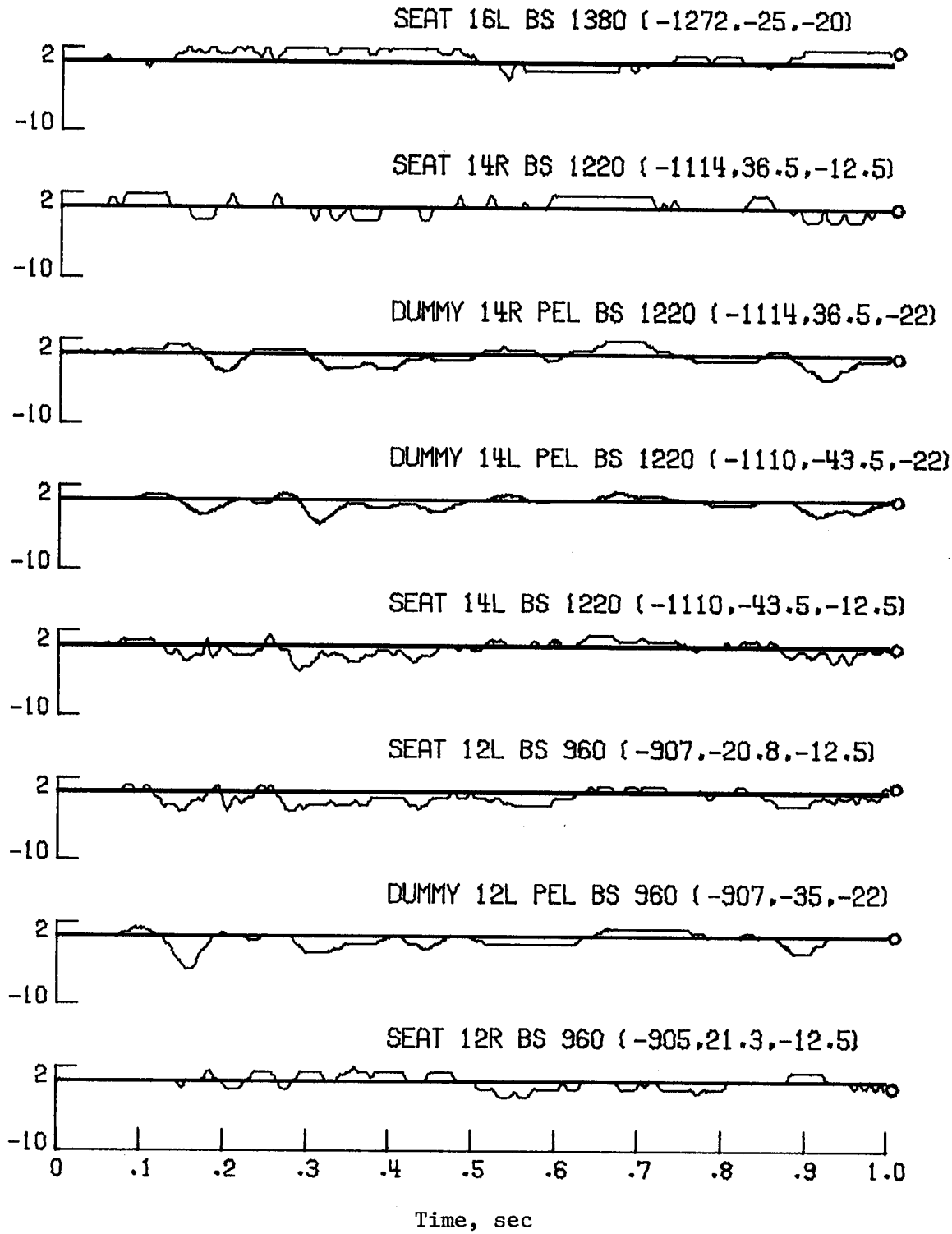

(e) BS 960 to 1380.

Figure C2. Concluded.

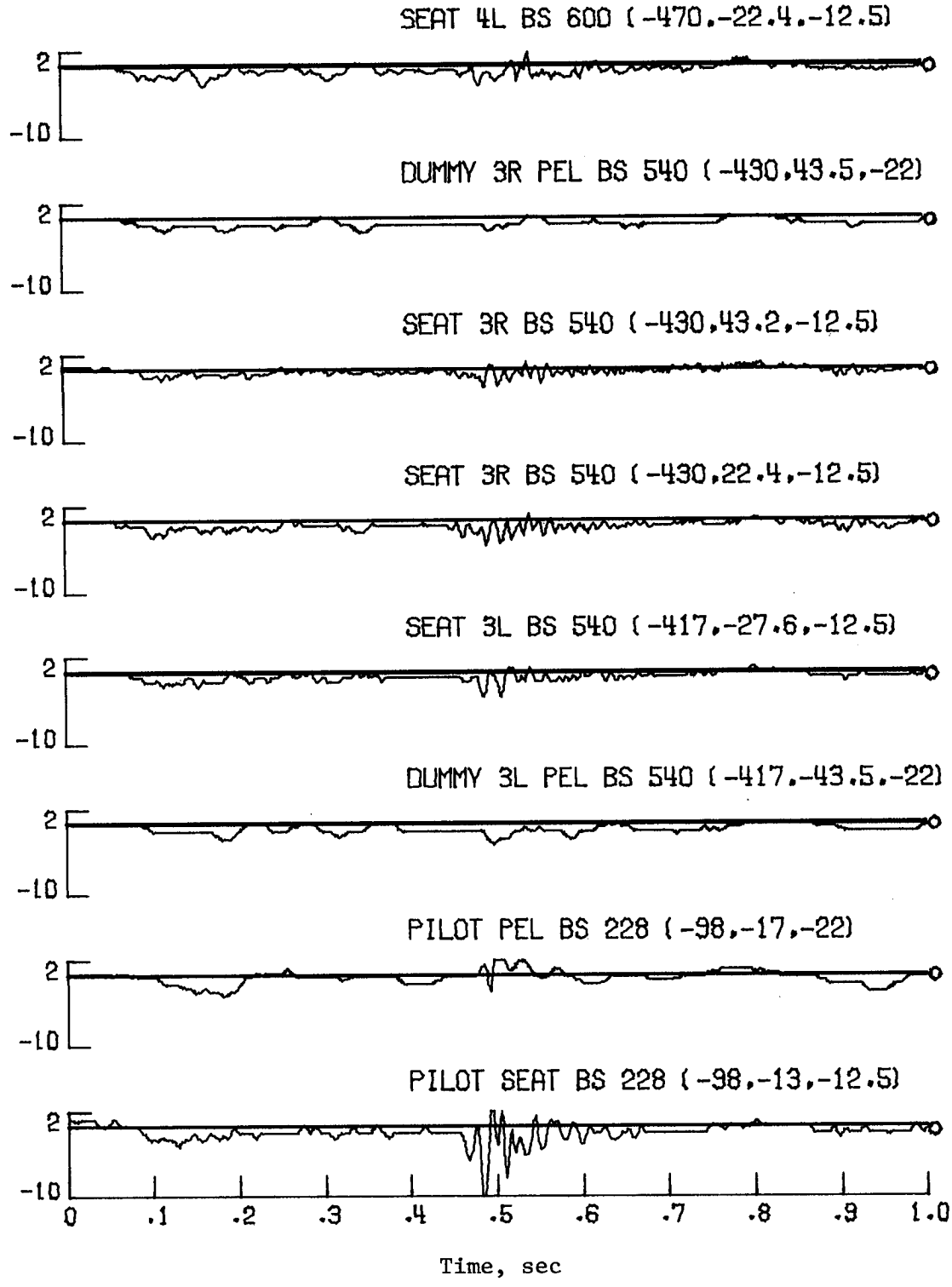

(a) BS 228 to 600.

Figure C3. Seat and dummy longitudinal acceleration time histories.

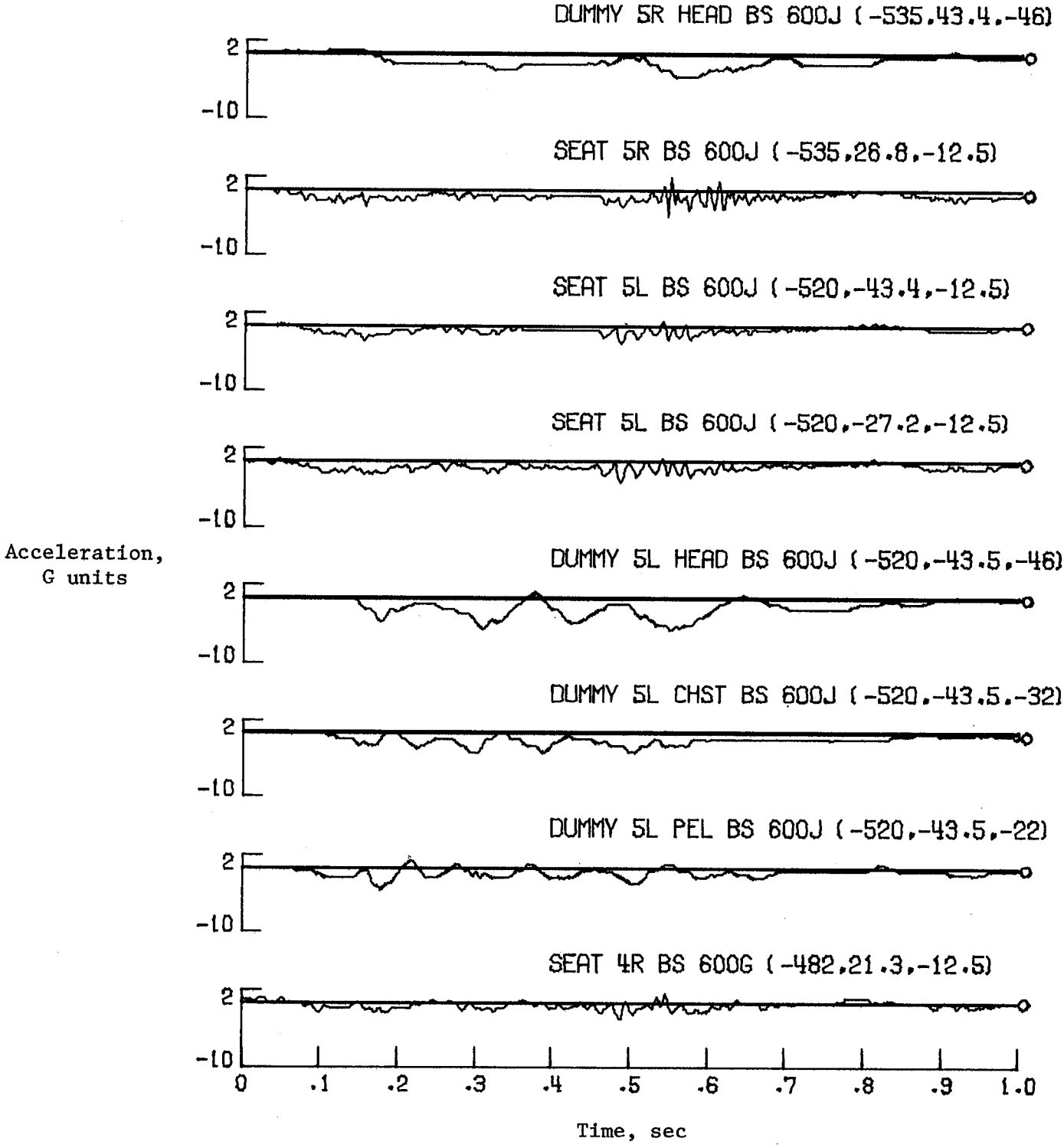

(b) BS 600G to 600J.

Figure C3. Continued.

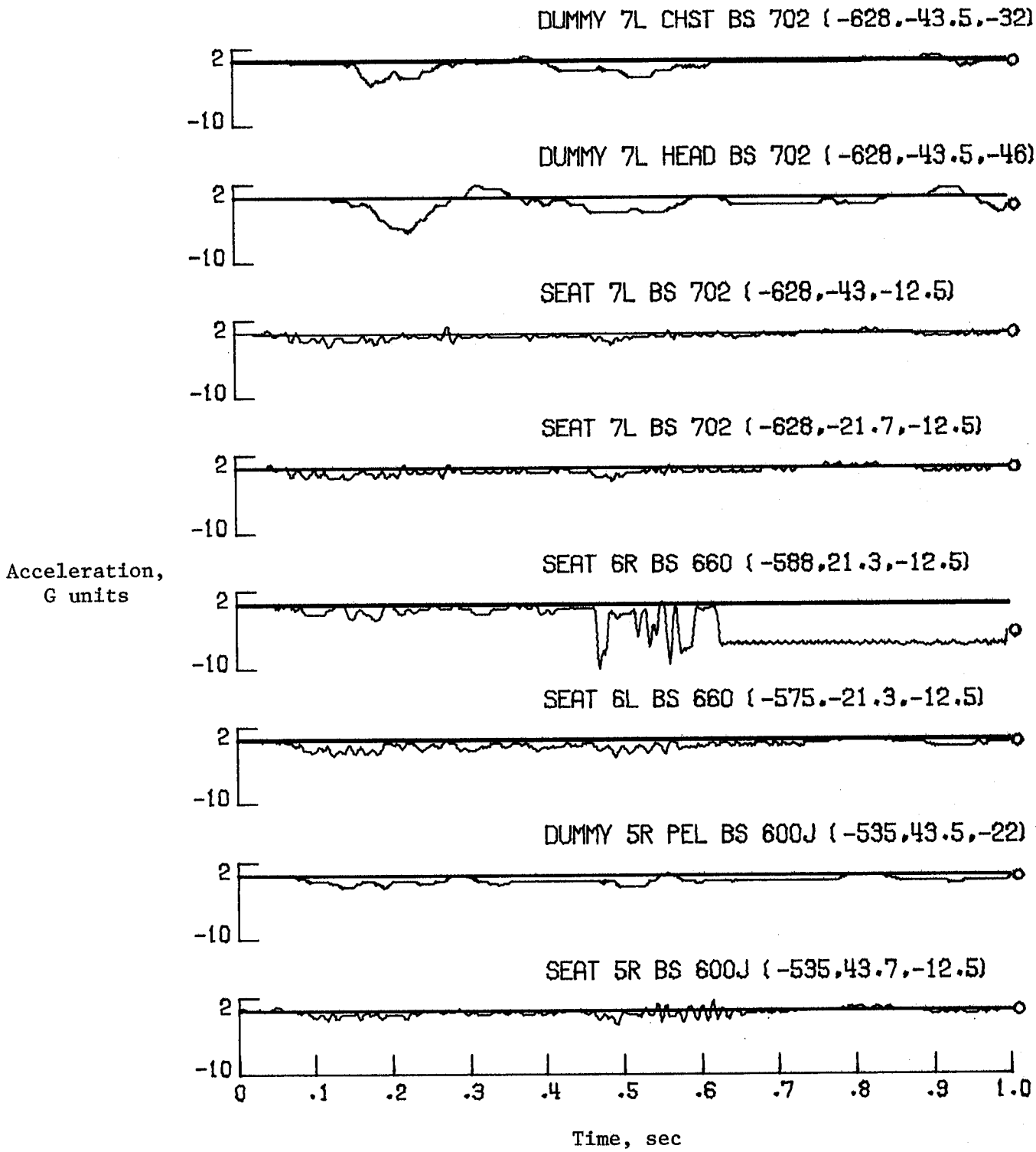

(c) BS 600J to 702.

Figure C3. Continued.

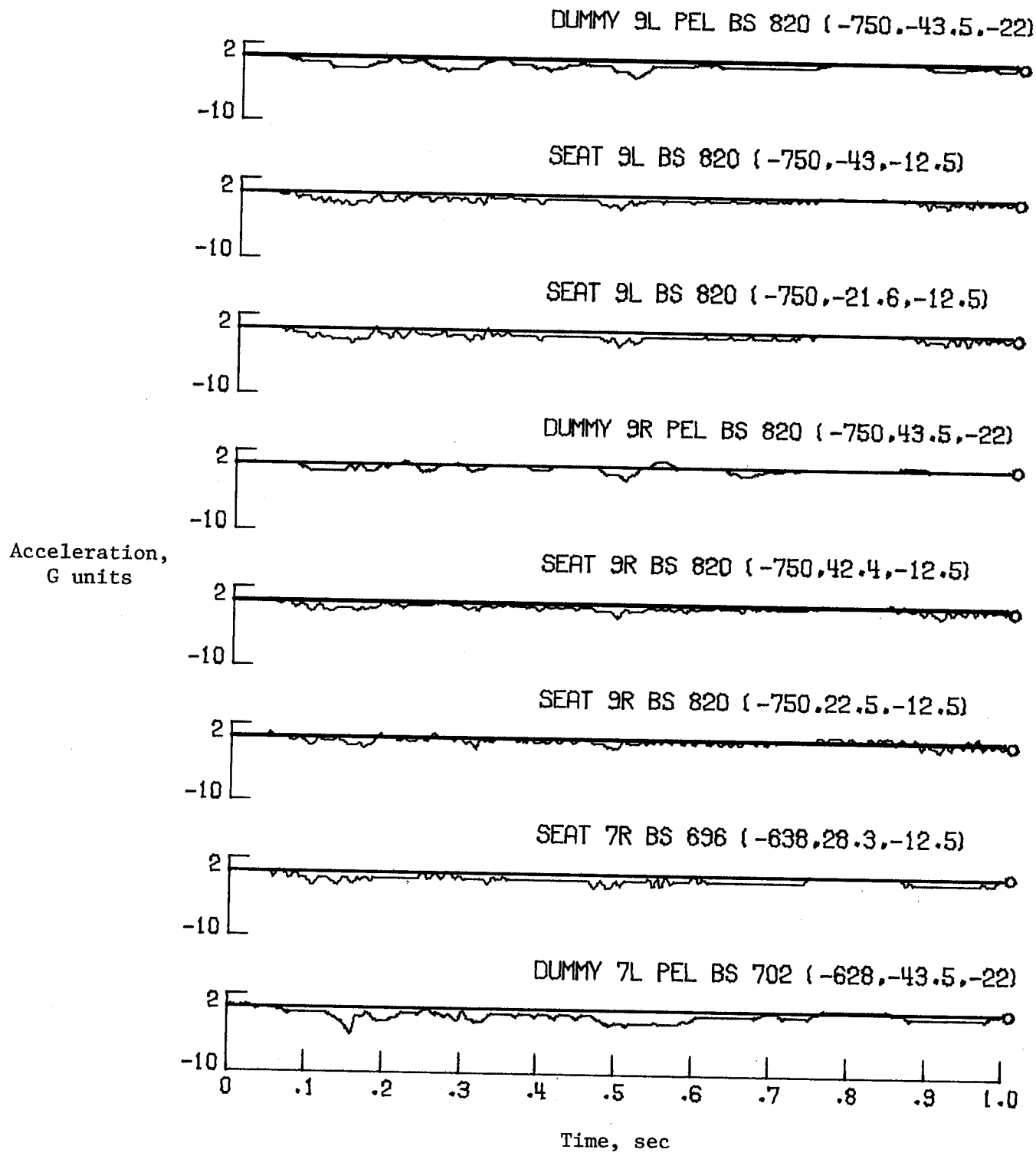

(d) BS 702 to 820.

Figure C3. Continued.

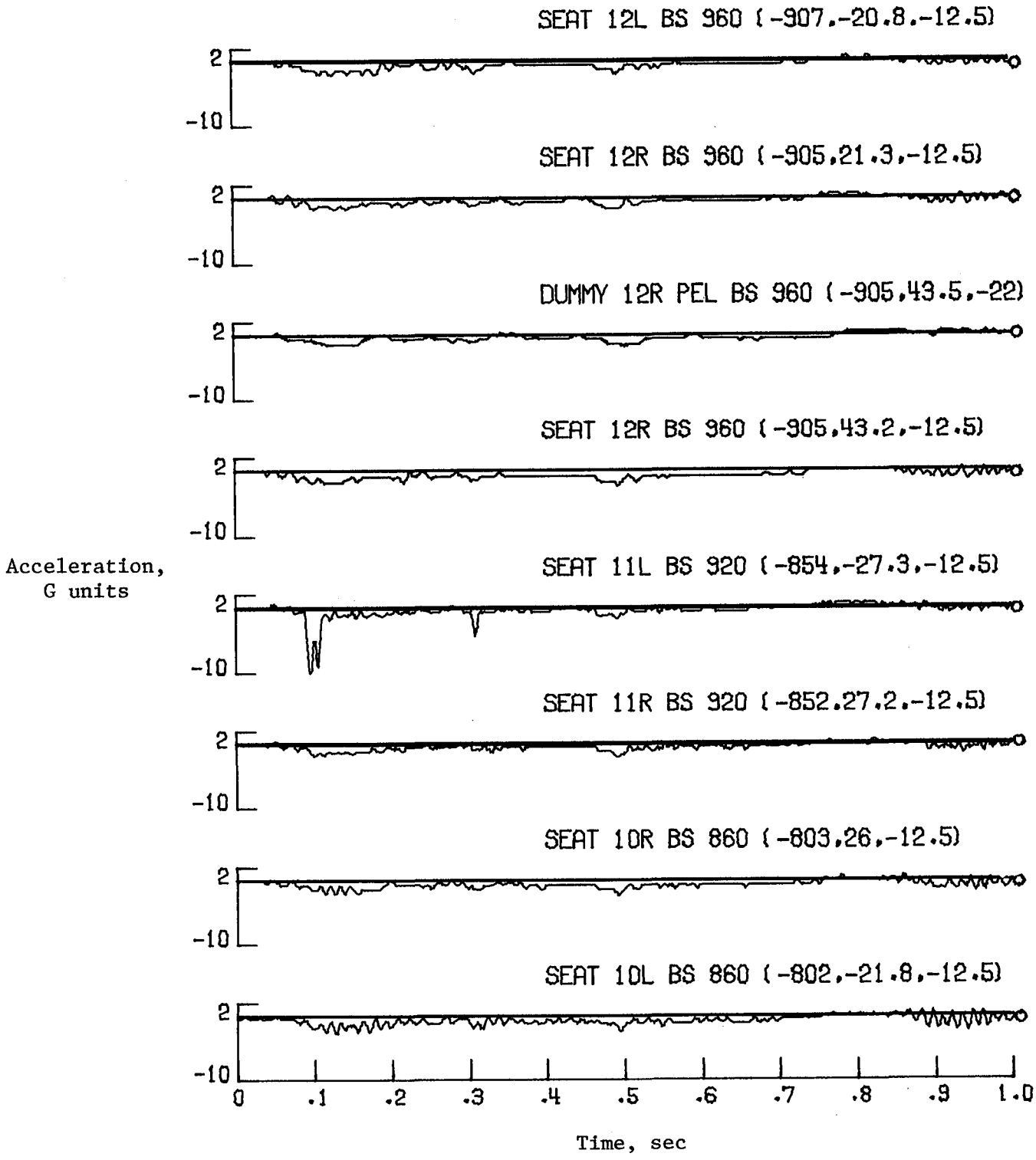

(e) BS 860 to 960.

Figure C3. Continued.

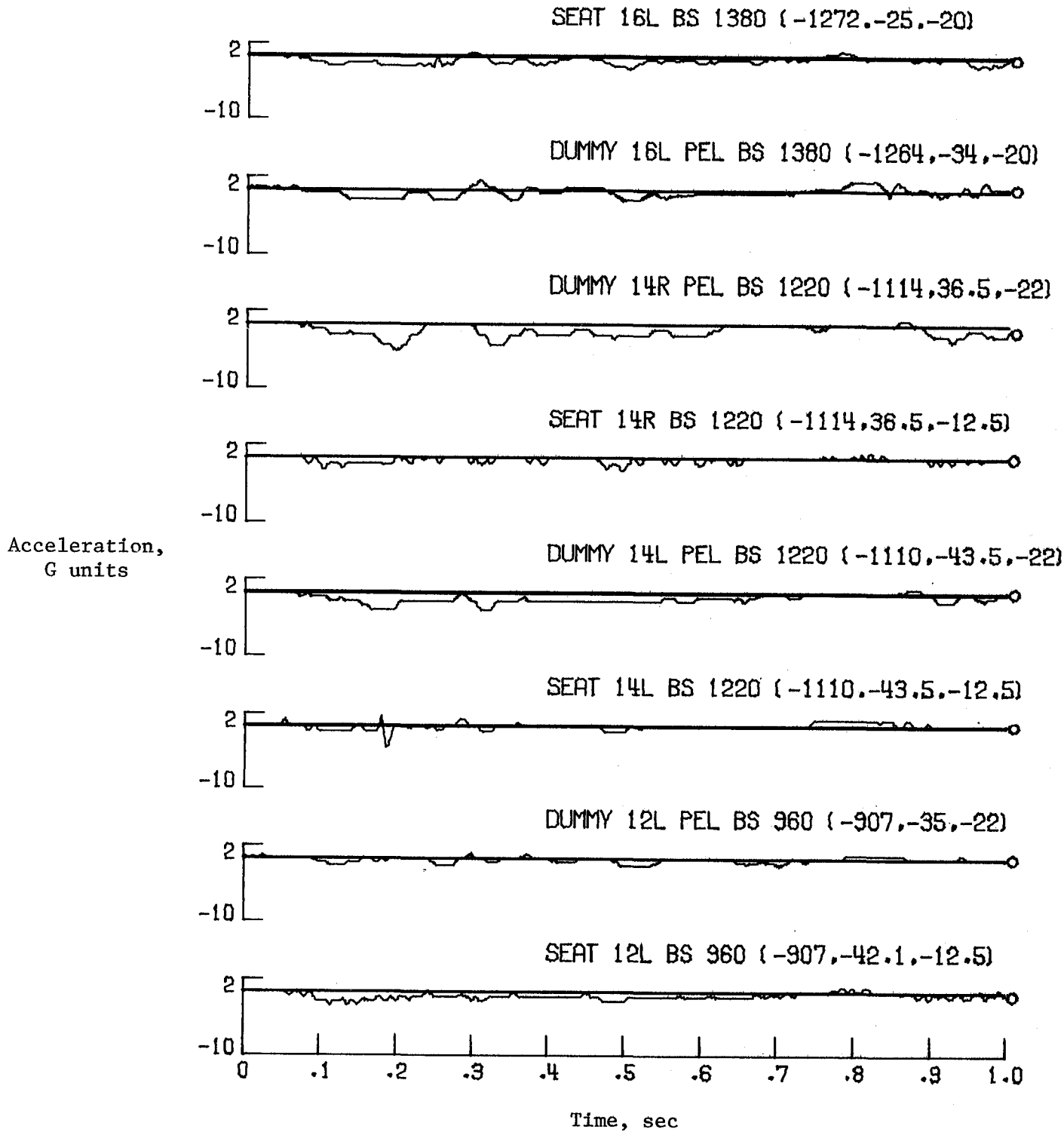

(f) BS 960 to 1380.

Figure C3. Concluded.

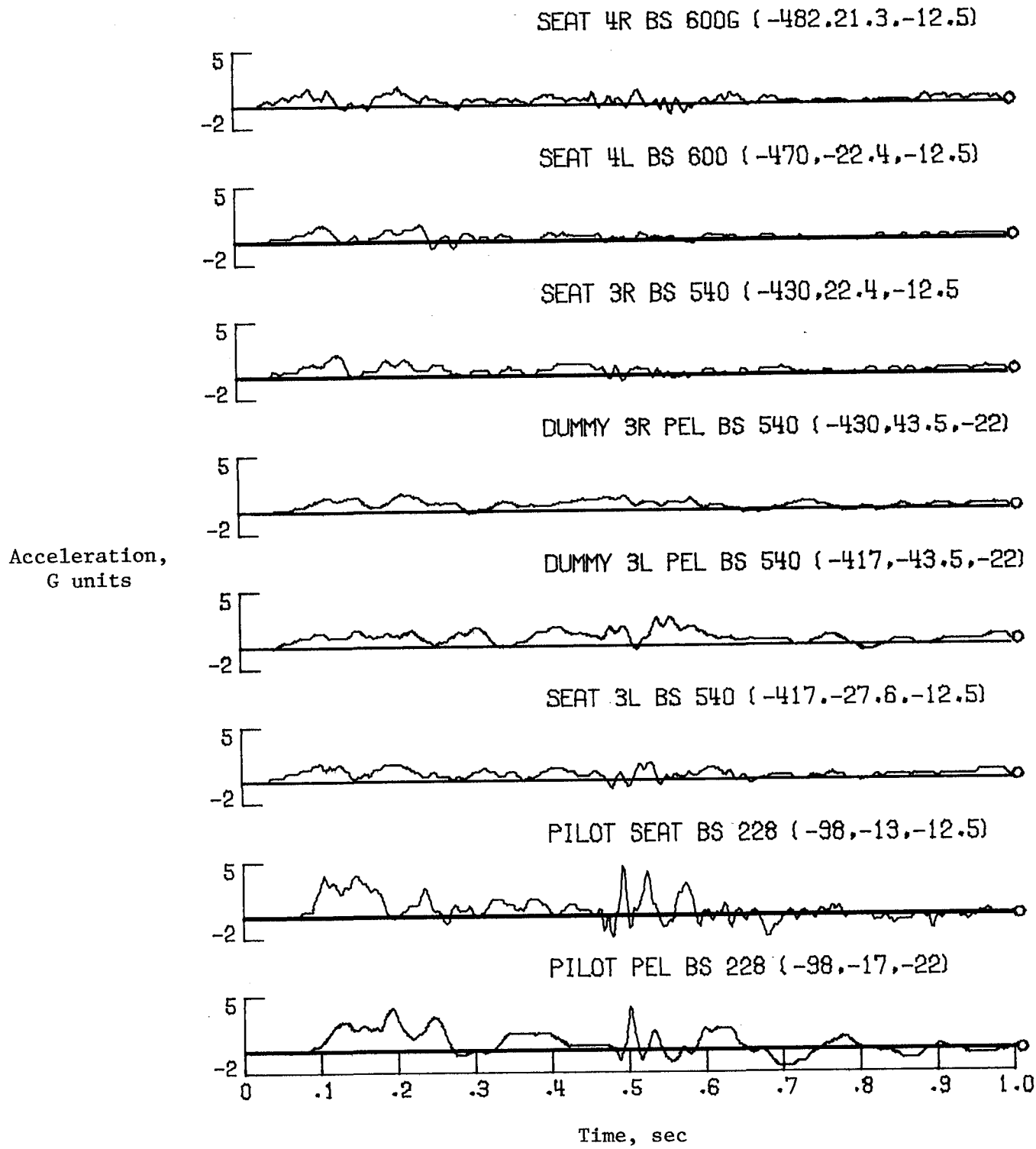

(a) BS 228 to 600G.

Figure C4. Seat and dummy transverse acceleration time histories.

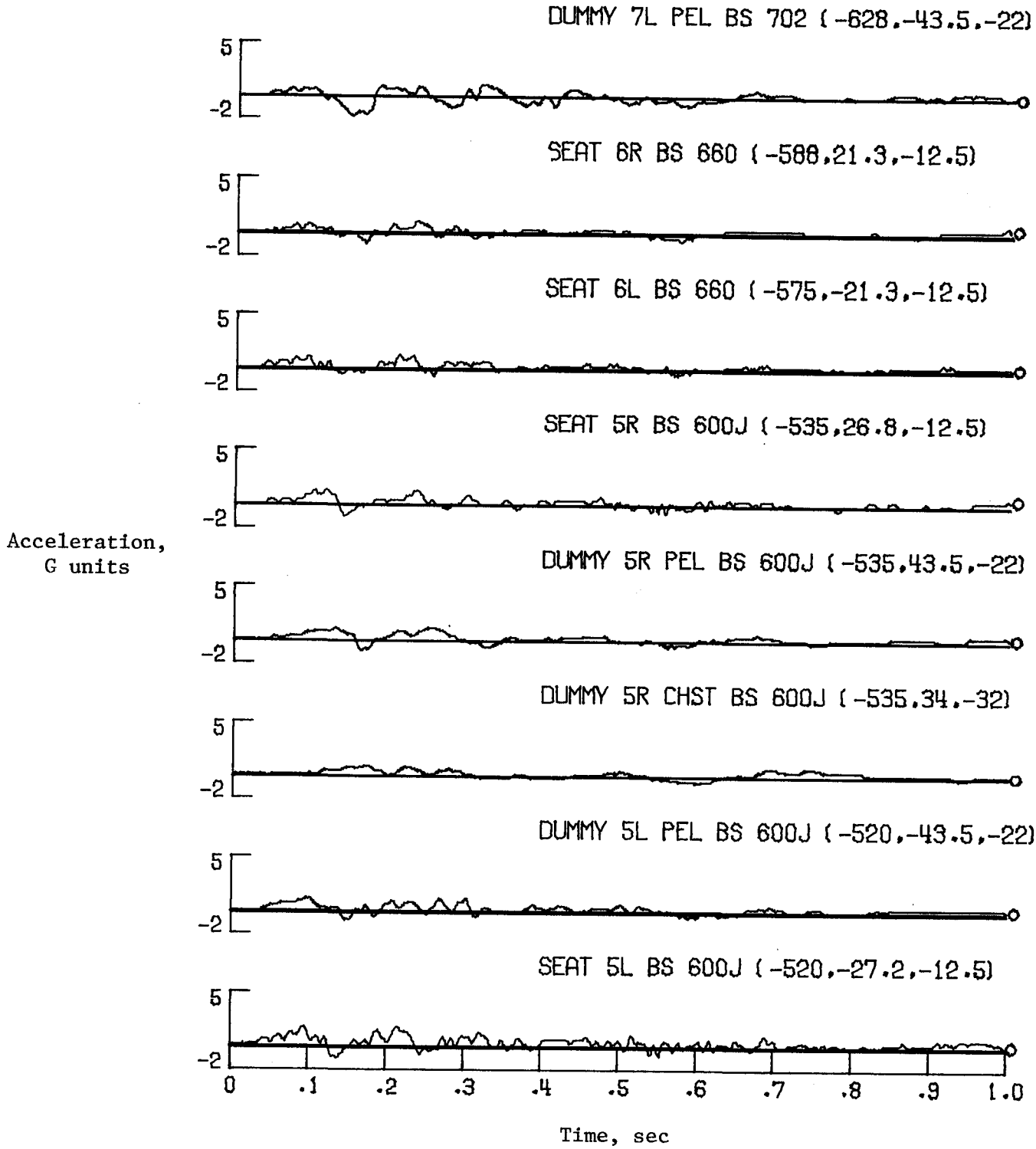

(b) BS 600J to 702.

Figure C4. Continued.

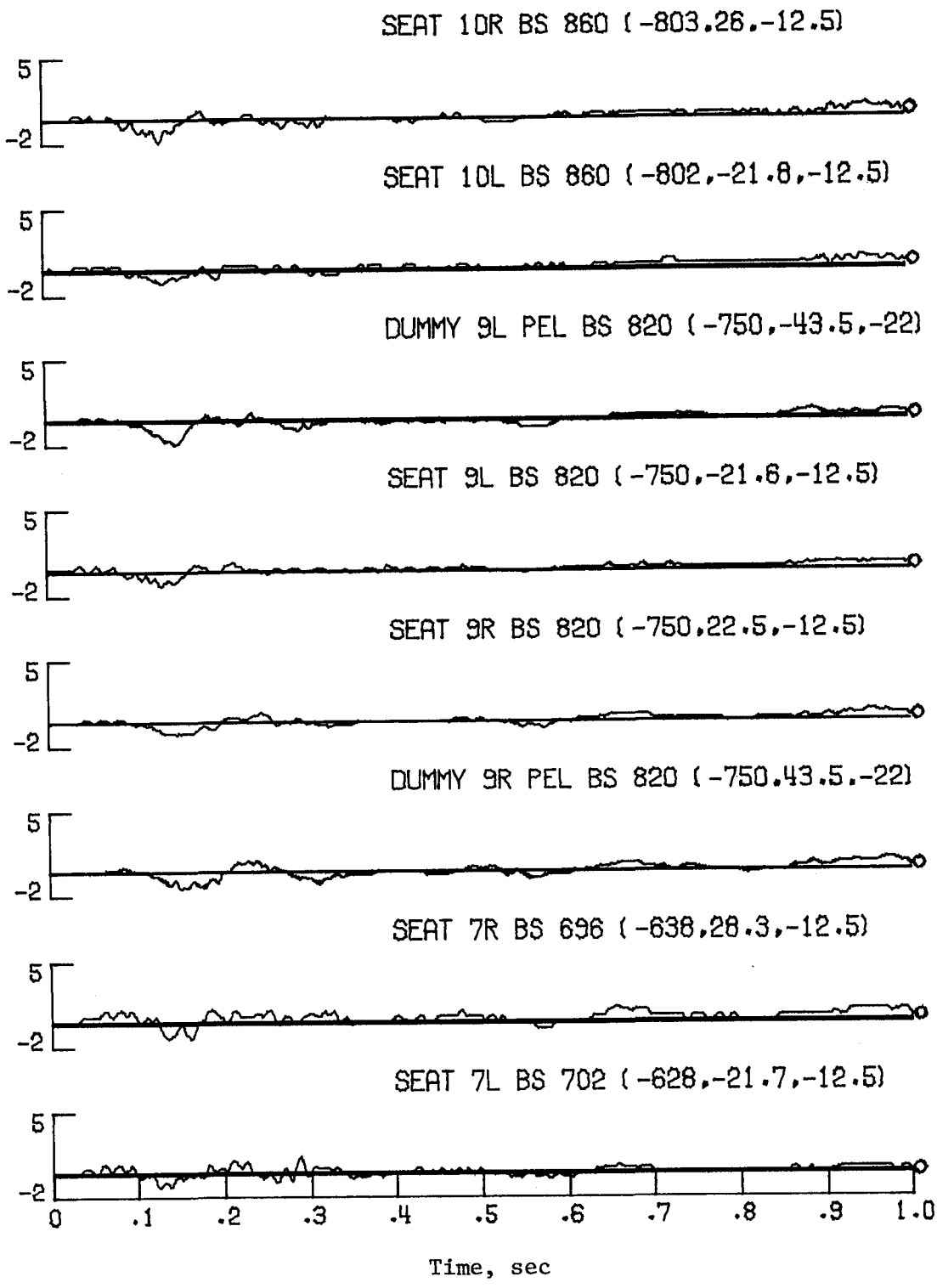

(c) BS 702 to 860.

Figure C4. Continued.

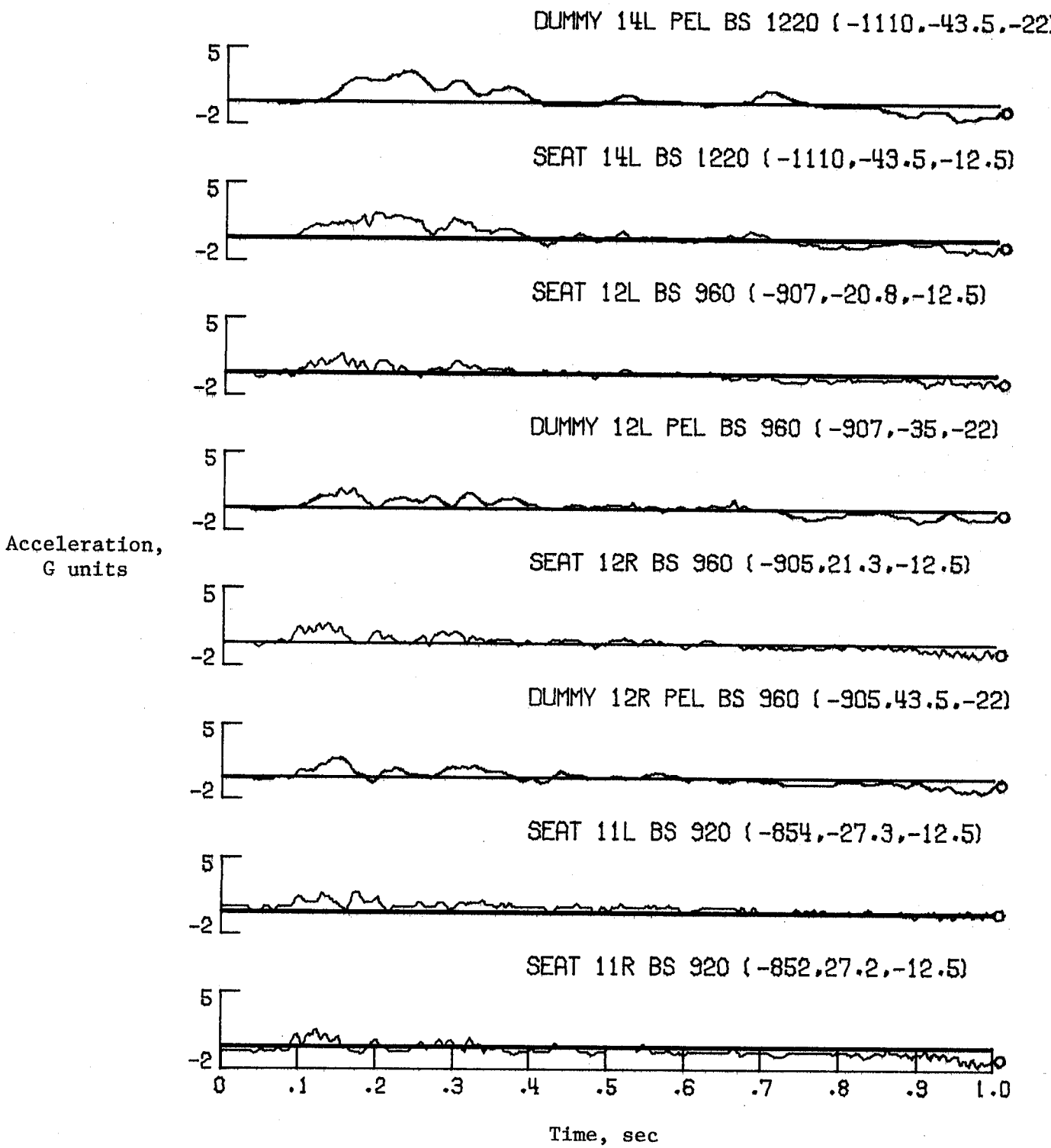

(d) BS 920 to 1220.

Figure C4. Continued.

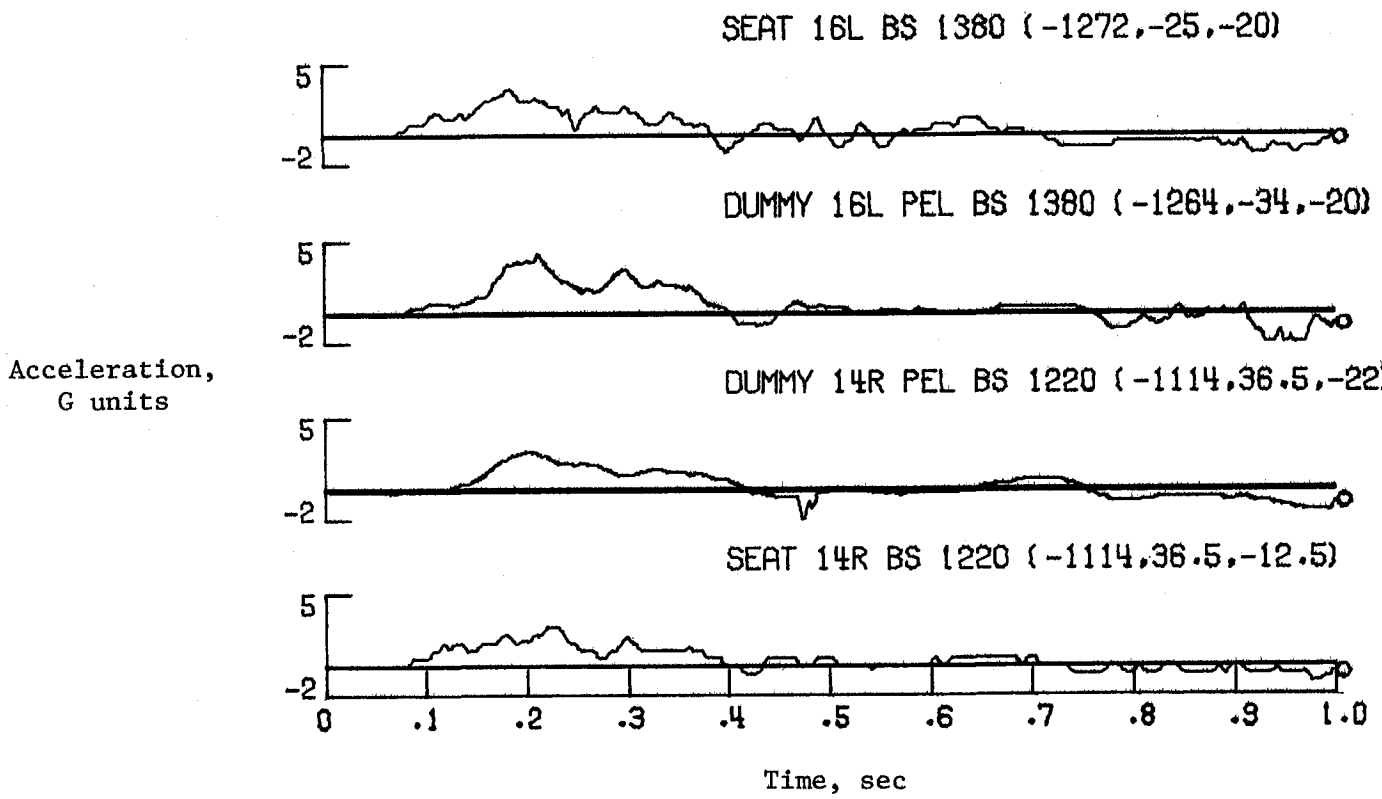

(e) BS 1220 to 1380.

Figure C4. Concluded.

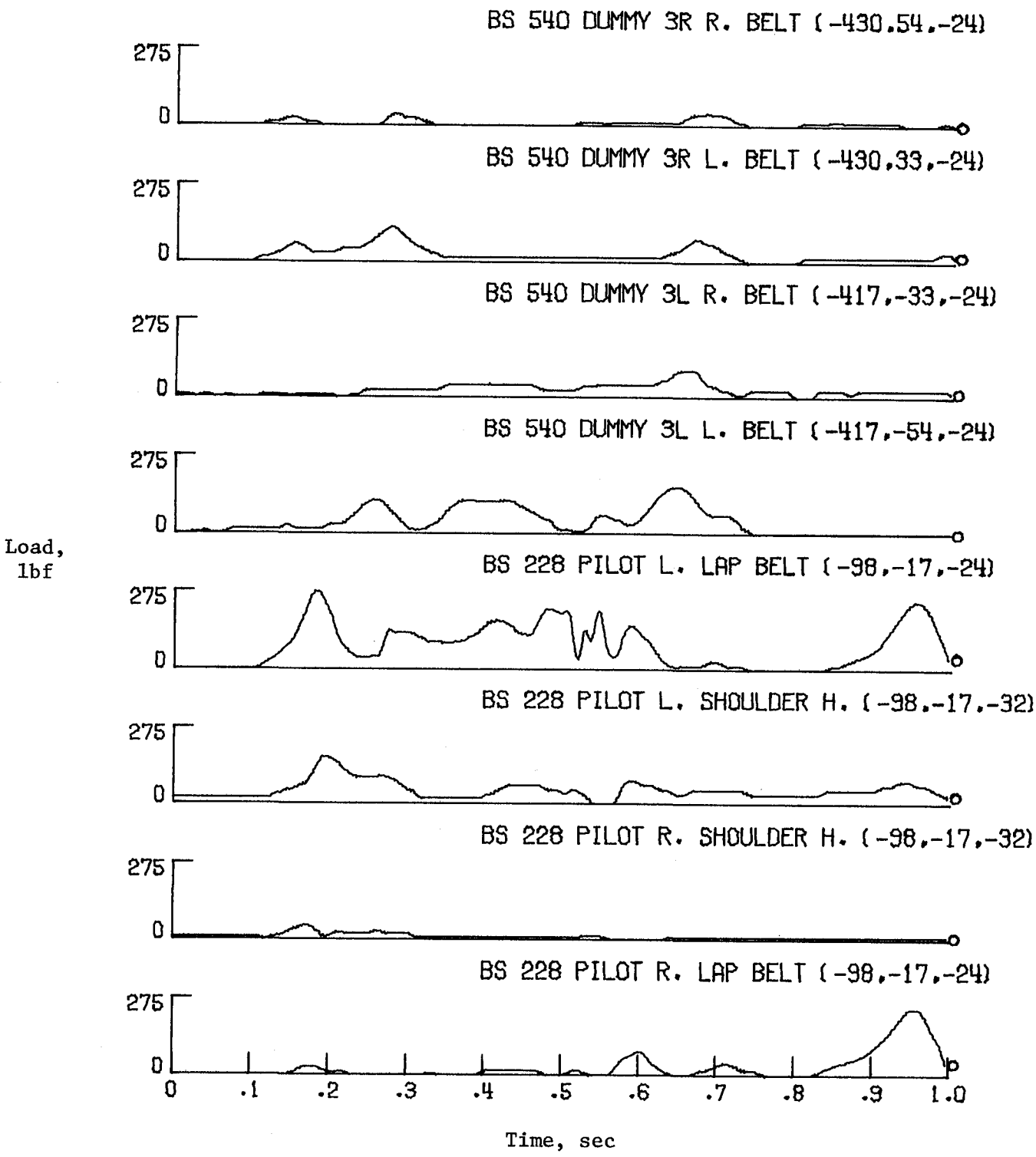

(a) BS 228 to 540.

Figure C5. Lap-belt and shoulder-harness load time histories.

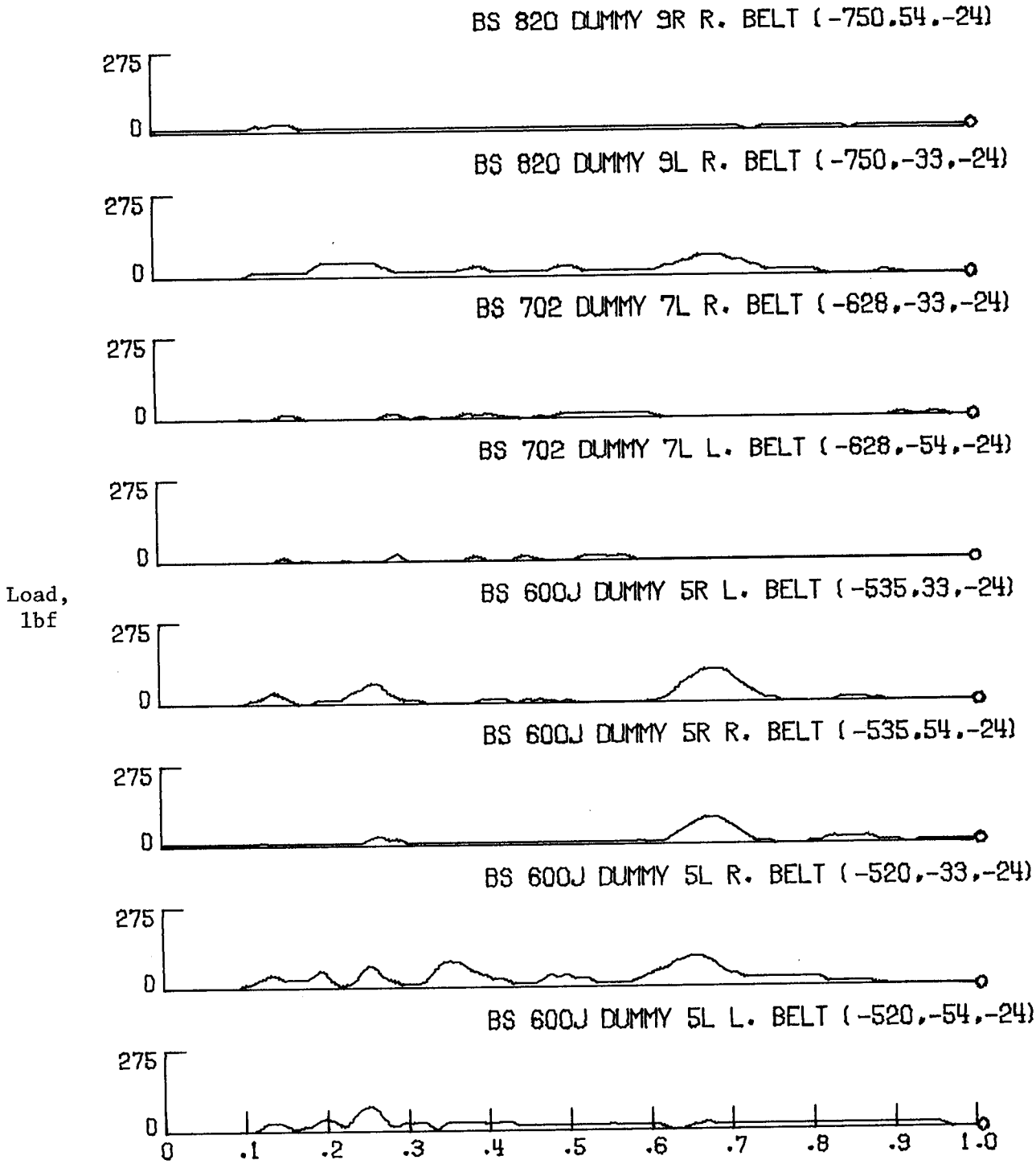

(b) BS 600J to 820.

Figure C5. Continued.

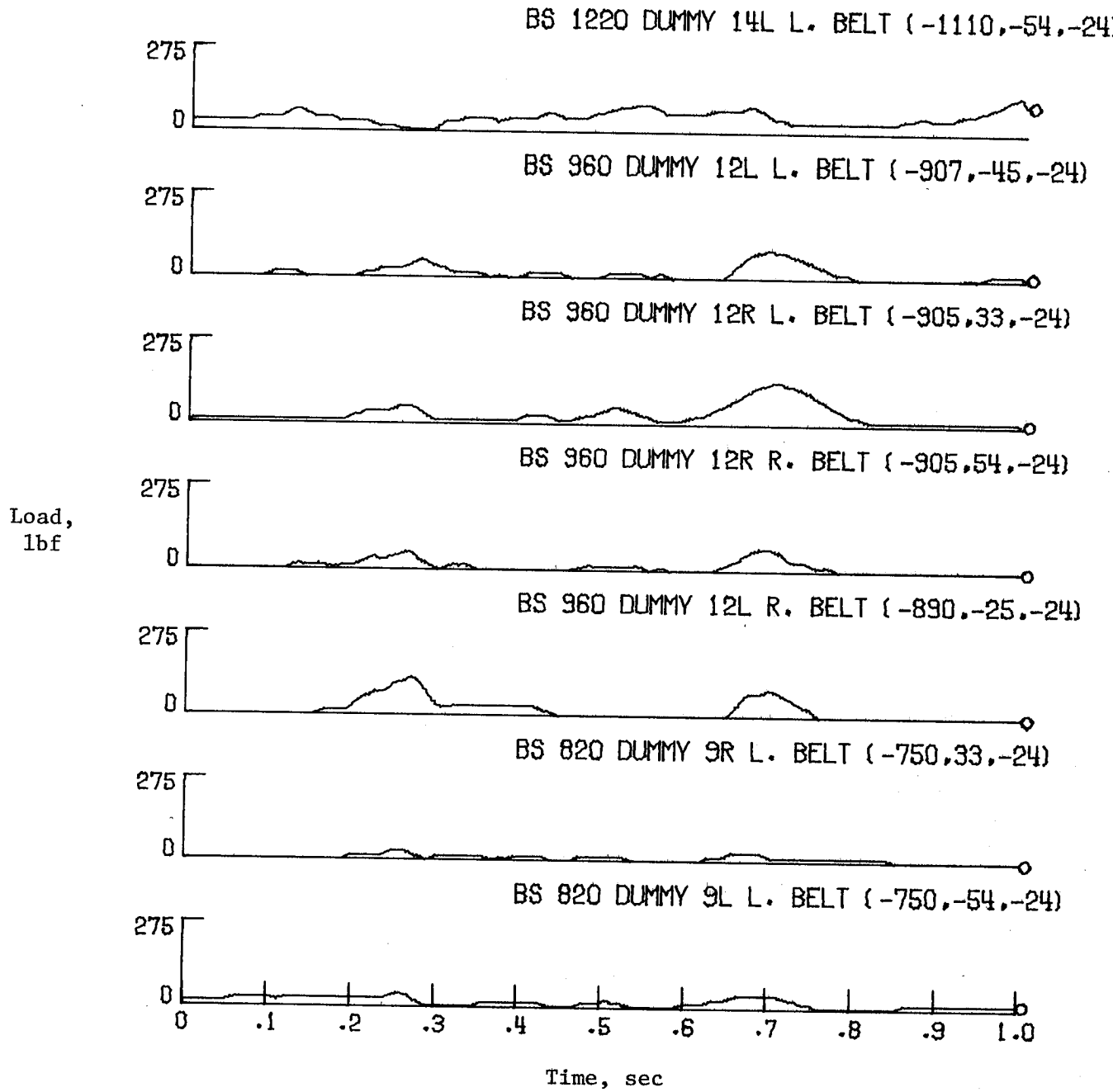

(c) BS 820 to 1220.

Figure C5. Continued.

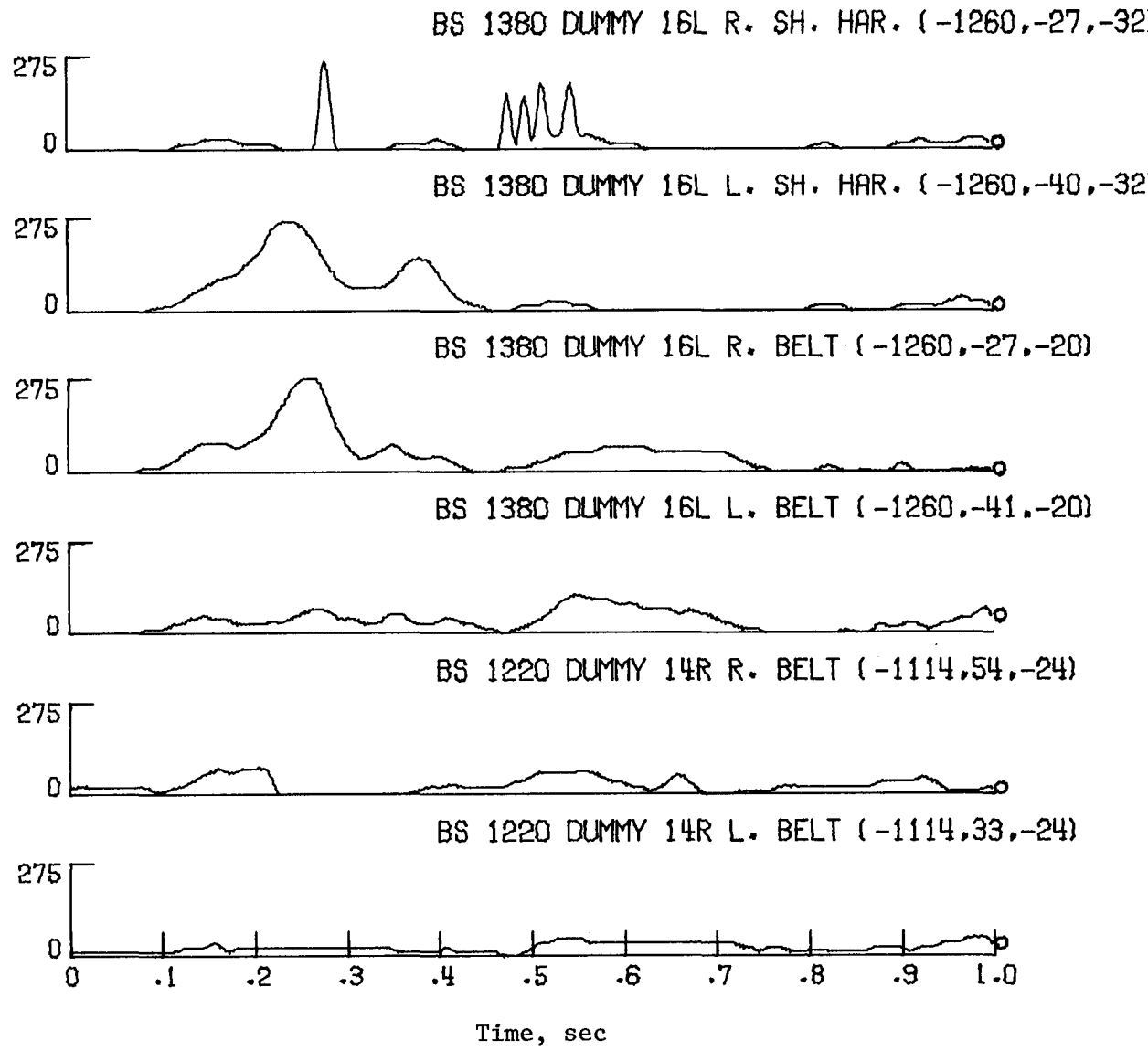

(d) BS 1220 to 1380.

Figure C5. Concluded.

References

1. Thomson, Robert G.; Carden, Huey D.; and Hayduk, Robert J.: *Survey of NASA Research on Crash Dynamics.* NASA TP-2298, 1984.
2. Alfaro-Bou, Emilio; Fasanella, Edwin L.; and Williams, M. Susan: Crashworthy Design Considerations for General Aviation Seats. SAE Tech. Paper Ser. 850855, Apr. 1985.
3. Fasanella, E. L.; Hayduk, R. J.; Robinson, M. P.; and Widmayer, E.: Analysis of a Transport Fuselage Section Drop Test. *Research in Structures and Dynamics—1984*, Robert J. Hayduk and Akmed K. Noor, compilers, NASA CP-2335, 1984, pp 347–368.
4. Fasanella, Edwin L.; Widmayer, E.; and Robinson, Martha P.: Structural Analysis of the Controlled Impact Demonstration of a Jet Transport Airplane. AIAA-86-0939, May 1986.
5. Hayduk, Robert J., compiler: *Full-Scale Transport Controlled Impact Demonstration.* NASA CP-2395, 1986.
6. Hayduk, Robert J.; Fasanella, Edwin L.; and Alfaro-Bou, Emilio: Structural Crashworthiness Experiments of the Controlled Impact Demonstration. Paper presented at the International Society of Air Safety Investigators 16 International Seminar (Scottsdale, Arizona), Sept. 1985.
7. Hayduk, Robert J.; Fasanella, Edwin L.; and Alfaro-Bou, Emilio: NASA Experiments Onboard the Controlled Impact Demonstration. SAE Paper 851885, Oct. 1985.
8. Thomson, R. G.; and Caiafa, C.: *Structural Response of Transport Airplanes in Crash Situations.* NASA TM-85654, 1983.
9. *Full-Scale Transport Controlled Impact Demonstration Program.* DOT/FAA/CT-82/151, Jan. 1984.
10. Eichelberger, Charles P.; Alfaro-Bou, Emilio; and Fasanella, Edwin L.: Development of an Energy-Absorbing Passenger Seat for a Transport Aircraft. *19th Aerospace Mechanisms Symposium*, NASA CP-2371, 1985, pp. 39–58.
11. Fasanella, E. L.: Digital Filtering and Acceleration Pulse Interpretation. *Full-Scale Transport Controlled Impact Demonstration*, Robert J. Hayduk, compiler, NASA CP-2395, 1986, pp. 103–123.
12. Eiband, A. Martin: *Human Tolerance to Rapidly Applied Accelerations: A Summary of the Literature.* NASA MEMO 5-19-59E, 1959.
13. Williams, M. Susan; and Hayduk, Robert J.: *Vertical Drop Test of a Transport Fuselage Center Section Including the Wheel Wells.* NASA TM-85706, 1983.

Standard Bibliographic Page

1. Report No.	2. Government Accession No.	3. Recipient's Catalog No.
NASA TP-2589		

4. Title and Subtitle	5. Report Date
Impact Data From a Transport Aircraft During a Controlled Impact Demonstration	September 1986
	6. Performing Organization Code: 505-63-41-01
7. Author(s): Edwin L. Fasanella, Emilio Alfaro-Bou, and Robert J. Hayduk	8. Performing Organization Report No.: L-16125
9. Performing Organization Name and Address: NASA Langley Research Center, Hampton, VA 23665-5225	10. Work Unit No.
	11. Contract or Grant No.
12. Sponsoring Agency Name and Address: National Aeronautics and Space Administration, Washington, DC 20546-0001	13. Type of Report and Period Covered: Technical Paper
	14. Sponsoring Agency Code

15. Supplementary Notes

Edwin L. Fasanella: PRC Kentron, Inc., Hampton, Virginia.
Emilio Alfaro-Bou and Robert J. Hayduk: Langley Research Center, Hampton, Virginia.

16. Abstract

On December 1, 1984, the FAA and NASA conducted a remotely piloted air-to-ground crash test of a Boeing 720 transport aircraft instrumented to measure crash loads of the structure and the anthropomorphic-dummy passengers. This paper contains over 330 time histories of accelerations and loads collected during the Full-Scale Transport Controlled Impact Demonstration (CID) for the 1-sec period after initial impact. Although a symmetric 1° nose-up attitude with a 17 ft/sec sink rate was planned, the plane was yawed and rolled 13° at initial (left-wing) impact. The first fuselage impact occurred near the nose wheel well with the nose pitched down 2.5°. Peak normal (vertical) floor accelerations were highest in the cockpit and forward cabin near the nose wheel well and were approximately 14G. The remaining cabin floor received normal acceleration peaks of 7G or less. The peak longitudinal floor accelerations showed a similar distribution, with the highest (7G) in the cockpit and forward cabin, decreasing to 4G or less toward the rear. Peak transverse floor accelerations ranged from about 5G in the cockpit to 1G in the aft fuselage.

17. Key Words (Suggested by Authors(s))	18. Distribution Statement
Crashworthiness Controlled impact demonstration Airplane crash test Transport crash test Impact test Crash dynamics	Unclassified—Unlimited Subject Category 05

19. Security Classif.(of this report)	20. Security Classif.(of this page)	21. No. of Pages	22. Price
Unclassified	Unclassified	88	A05

For sale by the National Technical Information Service, Springfield, Virginia 22161

NASA-Langley, 1986

National Aeronautics and
Space Administration
Code NIT-4

Washington, D.C.
20546-0001